

## INTRODUCTION

Hepatocellular carcinoma or HCC is the 5<sup>th</sup> most common cancer and the 3<sup>rd</sup> most lethal cancer worldwide. More worrisome is the fact that the historically low incidence rate in the US has started to climb, most likely due to exacerbating factors like chronic alcohol use, HCV infection, and perhaps most importantly obesity. Epidemiological studies have consistently shown that obesity is a major risk factor in the development of HCC, due to the development of NASH, which eventually leads and cirrhosis and finally ending in HCC. HCC patients who are obese have also been shown to have a much higher rate of morbidity, mortality, and overall a much poorer prognosis. Yet, little work has been conducted on the combinatorial effects of an obesogenic diet and exposure to an environmental or occupational carcinogen on the progression and development of HCC. Therefore the goal of our work was to investigate the effects of an obesogenic diet in combination with a known model carcinogen 4,4'-methylenedianiline (MDA).

MDA is considered an occupational carcinogen by the US National Institute for Occupational Safety and Health and is used in the manufacture of polyurethane foams used for insulation and in making coating materials, glues, Spandex®, fibers, dyes, and rubber. Exposure to MDA can occur through occupational contact, touching consumer goods containing MDA, or living near hazardous waste sites. Thus we expect the combination of an obesogenic diet and exposure to MDA will result in markedly more rapid and severe progression of HCC.

Analysis of current literature has shown two reliable and validated markers for documenting hepatic neoplastic and pre-neoplastic events, namely glutathione S-transferase P1 (GSTP1) and cyclin D1. GSTP1 is an important detoxification enzyme that catalyzes the conjugation of carcinogens with reduced glutathione for excretion. Cyclin D1 is a critical regulator of the cell cycle and is required by proliferating cells to progress from the G1 phase to the S phase, and has also been shown to be expressed in much higher levels in neoplastic foci than in surrounding livers. Thus we have used the levels of expression of these two proteins as a way to document the progression and severity of hepatocarcinogenesis in rats exposed to obesogenic diets and MDA.

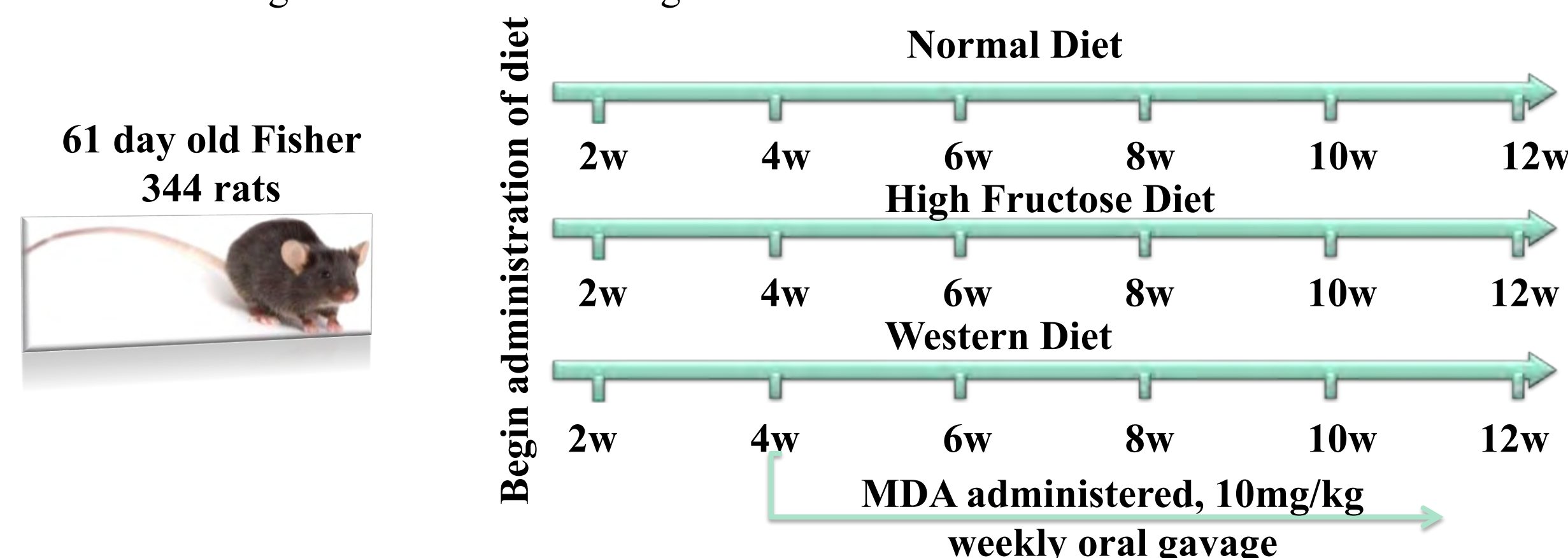
## ABSTRACT

Hepatocellular carcinoma (HCC) is the 5th most common malignancy in the world, and the third leading cause of cancer death due to a rapid progression, poor prognosis and high rate of mortality. Even in countries of historically low incidence rates particularly the US have experienced a steady increase in the occurrence of HCC. Yet in the US it has been reported that 15-50% of HCC patients had no exposure to established risk factors like heavy alcohol consumption, viral infection or aflatoxin B1 exposure. This highlights the role of predisposing factors such as diet and potential exposure to occupational and/or environmental carcinogens as being critical factors in HCC development and progression. Obesity, which has been on the rise for the last 30 years in the West, and high fat diets have been experimentally and epidemiologically linked to an increased risk of HCC incidence and mortality. Therefore the goal of our study was to investigate the carcinogenic potential of an environmental carcinogen 4,4 methylenedianiline (MDA) both singly, and in combination with obesogenic dietary components.

Sixty-one day old male F344 rats were exposed to either a normal diet, a high fructose diet (30% in drinking water), or a high fat/high cholesterol diet (Western diet, Open Source diets, 17% of calories from protein, 43% of calories from carbohydrates and 41 % from fat) with and without exposure to MDA. Those animals receiving MDA were administered a single oral gavage of 10 mg/kg MDA each week for eight weeks after four weeks of exposure to each respective diet. Livers obtained from these rats were subjected to immunohistochemical and Western blot analysis. Specifically, the effects on the hepatic cell cycle regulator cyclin D1 and the detoxification enzyme glutathione S-transferase P-form (GST-P) which are established pre-neoplastic and neoplastic markers of HCC were examined. Both the HCC neoplastic markers were observed to be increased in response to MDA in animals receiving normal diet according to immunohistochemical staining. Importantly, a further increase in the expression of these markers was observed as a consequence of the combinatorial effect of MDA and diet. Overall, our findings suggest that carcinogenic potential of environmental/occupational carcinogens could be significantly enhanced by dietary components.

## MATERIALS AND METHODS

- F344 male rats (61 days old) were fed either normal, high fructose or western diet for 4 weeks prior to the administration of MDA.
- The high fructose diet was administered ad libitum as a 30% solution in the drinking water, and the Western diet was obtained from Open Source Diets (17% of calories from protein, 43% of calories from carbohydrates and 41 % from fat). The animals weight was measured weekly.
- MDA was administered at a dosage of 10 mg/kg by a single oral gavage every week for 8 weeks at which time the rats were sacrificed, blood was collected, and liver tissues harvested.
- Visual inspection of livers showed no signs of overt toxicity and all 24 rats survived the experiment. Rats fed the Western and high fructose diets visibly had more visceral fat and a larger overall weight when compared to rats on normal diet.
- Rats were sacrificed at the end of the 12 weeks and blood, liver, and ileum samples were collected.
- Resected livers were embedded in paraffin after which cross-sectional slides made and subjected to analysis through immunohistochemistry. The slides were deparaffinized using the HEMO-DE solvent system, after which the tissues were rehydrated, blocked for non-specific peroxidases, then left in primary antibody over night. Slides were then developed using DAB+ substrate-chromogen solution which would bind to the primary antibody, be oxidized, and form an insoluble brown stain indicating positive identification of our target protein. Slides were then counterstained with methyl green to make the positive stain more distinguishable from the background.



## RESULTS

- As expected rats fed the Western diet and the high fructose diet had significantly higher body weights in both the treatment group as well as the control group. Both the treated and control groups gained approximately the same weight with the Western diet resulting in the largest gains.
- Both of these diets also caused the percent liver weight to body ratio to increase significantly when compared to the normal diet control. Interestingly both the Western and high fructose diets had approximately the same increase in liver to body weight ratios, suggesting that both diets cause an approximately equal increase in hepatic steatosis.
- Immunohistochemical staining showed both a greater overall positive staining of hepatic tissues in rats receiving MDA in combination with either the high fructose or Western diets. However rats receiving MDA and a normal diet showed a few localized regions of positive staining.
- Metamorph analysis of immunohistochemical staining revealed that both pre-neoplastic markers, GSTP1 and Cyclin D1 were increased by the high fructose and Western diets alone, yet the increase was greater in those animals treated with MDA in combination with the Western diet. Cyclin D1 expression was marginally increased by a combination of high fructose diet and MDA exposure.

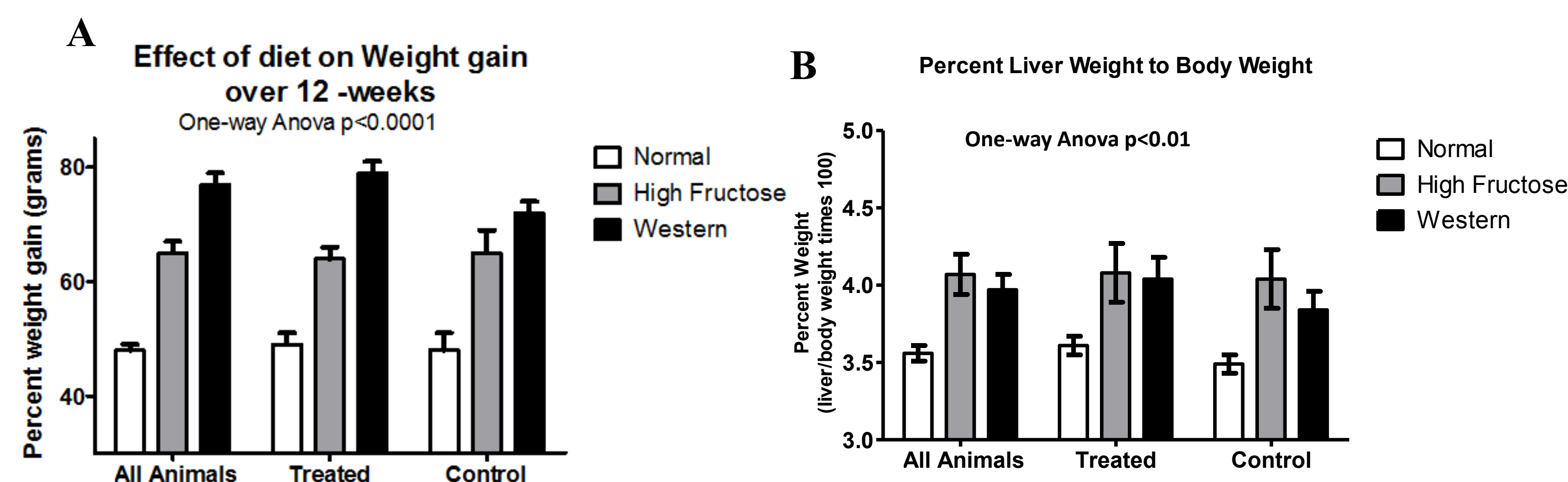


**Figure 1A** - At the end of the study both groups of rats that were fed a high fructose diet or a Western diet had significantly higher body weights and showed visible signs of obesity and excessive adiposity especially visceral fat. (Mean +/- SEM; n=24)

**Figure 1B** - Rats in both the high fructose group as well as the Western group also had significant amounts of fat deposited in their livers as shown by the increase in the liver to body percent weight ratio. (Mean +/- SEM; n=24)

## Combinatorial Effects of Diet and MDA on the Emergence of Early Preneoplastic Markers of HCC

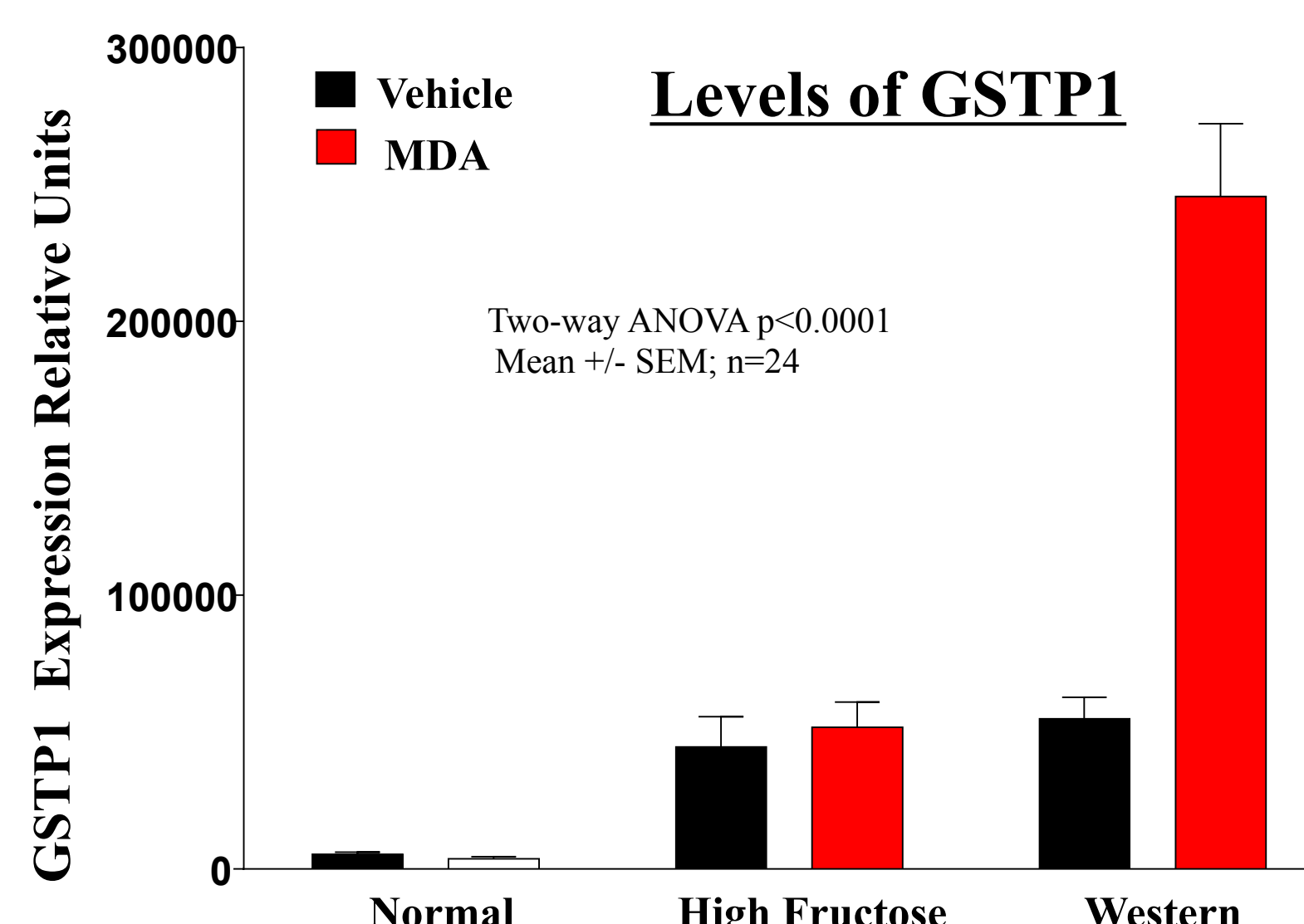
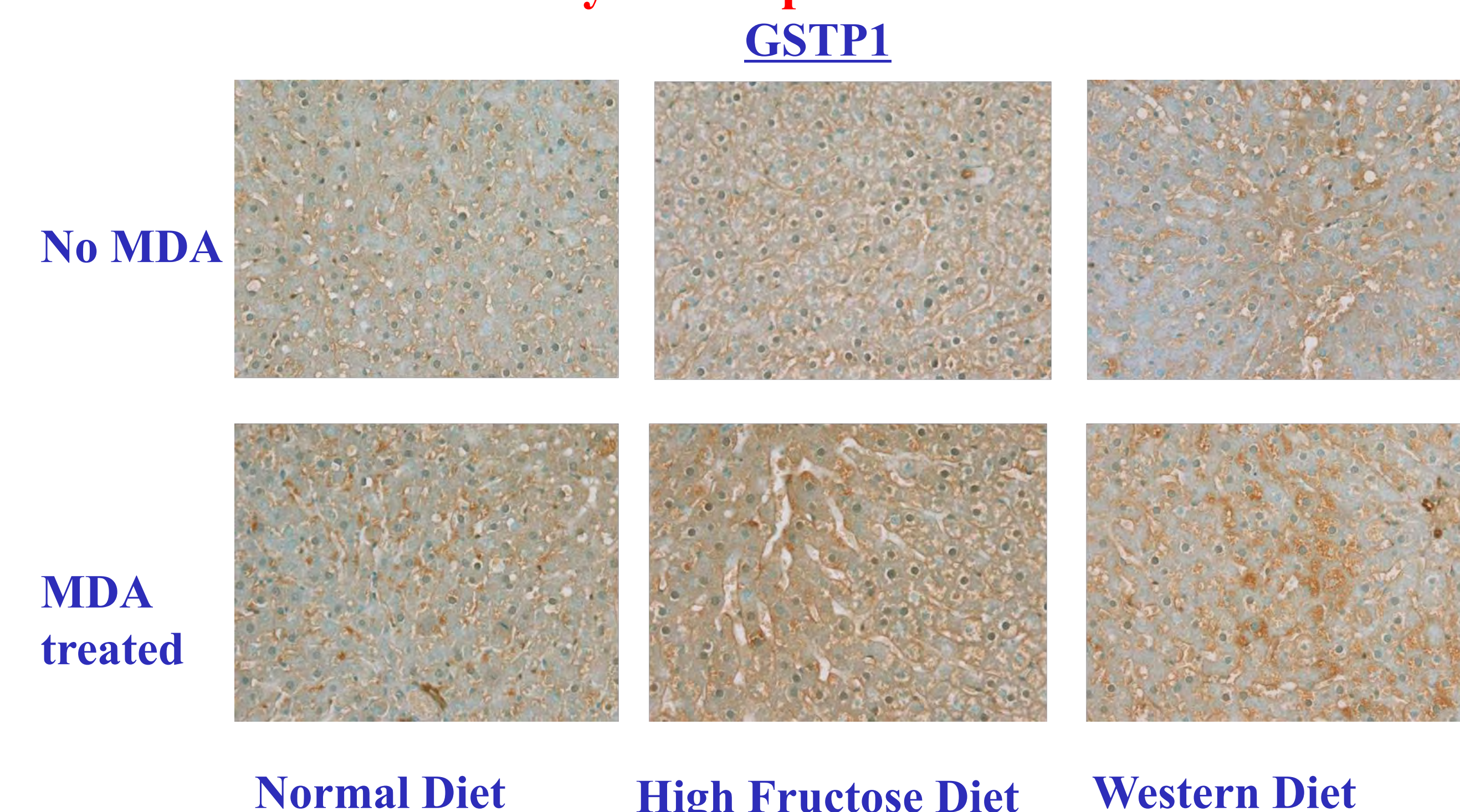


**Figure 2** - GSTP1 levels were quantified from the immunohistochemical staining through analysis with Metamorph software that was able to calculate the relative intensities of staining based on pixel density. High fructose diet in combination with MDA seems to have little to no effect but the combinatorial effect of the Western diet and MDA showed a marked increase of GSTP1.

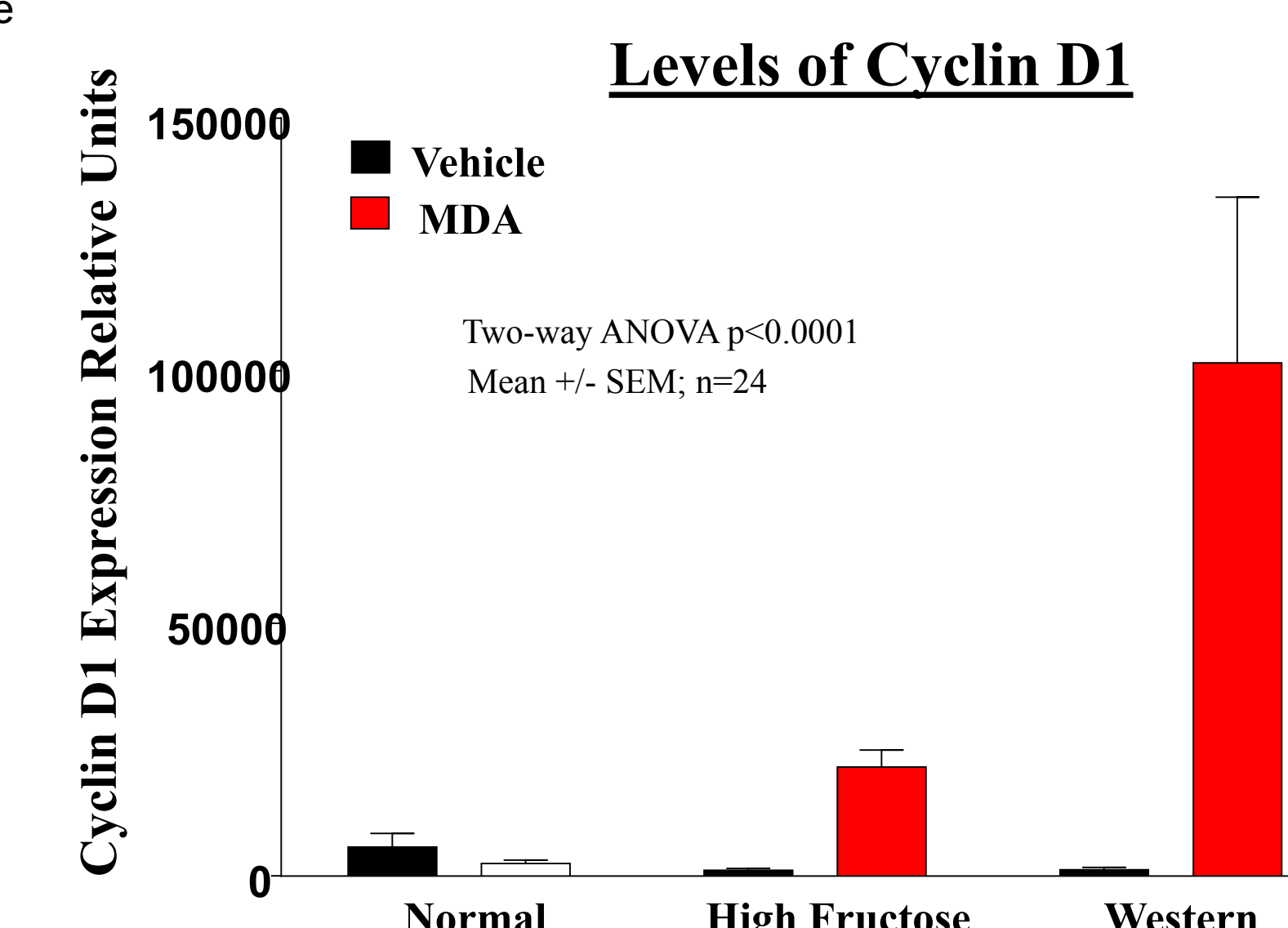
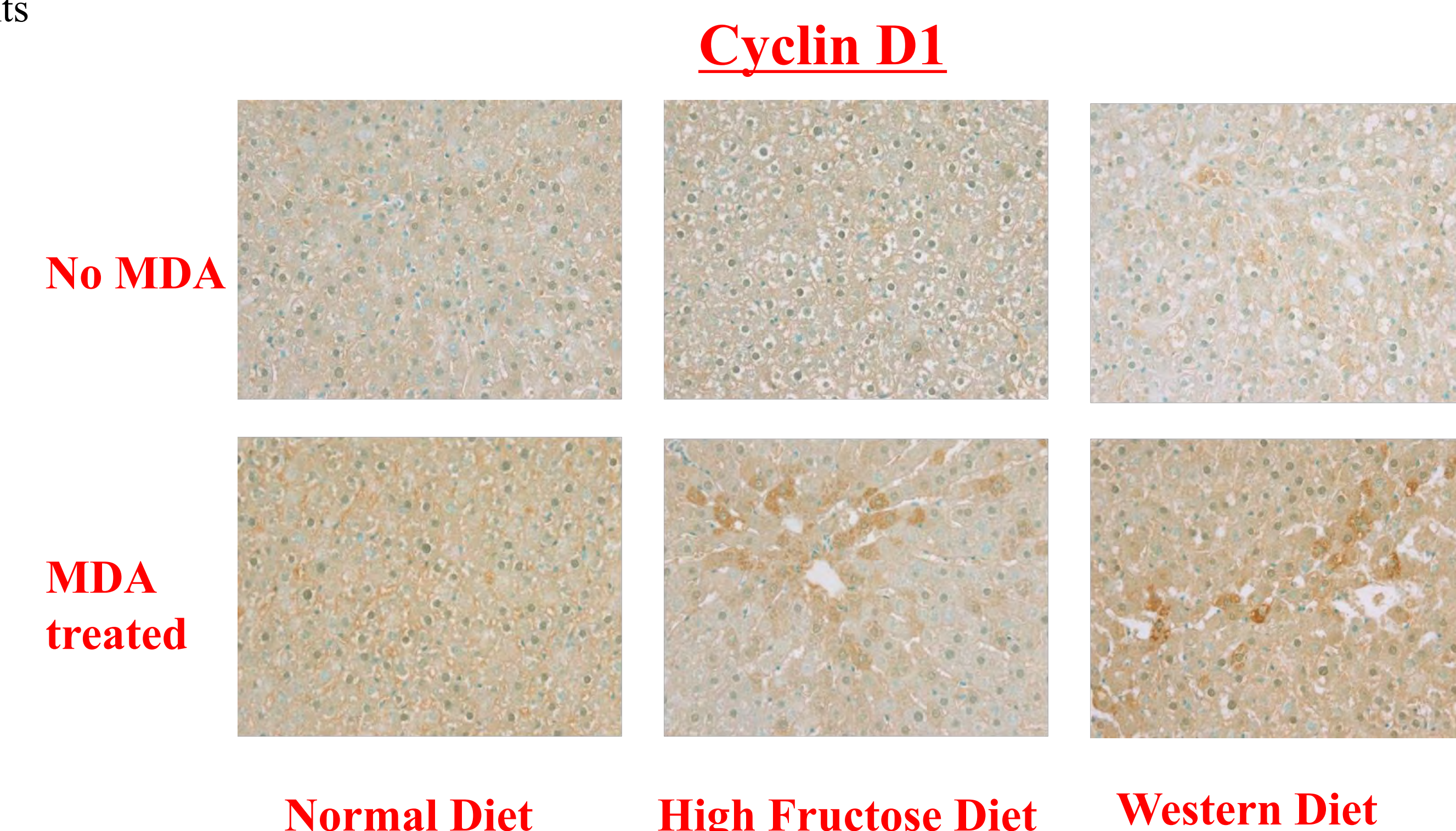


**Figure 3** - Cyclin D1 levels were quantified from the immunohistochemical staining through analysis with Metamorph software that was able to calculate the relative intensities of staining based on pixel density. High fructose diet in combination with MDA seems to have little to no effect but the combinatorial effect of the Western diet and MDA showed a marked increase of Cyclin D1.

## CONCLUSIONS

- Our hypothesis was validated as MDA causes pre-neoplastic events in the livers of rats, and these events are greatly amplified in rats fed a Western diet.
- Pre-neoplastic events were detected even using a dosage of MDA that is markedly lower than similar studies, highlighting the importance of the influence of predisposing factors, like diet, in addition to carcinogenic exposure.
- Rats receiving high fructose showed only marginal differences in the amount of cyclin D1 expression and showed no increase in GSTP1.
- The experimental data strongly suggests that the type of diet along with exposure to environmental or occupational carcinogens, like MDA, could greatly enhance the risk of developing HCC in obese and overweight individuals.

## ACKNOWLEDGEMENTS

- Funding provided by NCI Grant R25-CA134283

# Combination of Withaferin A and Cisplatin Eliminates Ovarian Cancer Stem Cells

Addison T. Bray<sup>1</sup>, Sham S. Kakar<sup>2,3</sup>

University of Louisville, College of Arts and Sciences<sup>1</sup>, Departments of Physiology & Biophysics<sup>2</sup>

and the James Brown Cancer Center<sup>3</sup>

University of Louisville, Louisville, Kentucky



## Abstract

Currently first round of chemotherapy for patients with ovarian cancer includes a platinum based drug called cisplatin. This treatment is often effective in 70% of women, however after a few months of treatment tumor relapse occurs and patients become platinum resistant, which happens in 70 to 80% of patients. The platinum-resistance and tumor renewal has been reported due to cancer stem cells that are present in small numbers in cancer. The purpose of the present study is to determine the effects of cisplatin in combination with withaferin A (WFA), a bioactive plant product. We looked for cancer stem cells that express high levels of aldehyde dehydrogenase 1 (ALDH1), a marker for cancer stem cells. The expression levels of ALDH1 were tested in vivo by using immunohistochemistry and western blot of mouse ovary cancer tissues after drug treatment. In vitro analysis includes western blot, ALDEFLOUR flow cytometry, and sphere forming assay of ALDH<sup>+</sup> and ALDH<sup>-</sup> sorted cells. In vivo results suggest that cisplatin resulted in a significant increase in ALDH1 expression levels, whereas WFA when used alone or in combination with cisplatin significantly suppressed the expression of ALDH1, suggesting that cisplatin increases the number of cancer stem cells. This helps better understand the high probability of secondary platinum resistant cancer in patients. In vitro results show that both cisplatin and WFA reduce ALDH1 expression and act synergistically in combination. The difference between in vivo and in vitro studies could be that cisplatin treatment may not have enough time to act on the cancer stem cells in vitro or the microenvironment could affect expression. The sphere forming assay shows that only ALDH<sup>+</sup> cells are able to form spheres on ultra-low attachment plates in stem cell media. In conclusion, we have shown that ALDH1 expression is up regulated with cisplatin treatment and down regulated with withaferin A or combination treatment. Cancer stem cells also appear to need abnormally high ALDH1 production in order to survive. Research supported by the NIH/NCI R25-CA-134283 grant.

## Introduction

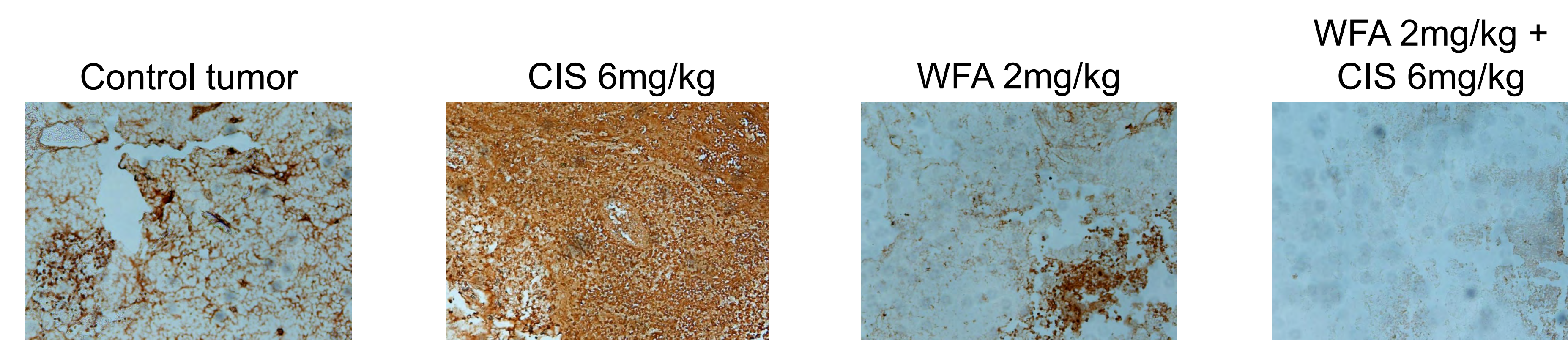
- Ovarian cancer is the leading cause of mortalities in gynecological malignancies.
- It is very difficult to detect early due to symptoms that are mild at first and often mimic other diseases. Most patients have advanced ovarian cancer when it is detected.
- 75% of women respond to the first round of platinum-based chemotherapy; however 75% of those patients who responded will relapse. If relapse occurs within six months the cancer is determined to be platinum resistant.
- Only about 30% of women survive beyond five years.
- The combination drug therapy of withaferin A (WFA) and cisplatin (CIS) offers an alternative to the current treatments in clinical practice.
- Aldehyde dehydrogenase 1 (ALDH1) is an enzyme which converts intracellular aldehydes into carboxylic acids.
- Increased ALDH1 activity has been linked to cancer stem cell properties in many cancer types.
- The goal of this present study was to analyze ALDH1 levels in response to WFA and CIS treatments and to understand the role of ALDH1 in ovarian cancer.

## Methods

- Cell Culture: Cell line A2780 maintained in RPMI-1640 medium supplemented with 10% fetal bovine serum and antibiotic solution. Cells were cultured at 37° C in humidified air with 5%CO<sub>2</sub>.
- Drug Treatment: A2780 cells seeded into 6 well plates and treated with WFA, CIS or a combination of WFA and CIS in varying concentrations for 48 hours. Cells were lysed and collected after 48 hours.
- Protein Assay: BSA used a standard for protein concentration determination of cells via spectrophotometry.
- Western Blot: Protein from the cell samples were resolved on SDS-PAGE gel and transferred to nitrocellulose paper. Diluted primary antibodies were applied to detect concentrations of ALDH. Peroxidase labeled secondary antibodies applied and detected using HRP chemiluminescence. Nitrocellulose paper was then washed and re-probed with β-actin to normalize protein concentrations.
- FACS Analysis and Cell Sorting: ALDEFLOUR kit used to detect ALDH<sup>+</sup> and ALDH<sup>-</sup> populations. The two subpopulations were sorted and collected using flow cytometry.
- Sphere Forming Assay: Cells collected from flow cytometry were plated on ultra low attachment plates with stem cell media. Growth factors added to the media every three days. Allowed to grow for two weeks and photographs were taken after one and two weeks.
- Immunohistochemistry: Previously xenografted tumors were sectioned and fixed in paraffin. Slides were prepared using ALDH1 antibodies and photographs were taken.

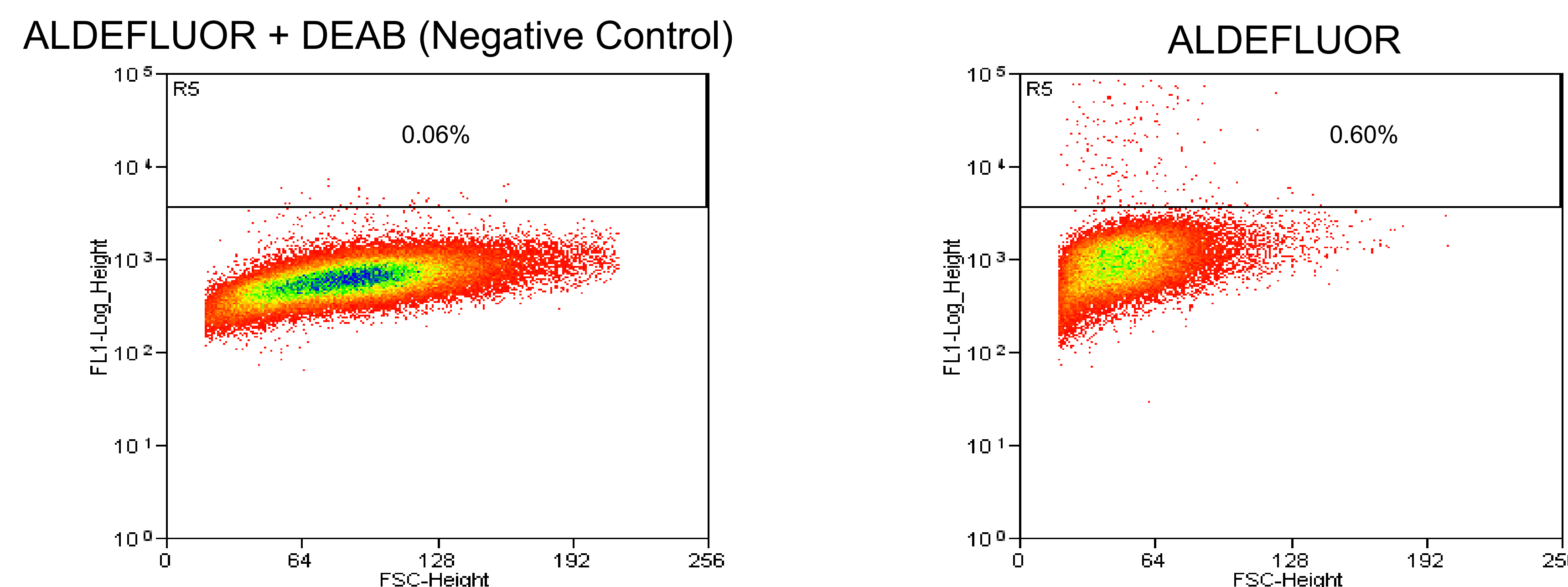
## Results

Figure 1: Combination Drug Therapy Immunohistochemistry of ALDH1



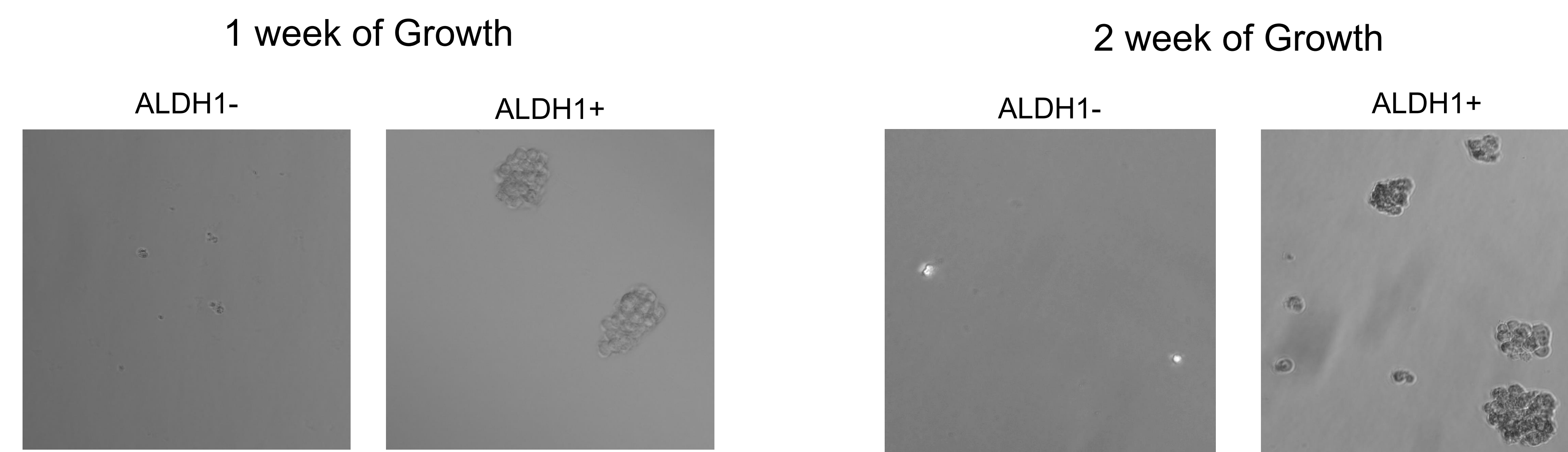
SCID mice were injected with A2780 cells directly into the ovaries and treated with Cisplatin, WFA or combination of both. Immunohistochemistry was performed using ALDH1-specific antibodies. Cisplatin increases ALDH1 expression, while withaferin A decreases ALDH1 expression. The combination treatment of cisplatin and withaferin A further decreases ALDH1 expression levels.

Figure 3: FACS Analysis of ALDH1 Positive Cells



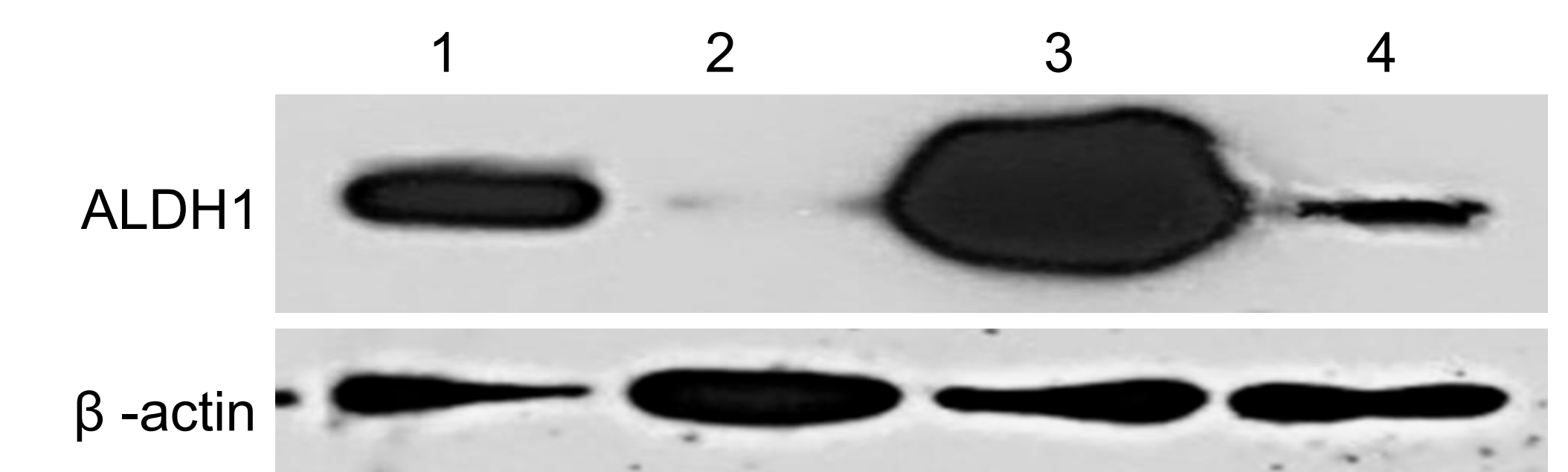
FACS analysis of ALDEFLOUR kit treated cells. Diethylaminobenzaldehyde (DEAB) is an inhibitor of ALDH1 activity and was used as the control to show baseline fluorescence. The cells that appear above the indicated line for ALDEFLOUR were collected as ALDH1<sup>+</sup> and the cells below the line collected as ALDH1<sup>-</sup>.

Figure 5: Sphere Forming Assay



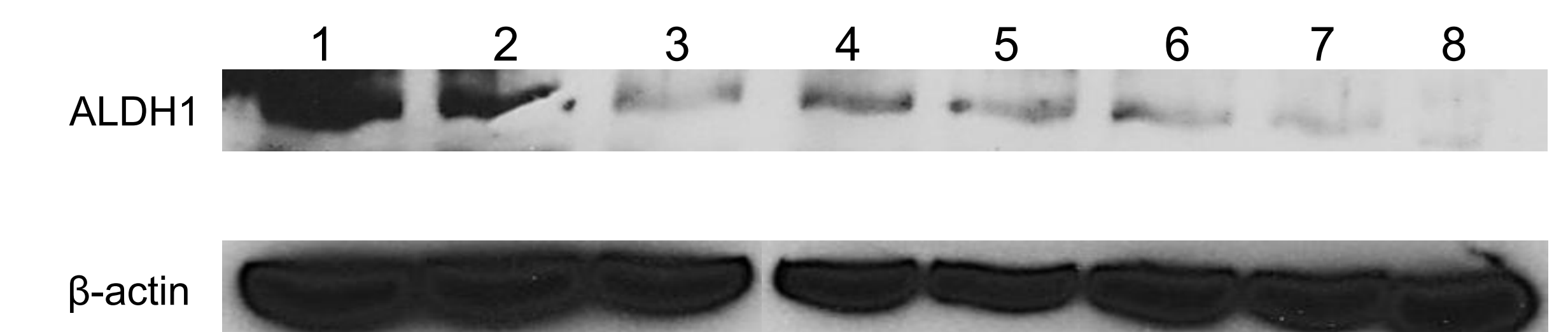
ALDH<sup>-</sup> and ALDH<sup>+</sup> cells that were sorted from FACS analysis were plated on ultra low attachment plates with stem cell media. Pictures shown taken after 1 week and 2 weeks of growth. ALDH<sup>+</sup> cells are able to form spheres while ALDH<sup>-</sup> cells are unable to form spheres.

Figure 2: In Vivo Western Blot Analysis



Lane 1: Control. Lane 2: WFA 2mg/kg body weight. Lane 3: CIS 6mg/kg bodyweight. Lane 4: (WFA 2mg + CIS 6mg)/kg body weight. Analysis of tumor for ALDH1 expression. Ovarian tumor tissue was used for protein extraction for the western blot. WFA down regulates ALDH1 and cisplatin up regulates ALDH1. The combination of WFA + CIS down regulates ALDH1.

Figure 4: In Vitro Western Blot Analysis of A2780 Cells



Lane 1: Control. Lane 2: WFA 0.5μM. Lane 3: WFA 1.5μM. Lane 4: CIS 20μM. Lane 5: CIS 50μM. Lane 6: WFA 0.5μM + CIS 20μM. Lane 7: WFA 1.5μM + CIS 20μM. Lane 8: WFA 1.5μM + CIS 50μM. In vitro analysis of ALDH1 using cell cultures following a 48 treatment. ALDH1 protein is down regulated with increasing WFA concentrations, slightly down regulated with increasing CIS concentrations and WFA + CIS acts synergistically to down regulate expression.

## Conclusions

- ALDH1 is an important biomarker for ovarian cancer stem cells
- Only cancer stem cells with high ALDH activity are able to form spheres on ultra low attachment plates in stem cell media.
- Cisplatin increases ALDH1 levels
- Withaferin A decreases ALDH1 levels
- Combination therapy of CIS + WFA decreases ALDH1 synergistically
- Further studies need to be performed on the roles of signaling pathway molecules with ALDH1 (Notch 1, HES1, HEY1, Nf-κB) as well as generation of tumor in mice by injecting ALDH1<sup>+</sup> cells into SCID mice and subsequent treatment with cisplatin, withaferin A or in combination.

## Acknowledgements

Research supported by the NIH/NCI R25-CA-134283 grant and the University of Louisville Cancer Education Program

## References

1. Fong M.Y., Jin S.Y., Rane M., Singh R.K., Gupta R., Kakar S.S. Withaferin A synergizes the therapeutic effect of doxorubicin through ROS-mediated autophagy in ovarian cancer. *PLoS One*. 2012;7:1-16.
2. Gimester C, Hur M.H, Charafé-Jauffret E, Morville F, Dutcher J, Brown M, Jacquemier J, Viens P, Kleer CG, Liu S, Schott A, Hayes D, Birnbaum D, Wicha MS, Dontu G. ALDH1 is a marker of normal and malignant human mammary stem cells and a predictor of poor clinical outcome. *Cell Stem Cell*. 2007;1:555-567.
3. Kakar, S.S., V.R. Jala, and M.Y. Fong. 2012. Synergistic cytotoxic action of cisplatin and withaferin A on ovarian cancer cell lines. *Biochemical and Biophysical Research Communications* 423: 819-825.



# A Proposed Treatment Algorithm for Stage III Pancreatic Adenocarcinoma

Thomas Brenzel, Robert CG Martin II, MD, PhD

Department of Surgery, Division of Surgical Oncology, University of Louisville, Louisville, KY



## Introduction

Pancreatic adenocarcinoma has seen new advancements in therapy in recent years, but the 5 year overall survival remains at 5%. About 50,000 cases of pancreatic adenocarcinoma are diagnosed each year in the United States. Of these cases, 30% present as locally advanced, stage III. The management of stage 3 pancreatic adenocarcinoma remains a challenge in oncology. Balancing quality of life management with active and effective therapies remains the key goals in optimal care. Currently there are no well established guidelines for optimal staging and treatment in locally advanced pancreatic cancer. The current NCCN guidelines include SIX different chemotherapeutic strategies with significant variability of active agents ranging from FOLFIRINOX based chemotherapy to just 5FU alone (<http://www.nccn.org/patients/guidelines/pancreatic/files/assets/basic-html/page66.html>). This significant variability in chemotherapy and the lack of concised guidelines has lead to wide spread therapies based on historical and in some instances nihilistic bias's.

## Hypothesis and Aims

Hypothesis:

- There is currently no standardized treatment or staging algorithm for unresectable locally advanced pancreatic adenocarcinoma.

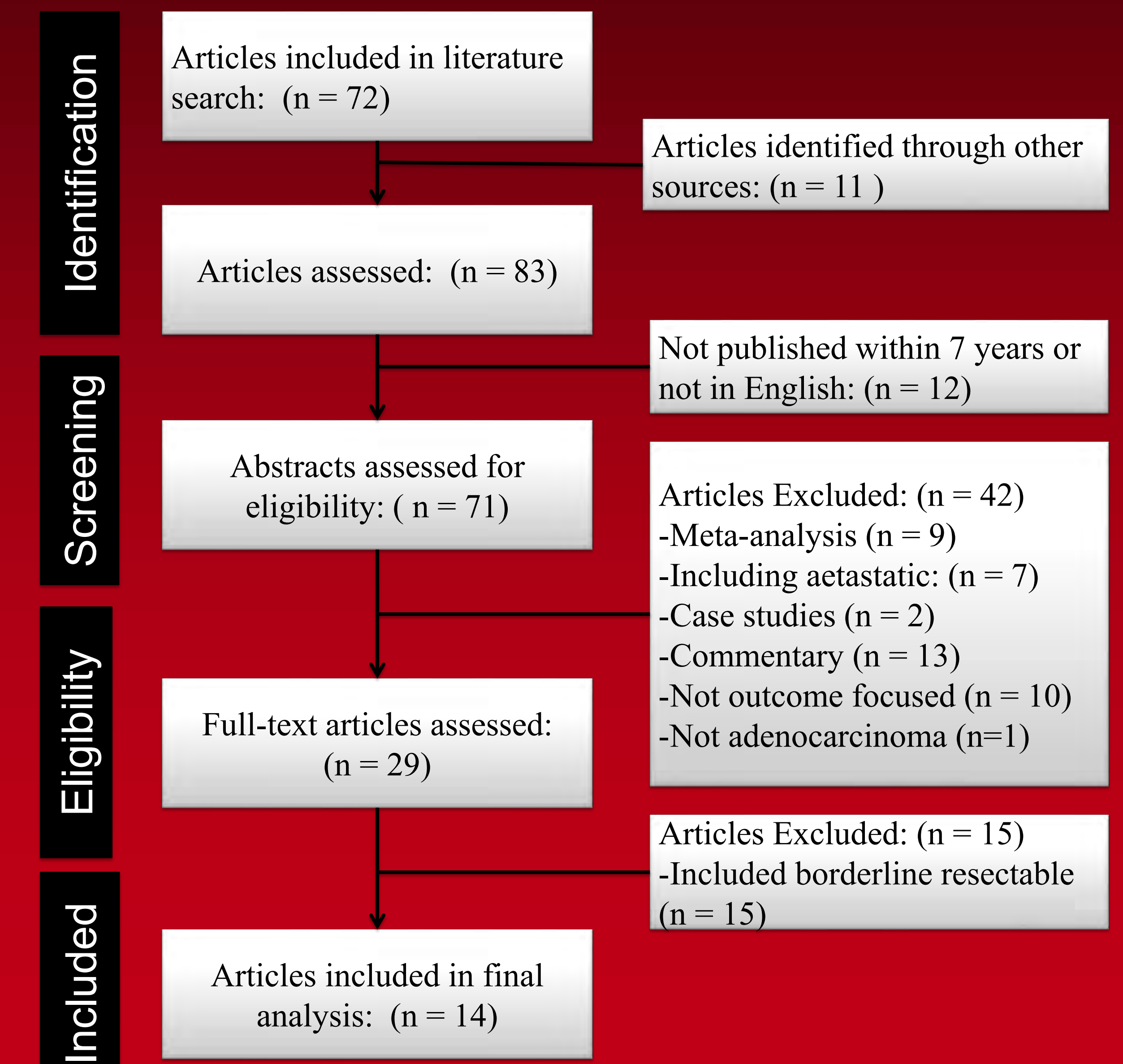
Aims:

- Evaluate current reported strategies in the care and treatment of locally advanced unresectable pancreatic adenocarcinoma.
- Propose and establish an acceptable treatment strategy to optimize diagnosis and treatment outcomes.

## Methods

- A literature review was conducted using the PubMed, EmBase, and Library of Congress Database for articles with the title containing, "Pancreatic Cancer" Locally Advanced", "Stage 3 Pancreatic Cancer", "Locally Advanced Pancreatic Adenocarcinoma".
- For the purpose of this analysis articles were excluded if:
  - they were not published in the last 7 years or not published in English.
  - Abstracts of the remaining articles were assessed and case studies, previous meta-analysis articles, and articles not treatment or outcome focused were removed.
- The selection process is demonstrated in Figure 1. Fourteen Articles met the criteria and were then summarized in Table 1.

Figure 1: Article Selection Flow Chart



## Results

Table 1: Analysis Articles

| Study (Year)              | # Patients | Treatment  | Level of Evidence | Chemo type  | Radiation     | Toxicity Grade 3/4 | Morbidity                          | Mortality       | Resected % | R0 %       | PFS med.   | Med. OS  |
|---------------------------|------------|--|-------------------|---|---------------|--------------------|------------------------------------|-----------------|------------|------------|--|--|
| Baumgartner et al. (2012) | 11         | Neoadjuvant Chemoradiotherapy before resection   | 2b                | Gem Based. But + other in 45%                             | 72% received  | NR                 | 45% post-op, n=5                   | 18%, n=2        | 100%       | 91% n=10   | 5.25 m   | 26 m (31 from Diagnosis)                                 |
| Cantore et al. (2012)     | 107        | Primary RFA + adjuv<br>Secondary RFA + adjuv   | 2a                | Gem-Cis or Gem-Epirubicin                                 | 54.0-59.4 Gyn | NR                 | Overall: 28% n=30 RFA / 8.4% Surg. | 1.9% in 30 days | N/A        | N/A        | NR   | 14.7 m<br>25.6m  |
| Chauffert et al. (2008)   | 119        | Chemo Alone vs. CRT + maintenance Chemo  | 1                 | Gemcitabine   | n/a           | 40%                | NR                                 | 0%              | 5% (n=3)   | NR         | NR   | 13.0 m<br>8.6 m  |
| Faisal et al. (2013)      | 100        | Only Chemo (n=18)<br>CRT alone (n=10)<br>CRT followed by Chemo (n=25)<br>Induction Chemo followed by CRT: (n= 44) 0 to 2 Cycles (n=36) >2 Cycles (n= 18) | 2b                | Various Standard dose Chemo used for all Chemo treatments | 0             | NR                 | NR                                 | NR              | NR         | NR         | 4.5 m<br>2.2 m<br>8.4 m<br>12.6 m<br>8.2 m<br>15.0 m | 15.9 m<br>11.1 m<br>11.0 m<br>18.1 m<br>15.7 m<br>19.4 m |
| Faris et al. (2013)       | 22         | Induction Chemo followed by CRT  | 2a                | Folfirinnox   | 50.4 Gy       | 32%                | NR                                 | 0%              | 23% (n=5)  | 100% (n=5) | 11.7   | NR   |
| Haddock et al. (2007)     | 48         | Chemo Rad (Gem-Cis) + Adj. Gem   | 2a                | Gem-Cis during RT followed by Adj. Gem                    | 50.4 Gy       | 92% (n=44)         | NR                                 | 2.1% (n=1)      | NR         | NR         | 7.3 m  | 10.3 m   |
| Hazard et al. (2012)      | 62         | Chemo-Rad Comparison   | 2a                | CapOx + RT (n=13)<br>5FU + RT (n=20)<br>Gem + RT (n=30)   | 45 Gy         | 15.4%              | NR                                 | 0%              | 8%         | NR         | NR   | 11 m<br>13 m<br>12 m                                     |

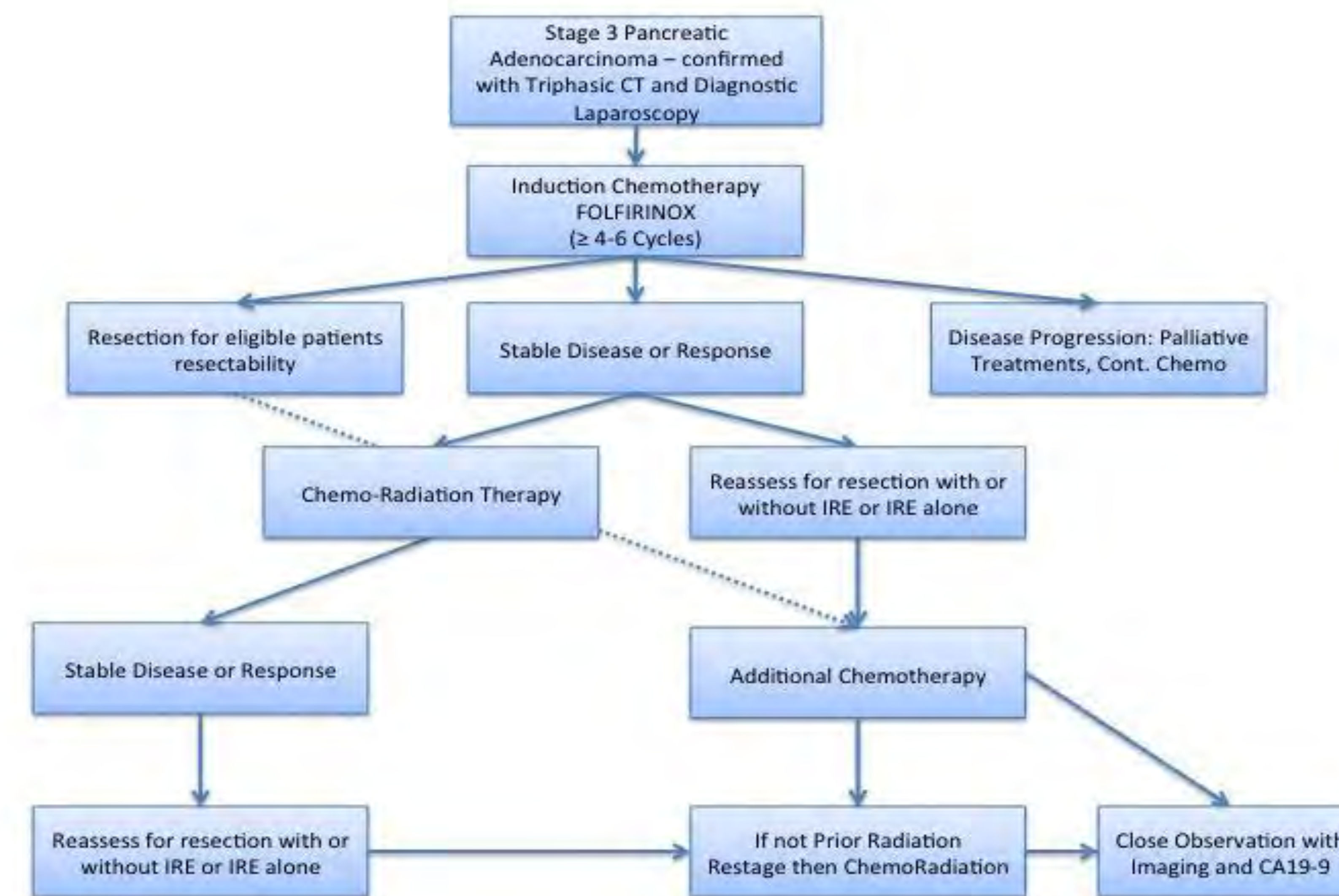
- Currently, there is no well-defined and established treatment algorithm for stage III pancreatic cancer. In the last 7 years patients have been treated by chemotherapy alone, chemo-radiotherapy (CRT), induction chemo followed by CRT, or CRT followed by chemo. Other patients received irreversible electroporation (IRE) or ablation.
- Only a limited number (n = 3) of randomized control trials were found for specifically stage 3 PDAC.
- Patients who become eligible for surgical resection have the greatest survival benefit.
- Gemcitabine was the most common chemo agent used. Only 9 of the 14 articles define extensively the chemotherapy agents used, the dosages, and durations.
- New combinations of chemotherapy drugs are being studied for patients with stage 3 PDAC. Notably FOLFIRINOX, which is 5-fluorouracil [5-FU], oxaliplatin, irinotecan, and leucovorin.
- The most frequent dose of radiation given in patients with chemo-radiation therapy was 50.4 Gy. These articles show a consensus of recommending between 50-60 Gy.
- Treatment with CRT has higher toxicity than chemo alone
- CRT has no clear survival advantage over chemo alone.
- Chemo followed by CRT reported the highest OS.
- The single article reporting on FOLFIRINOX showed an improved progression free survival but did not calculate OS

| Study (Year)          | # Patients | Treatment   | Level of Evidence | Chemo type                                    | Radiation       | Toxicity Grade 3/4    | Morbidity         | Mortality           | Resected % | R0 %      | PFS med.                   | Med. OS                        |
|-----------------------|------------|---|-------------------|---|-----------------|-----------------------|-------------------|---------------------|------------|-----------|----------------------------|--------------------------------|
| Herman et al.         | 304        | SOC<br>SOC + TNFerade                                   | 1                 | Varied, NR for either arm                     | NR              | 65.6%                 | 9.6%              | NR                  | 11% (n=10) | 78%       | 7.0                        | 10.0                           |
| Huguet et al. (2007)  | 181        | Chemo(3m) then PD<br>Chemo, No 3 m PD<br>Chemo then CRT | 2b                | Varied combination Chemo Drugs                | 55 Gy           | NR                    | NR                | NR                  | NR         | NR        | 2.0<br>7.4<br>10.8         | 4.5 m<br>11.7 m<br>15.0 m      |
| Loehrer et al. (2011) | 74         | Chemo (n = 37)<br>v. Chemo-Rad (n=34)                   | 1                 | Gemcitabine<br>Gemcitabine                    | None<br>50.4 Gy | 77%<br>79%            | NR                | 2.7%<br>2.9%        | NR         | NR        | 6.7 m<br>6.0 m             | 9.2 m<br>11.1m                 |
| Mamon et al. (2011)   | 78         | Chemo-Rad   | 2b                | Gemcitabine + 5-FU + RT                       | 50.4 Gy         | 71%                   | NR                | 2% (n=2)            | NR         | NR        | 10 m                       | 12.2 m                         |
| Martin et al. (2012)  | 27         | Surgical IRE  | 2b                | Varied, (85%) had previous chemo or chemo-rad | Varied;         | N/A                   | 33% (n=9)         | 3.7% (n=1, 90 day)  | 8          | NR        | NR                         | NR                             |
| Maximos et al. (2009) | 25         | Pre-op Chemo-Rad  | 2b                | Gemcitabine                                   | 54 Gy           | NR                    | Post-Op 25% (n=2) | Post-Op 12.5% (n=1) | n = 8      | NR        | NR                         | 12 m resected; 8 m un resected |
| Reni et al. (2009)    | 91         | Chemo followed by Chemo-Rad                             | 2a                | PEFG<br>PEFG<br>PEFG<br>PDMG                  | 50-60 Gy        | High<br>Low<br>Lowest | NR                | NR                  | n = 13     | 69% (n=9) | 10.4<br>10.5<br>7.7<br>7.8 | 14.1<br>16.2<br>12.7<br>16.8   |

Table 1 Legend:

NR = not reported; N/A = Not Applicable; Os = Overall survival; PFS = Progression Free survival; RFA = Radio-Frequency Ablation; Gem. = Gemcitabine; IRE = Irreversible Electroporation; PEFG = (cisplatin, epirubicin, 5-Xuorouracil, gemcitabine); PEXG = cisplatin, epirubicin, capecitabine, gemcitabine; PDXG = cisplatin, docetaxel, capecitabine, gemcitabine; SOC = Standard of Care; TNF = Tumor Necrosis Factor Alpha; PD = Progressive Disease

## Proposed Treatment Algorithm



## Discussion

- No established or well-defined treatment algorithm was found for Stage III (locally advanced unresectable) pancreatic cancer. Stage III should be treated uniquely from stage II or stage IV by the proposed algorithm.
- Pancreatic adenocarcinoma should be staged with a triphasic CT scan and diagnostic laparoscopy.
- CRT should be the second-line treatment in patients that have stable disease or response following 4-6 cycles of induction chemotherapy.
- Patients with progressive disease should be treated with chemotherapy
- FOLFIRINOX is the recommended first line chemo combination. Reports have demonstrated improved survival in metastatic patients

## Acknowledgements

National Cancer Institute 5R25CA134283-03 – Cancer Education Program Grant

## ABSTRACT

**Background.** Vinyl chloride (VC) is a ubiquitous environmental contaminant and ranks 4<sup>th</sup> on the ATSDR Hazardous Substances Priority List. It has been shown to cause liver cancer and other hepatic dysfunctions. We have previously reported increased hepatocellular necrosis in a highly exposed occupational cohort and *in vitro* models. The purpose of this study is to investigate hepatic injury *in vivo* and its mechanisms including the role of endoplasmic reticulum (ER) stress *in vitro*. **Methods.** Chow-fed C57BL/6J mice received chloroethanol (ClEtOH), a major metabolite of VC, and lipopolysaccharide (LPS) after ClEtOH. High fat diet (HFD)-fed mice received a bolus dose of ClEtOH after 10 weeks, 24 hours prior to sacrifice. Samples were harvested for determination of liver damage, inflammation, ER stress and changes in carbohydrate and lipid metabolism. Apoptosis and necrosis biomarkers were measured in human serum. *In vitro*, HepG2 cells were treated with varying concentrations of chloroacetaldehyde (CLA), a metabolite of VC. RNA was extracted for analysis of markers of ER stress (*Atf3*, *Atf4*, *Hsp90b1*, and *Chop*). **Results.** In chow-fed mice, ClEtOH alone caused no detectable liver damage but caused changes in carbohydrate and lipid regulating genes. LPS exposure caused oxidative stress, lipid accumulation and inflammation, which was exacerbated by ClEtOH preexposure. ClEtOH increased activation of recruited and resident monocytes as well as neutrophils and was coupled with an increase in transaminases over LPS alone, an increase in necroinflammatory foci and an increase in free fatty acids. The combination of ClEtOH and LPS decreased TUNEL-positive cells, suggesting a switch to necrotic cell death. In HFD-fed mice, ClEtOH caused an increase in HFD-induced liver damage, steatosis, hepatocyte ballooning, infiltrating inflammatory cells, hepatic expression of proinflammatory cytokines and genes involved in the ER stress response. *In vitro*, CLA decreased oxygen consumption, depleted ATP levels and decreased mitochondrial membrane integrity. **Conclusions.** Taken together, VC and its metabolites sensitize the liver to a "second hit." This serves as proof-of-concept that VC hepatotoxicity may be modified by underlying liver diseases, which commonly occurs in diet-induced obesity and NAFLD. These data implicate VC exposure as a risk factor in the development of liver disease in susceptible populations. (supported, in part, by a grant from NIDDK and NIH/NCI R25-CA134283)

## BACKGROUND

Over 33% of US adults are obese (BMI ≥ 30) with another 34.2% being overweight (BMI ≥ 25).<sup>1</sup> One of the major health effects of obesity is non-alcoholic fatty liver disease (NAFLD). Indeed, the burden of liver disease has increased in the US in parallel with the obesity epidemic.<sup>2</sup> However, it is assumed that there are other contributing factors (e.g., environmental factors) that determine overall risk for developing the disease. Vinyl chloride is found in significant concentrations in the ambient air and the ground water surrounding manufacturing complexes. Therefore, exposure to VC is widespread in industrialized nations. Historically VC-exposure has been associated with hemangiosarcoma, HCC and fibrosis. The Louisville industrial area ('Rubbertown') is a well documented site for VC-induced liver diseases.<sup>3</sup> What is unknown is what low level (sub-NOAEL) exposure will do to the risk of underlying liver diseases. While it is clear that high doses of VC are directly hepatotoxic to humans, the effects of lower doses of VC and its interactions with overnutrition on overall liver health have not been determined. The risk for developing fatty liver disease is not based solely on one factor, but rather is modified by other mitigating conditions, such as genetic (e.g., polymorphisms in key genes) or environmental (e.g., diet, lifestyle, etc) factors. Numerous studies have now established that physiological/biochemical changes to liver that are pathologically inert can become hepatotoxic in response to a second agent. This '2-hit' paradigm has been best exemplified in non-alcoholic fatty liver diseases.<sup>4</sup> We propose that low-dose VC may also serve as a second hit. The metabolism of VC is similar to that of ethanol, which also causes fatty liver disease. VC is metabolized via an CYP2E1 and aldehyde dehydrogenase dependent pathway. Indeed, a key pathologic characteristic of VC-induced TASH in humans is steatohepatitis analogous to ASH or NASH. VC-metabolites may therefore be important mediators of VC-enhanced NAFLD. Recent work has suggested that the development of 'classical liver diseases' (e.g., ASH and NASH) involve endoplasmic reticulum (ER) stress. ER stress is induced when homeostasis of synthesis, folding, and secretion of proteins is disrupted.<sup>5</sup> It is not known if TASH i.e., exposure to VC and its metabolites induces ER stress.

## MATERIALS AND METHODS

**Animals and treatments.** Eight week old male C57BL/6J mice were obtained from Jackson Laboratory (Bar Harbor, ME). Animals were administered chloroethanol (50 mg/kg i.g.) and/or LPS (10mg/kg i.p.) 24 hours later. They were anesthetized with ketamine/xylazine (100/15 mg/kg, i.m.) 0h, 4h and 24h after injection of LPS. Animals were sacrificed and blood and tissue were collected for further analyses. **Cell culture and treatments.** HepG2 cells from ATCC (Manassas, VA) were exposed to (20 μM, 50 μM, 80 μM, and 100 μM of chloroacetaldehyde) and (60 μM) acrolein. Cells were plated at 200,000 cells per well for 12-well plate. RNA was extracted after 6 hours. **Biochemical analyses and histology.** Plasma levels of ALT, AST were determined using standard kits (ThermoTrace, Melbourne, Australia). Paraffin-embedded sections of liver were stained with hematoxylin & eosin (H&E) to assess overall hepatic structure, and Periodic acid-Schiff reagent (PAS) to detect glycogen. Neutrophil accumulation in the livers was assessed by staining tissue sections for chloroacetate esterase (CAE), a specific marker for neutrophils, using the naphthol AS-D chloroacetate esterase kit (Sigma, St. Louis MO). Frozen sections of liver were stained with Oil Red O to detect neutral lipids, and counterstained with hematoxylin. **RNA isolation and real-time RT-PCR.** Total RNA was extracted from liver tissue samples by a guanidium thiocyanate-base method (RNA STAT 60 Tel-Test). 1 μg total RNA per sample was reverse transcribed. PCR was performed using the ABI StepOne Plus. The comparative C<sub>T</sub> method was used to determine fold differences between samples. **Oxygen Consumption assays:** Cells were plated in a XF24 cell culture plate (15,000 cells per well) and allowed to recover o.n. Media was changed to unbuffered DMEM and the oxygen consumption measured using a Seahorse XF24 Extracellular Flux analyzer. **ATP determination:** ATP was determined in cell lysates using a kit from Sigma-Aldrich. **Cellomics HCS.** After the predetermined incubation period with 4-HNE, the media was removed and media containing: Hoechst (nuclear fluorescence), TMRM (mitochondrial membrane potential), Fluo-4 (free calcium), and TOTO-3 (cell membrane permeability) dyes were added to the wells. Following a 1h incubation with the dyes, the plate was placed into the Cellomics Array Scan VTI HCS reader. Cellomics Array Scan 60 software (7.6.2.1-1.00x) was used for determining the intensity of the dyes listed above. Well averages, as well as individual cell data were recorded and analyzed. **Statistics.** Summary data represent means ± SEM (n = 4-6). ANOVA with Bonferroni's post-hoc test or the Mann-Whitney rank sum test was used for the determination of statistical significance among treatment groups, as appropriate. <sup>a</sup>, p < 0.05 compared to vehicle; <sup>b</sup>, p < 0.05 compared to animals exposed LPS alone.

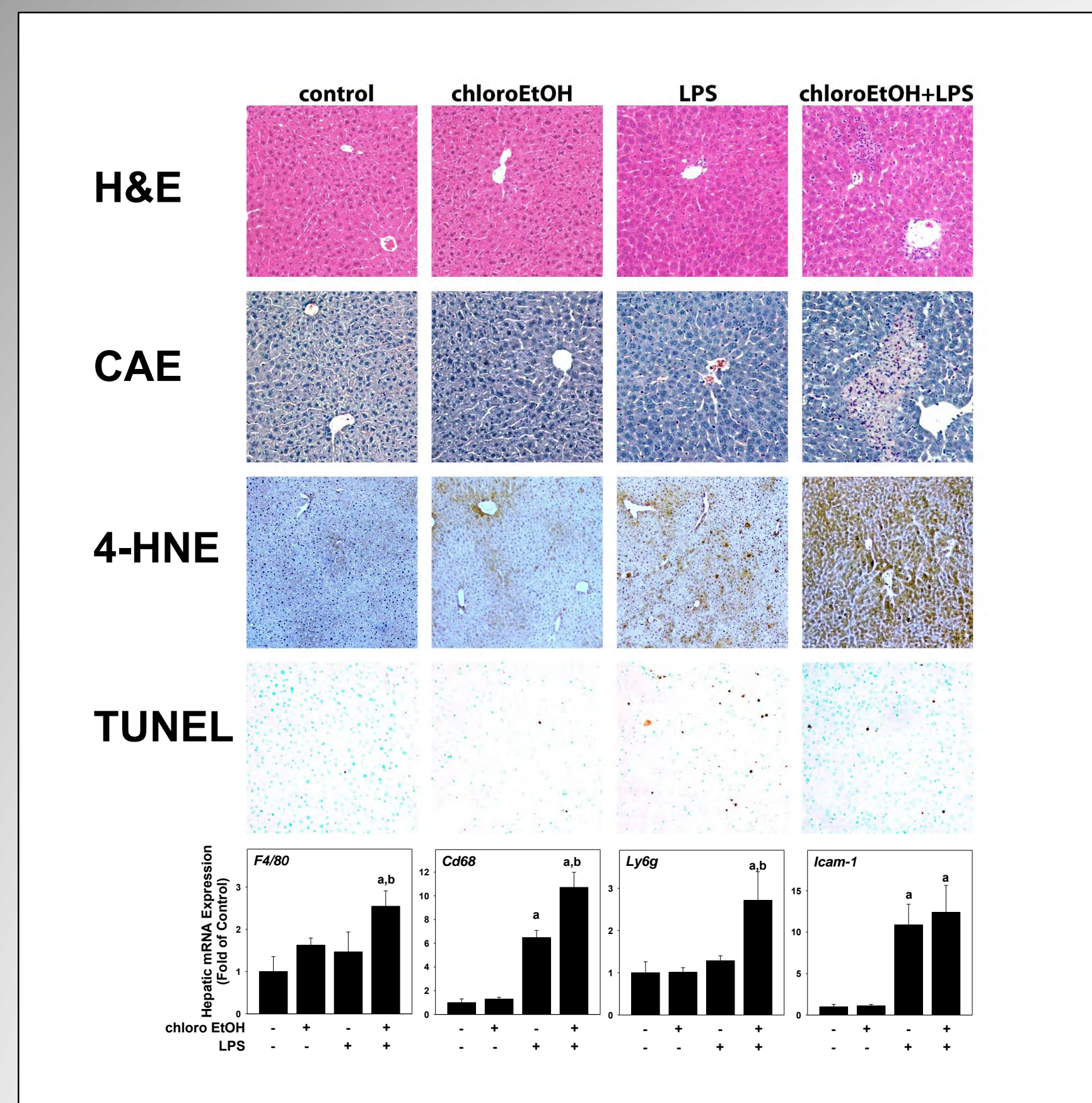


**Figure 1: Effects of chloroEtOH and LPS on liver health and inflammation.** Mice were treated as described in *Materials and Methods*. Representative photomicrographs of hematoxylin & eosin (H&E), chloroacetate esterase (CAE) and TUNEL stains are shown. Real-Time RT-PCR was performed as described in *Materials and Methods*.

There were no gross morphologic changes in the untreated or chloroEtOH groups. LPS induced inflammation, necrosis and apoptosis. ChloroEtOH increased the number of LPS-induced necroinflammatory foci and the number of neutrophils. However, chloroEtOH blunted the number of TUNEL positive cells, suggesting a necrotic cell death rather than apoptotic. Hepatic gene expression levels of macrophage marker *F4/80*, monocyte marker *Ccl68* and neutrophil marker *Ly6g* were significantly increased in the chloroEtOH + LPS group. Whereas the expression of intercellular adhesion molecule 1 *Icam-1* was increased with LPS, chloroEtOH did not alter this effect at the 24 h timepoint.

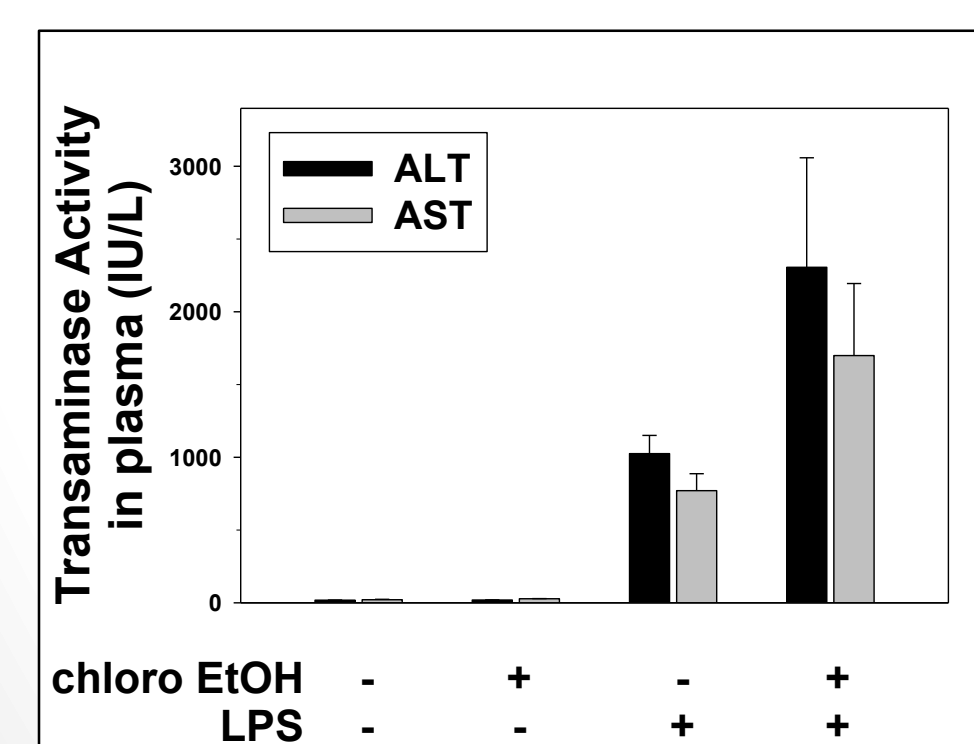


**Figure 2: Effect of chloroEtOH and LPS on plasma transaminases.** Mice were treated as described in *Materials and Methods*. Alanine aminotransferase (ALT) and aspartate aminotransferase (AST) were determined in plasma samples collected 24 hours after injection of LPS.

Whereas having no effect in absence of LPS, chloroEtOH strongly increased plasma levels of indices of liver damage (AST, ALT) 24 hours after LPS.

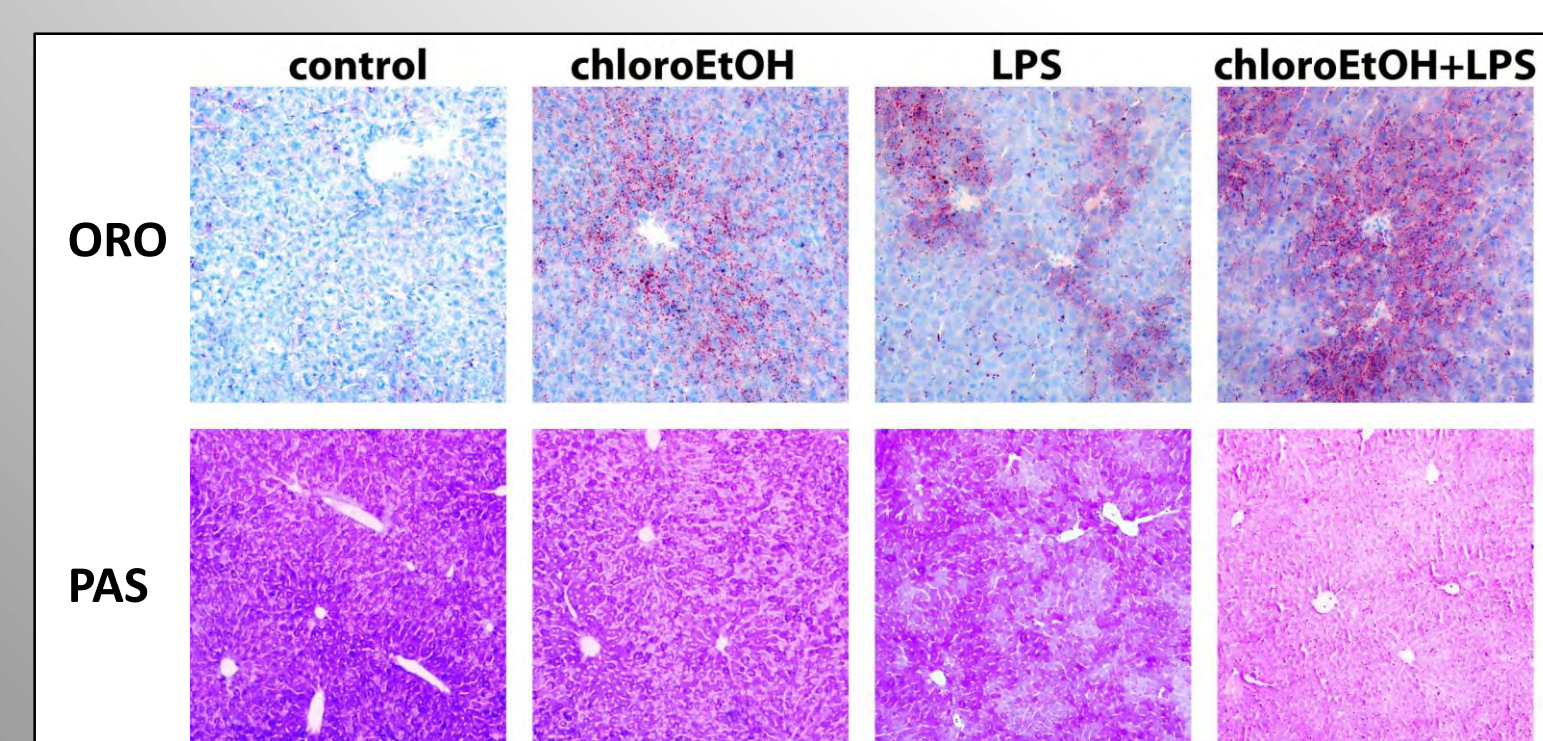


**Figure 3: Effect of chloroEtOH and LPS hepatic lipids and glycogen.** Mice were treated as described in *Materials and Methods*. Representative photomicrographs of Oil Red O-staining (ORO) and Periodic acid-Schiff stain (PAS) for glycogen at the 4 h time point are shown.

ChloroEtOH significantly enhanced LPS-induced steatosis as shown by ORO. Accordingly chloroEtOH significantly enhanced the increase in NEFAs caused by LPS (LPS: 1.2378±0.0281; chloroEtOH+LPS: 1.3687±0.0803 nmol/mg wet weight. Whereas chloroEtOH slightly and LPS dramatically depleted unfasted glycogen reserves in liver, their combined effect is blunted.

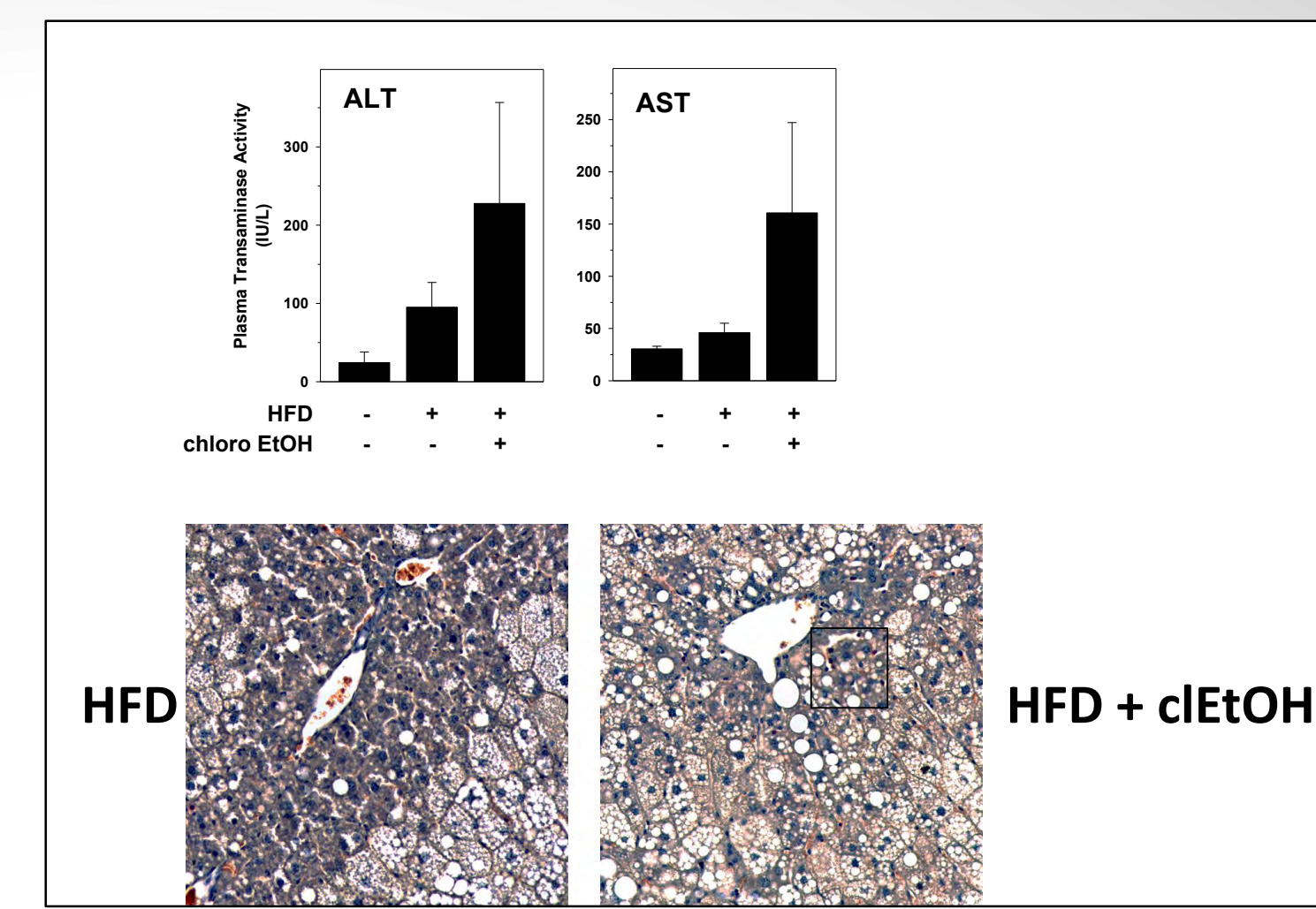


**Figure 4: Effects of HFD and chloroEtOH on liver health and inflammation.** Mice were treated as described in *Materials and Methods*. Representative photomicrographs of chloroacetate esterase (CAE) stains are shown. Alanine aminotransferase (ALT) and aspartate aminotransferase (AST) were determined in plasma samples collected 24 hours after chloroEtOH.

ChloroEtOH strongly increased plasma levels of indices of liver damage (AST, ALT) and the number of infiltrating neutrophils after chronic HFD feeding.

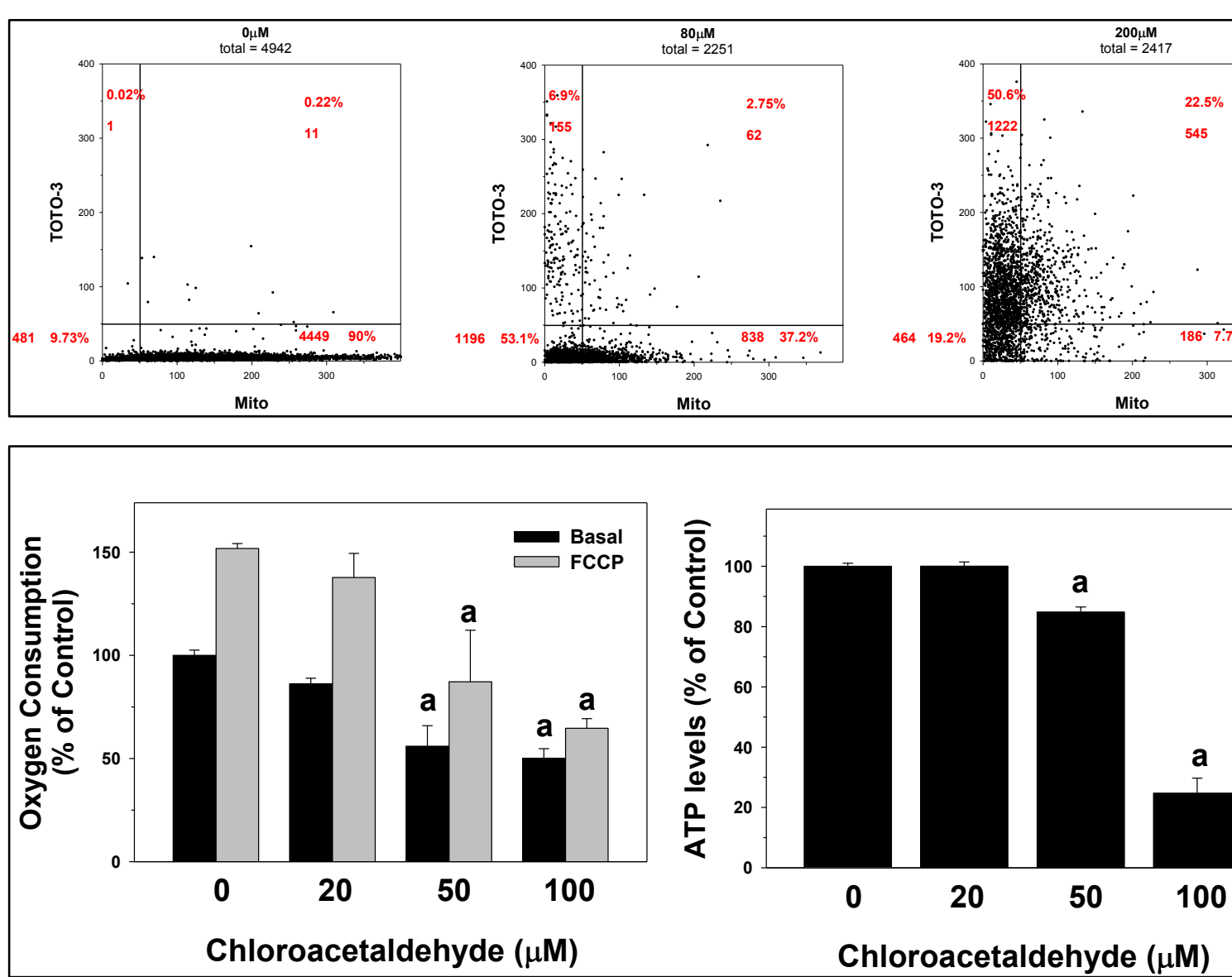


**Figure 5: Chloroacetaldehyde toxicity in HepG2 cells.** HepG2 cells were grown in 96-well plates and incubated with chloroacetaldehyde. Nuclear area (Hoechst fluorescence), mitochondrial membrane potential (TMRM fluorescence), cell membrane permeability (TOTO-3) were determined using the Cellomics HCS. Oxygen consumption rate was measured using a Seahorse. ATP levels were determined using a luminometer.

Chloroacetaldehyde caused cell toxicity as seen in the decreased mitochondrial membrane potential prior to increasing cell permeability. Chloroacetaldehyde also causes a dose dependent decline in oxygen consumption in ATP-linked oxygen consumption. Accordingly, ATP was decreased by up to 75% 100 μM chloroacetaldehyde.

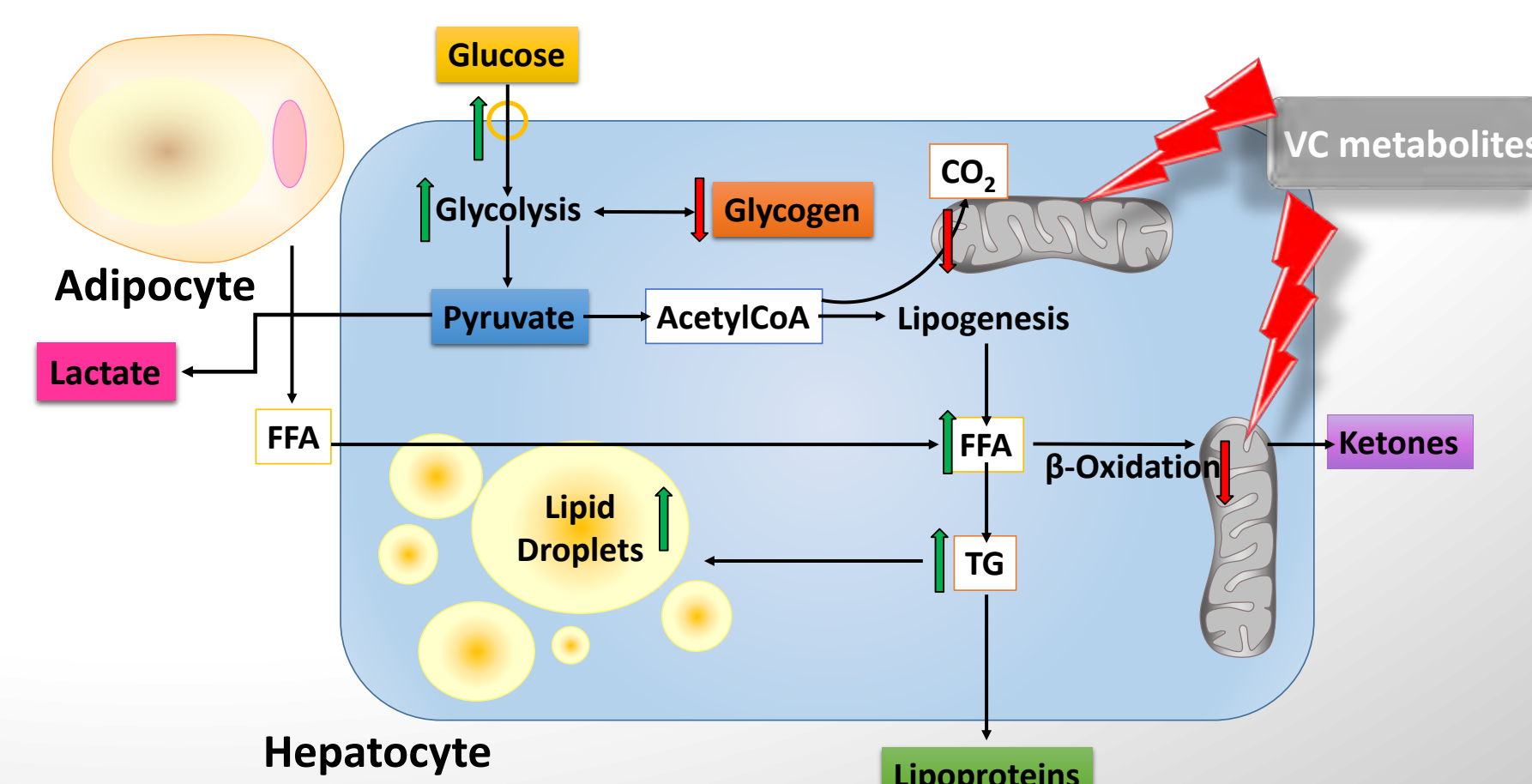


**Figure 6: Working Hypothesis (so far).** VC metabolites cause mitochondrial damage, which impairs oxidative phosphorylation; the cell increases flux through anaerobic glycolysis to compensate for this loss of ATP yield. The increased demand for glucose depletes glycogen stores and the cell becomes 'pseudo-fasted,' this latter state likely increases AMPK activity. Interestingly, mTOR, which is usually regulated in opposition to AMPK, also appears to be activated by VC exposure. This concomitant activation of catabolic (AMPK) and anabolic (mTOR) signals likely explains why acetylCoA is being shunted to lipid synthesis instead of β-oxidation, even under conditions of ATP depletion. The combined metabolic stress of VC exposure likely sensitizes the hepatocyte to oncotic cell death caused by inflammation.

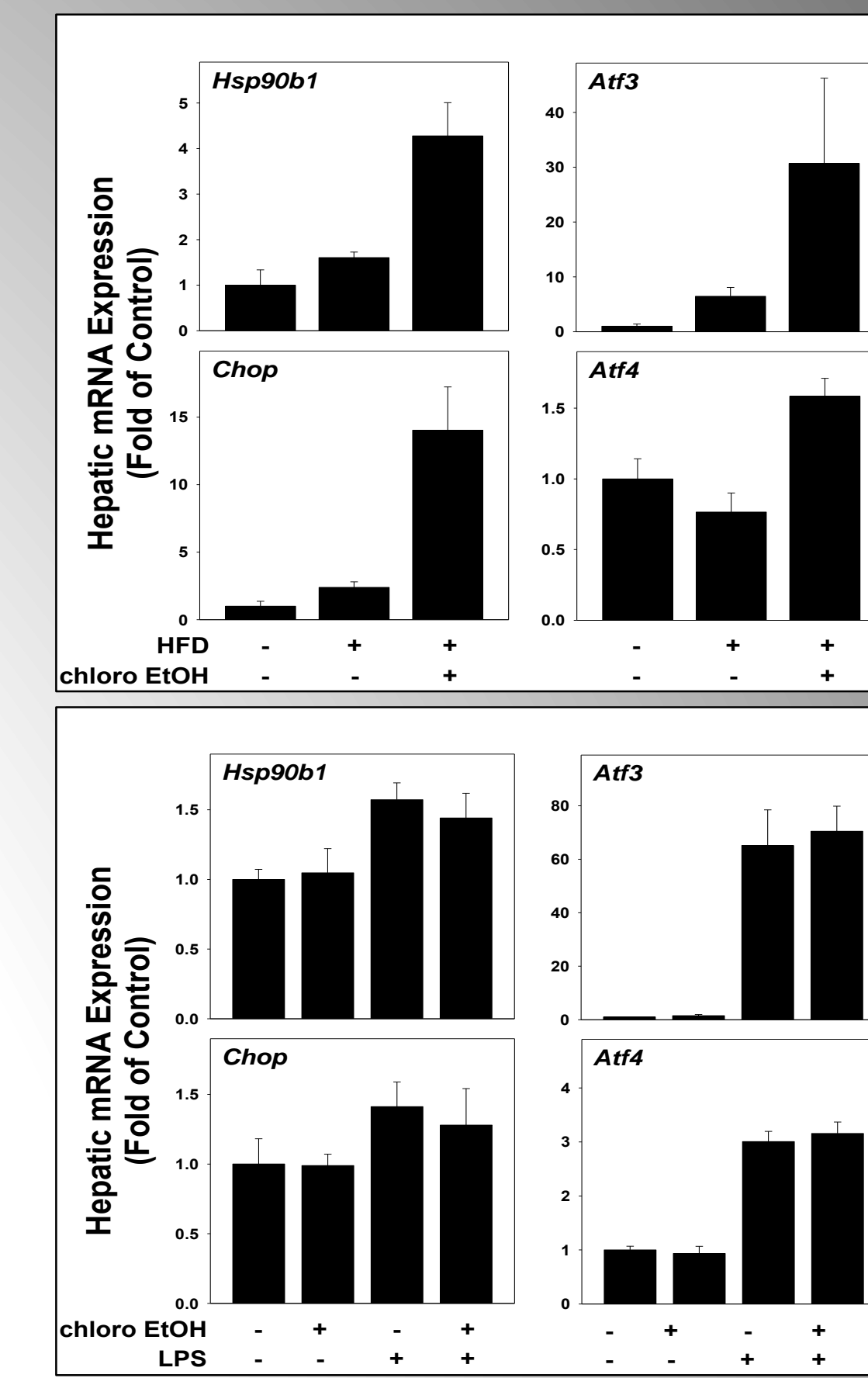


**Figure 7: Effect of chloroEtOH on markers of ER-stress in vivo.** Mice were treated and real-time RT-PCR for ER stress markers *Hsp90b1* (*Grp94*), *Atf3*, *Atf4* and *Chop* was performed as described in *Materials and Methods*.

Whereas HFD-induced hepatic gene expression levels of ER stress markers was significantly increased by chloroEtOH, chloroEtOH didn't alter the expression of these markers after LPS (4 and 24 hours).

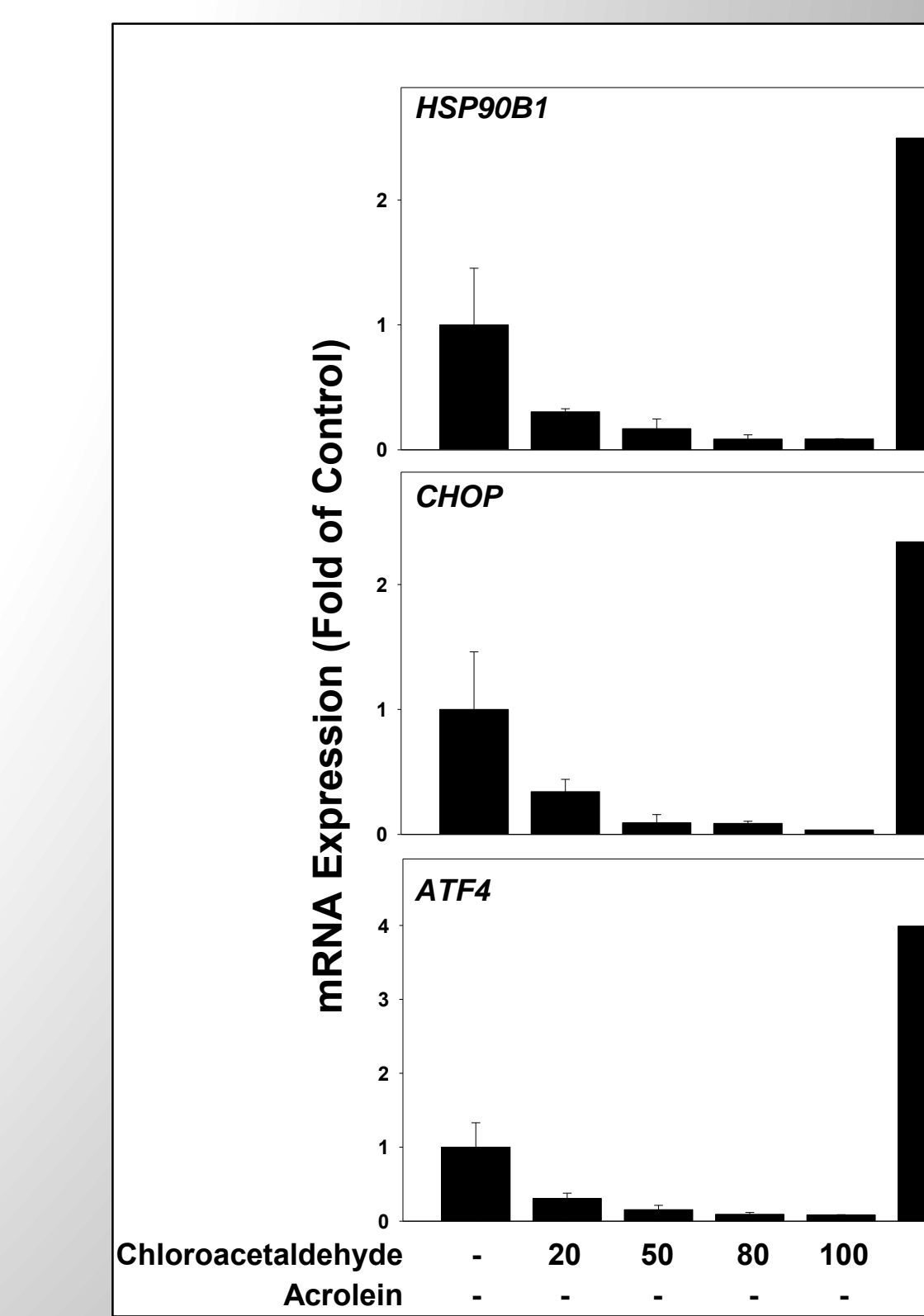


**Figure 8: Markers of ER-stress in Chloroacetaldehyde treated HepG2 cells.** HepG2 cells were grown in 12-well plates and incubated with chloroacetaldehyde (20, 50, 80, and 100 μM) and acrolein (60 μM) for 6 hours.

Chloroacetaldehyde (CLA) did not increase expression of ER stress markers as observed *in vivo*. Acrolein (+ control) induced markers of ER stress, as reported previously.<sup>6</sup>

## FUNDING SUPPORT

This research was supported in part by NCI (R25-CA134283 -AMB), NIDDK (JIB; CJM), NIEHS (MC), NIAAA (CJM), and the Veterans Administration (MC, CJM).

## SUMMARY

### MICE

Vinyl chloride metabolite chloroEtOH:

- 1) sensitizes the liver to necro-inflammation and steatosis.
- 2) increases LPS and HFD-induced inflammation.
- 3) enhances LPS-induced steatosis and NEFA.
- 4) exacerbates depletion of hepatic glycogen reserves.
- 5) causes ER-stress after HFD feeding (chronic) but not after LPS (acute)

### Cell Culture (HepG2)

Vinyl chloride metabolite chloroacetaldehyde:

- 1) decreases mitochondrial membrane potential prior to increasing cell permeability.
- 2) decreases oxygen consumption and depletes ATP levels.
- 3) decreases markers of ER stress response with increasing concentrations.

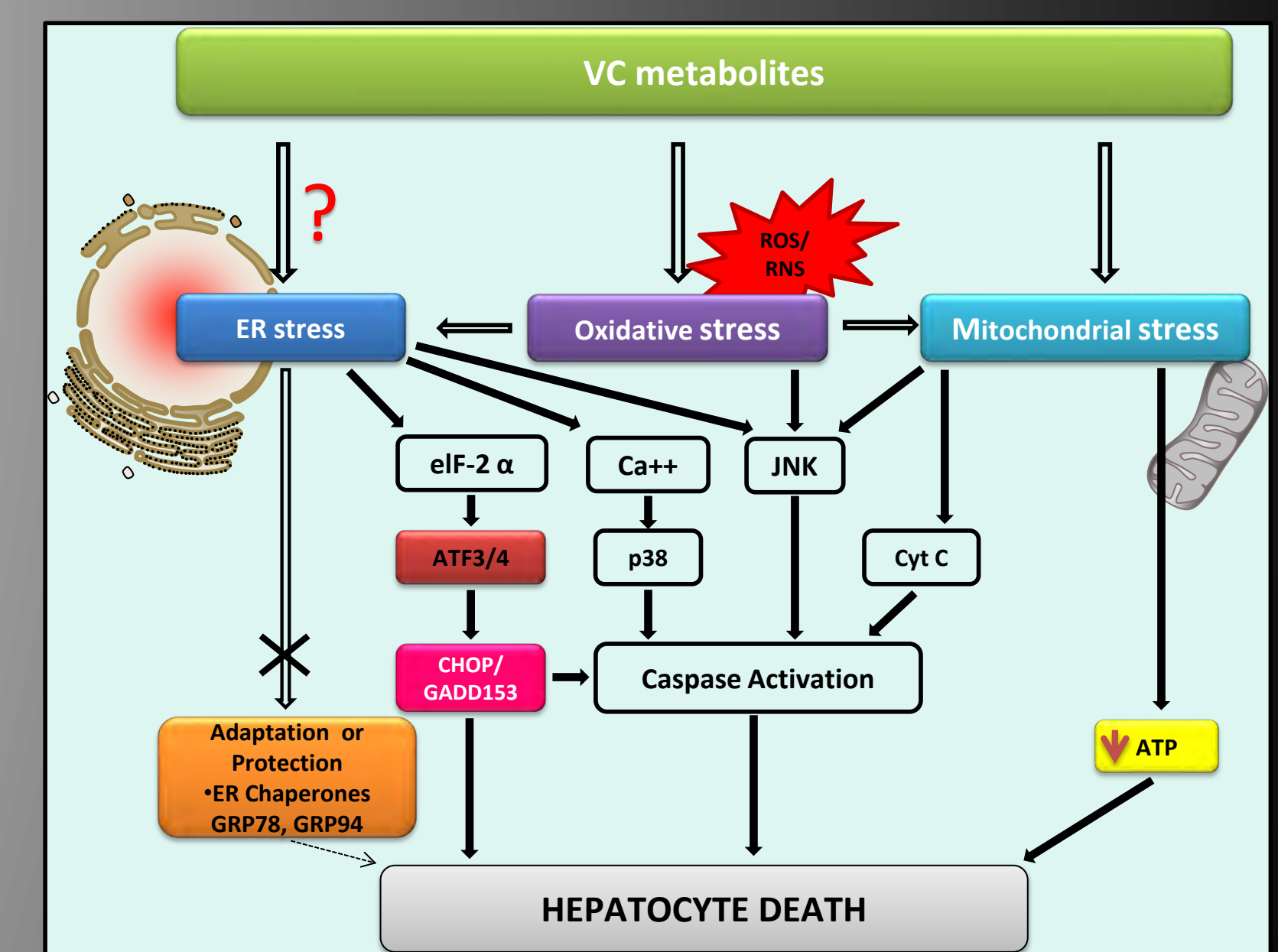


**Figure 9: Working Hypothesis.** VC metabolites cause oxidative stress and mitochondrial damage, which causes ATP depletion and hepatocellular death. VC indeed enhanced ER stress under some conditions; however this effect was unique to fatty liver and was not directly caused by the compound per se, as seen in the acute (LPS) model and in cell culture. These data therefore may explain why fatty livers are more sensitive to VC/metabolite exposure.

## REFERENCES

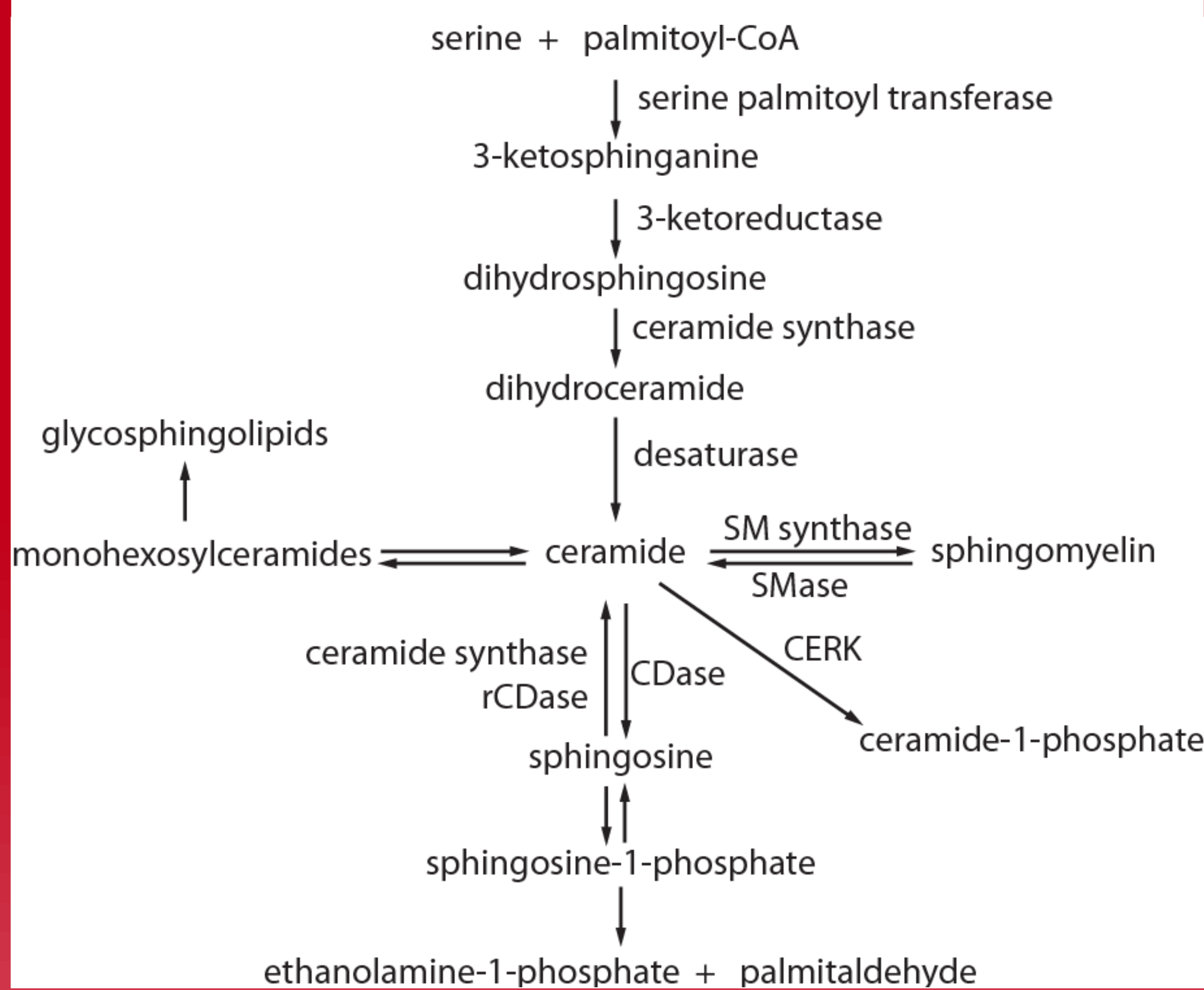
1. Cave M., Deacuciu I., Mendez C., Song Z., Joshi-Barve S., Barve S. & McClain C. Nonalcoholic fatty liver disease: predisposing factors and the role of nutrition. *J. Nutr. Biochem.* 18, 184-195 (2007).
2. Cave M et al., Toxicant associated steatohepatitis in vinyl chloride workers. *Hepatology.* 51:474-81 (2010).
3. Day C.P. & James O.F. Steatohepatitis: a tale of two "hits"? *Gastroenterology.* 114, 842-845 (1998).
4. Flegal K.M., Carroll M.D., Ogden C.L. & Curtin L.R. Prevalence and trends in obesity among US adults, 1999-2008. *JAMA.* 303, 235-241 (2010).
5. Wang X., Wang S., Liu Y., et al. The Hsp90 inhibitor SNX-2112 induces apoptosis of human hepatocellular carcinoma cells: the role of ER stress. *Biochemical and Biophysical Research Communications.* 446, 160-166 (2014).
6. Mohammad MK, Avila D, Zhang J, Barve S, Arteel G, McClain C, Joshi-Barve S. Acrolein cytotoxicity in hepatocytes involves endoplasmic reticulum stress, mitochondrial dysfunction and oxidative stress. *Toxicol Appl Pharmacol.* 265:73-82 (2012).

# Development of a shRNA library for high-throughput screening of the role of sphingolipids in tumorigenesis.

Cameron Conway<sup>1</sup>, Gauri Patwardhan<sup>2,4</sup>, Doug Saforo<sup>2,4</sup>, Levi J. Beverly<sup>2-4</sup>, and Leah J. Siskind<sup>2,4</sup>,  
<sup>1</sup>J. B. Speed School of Engineering, Departments of <sup>2</sup>Pharmacology and Toxicology and <sup>3</sup>Medicine,  
<sup>4</sup>James Graham Brown Cancer Center, University of Louisville, Louisville, KY

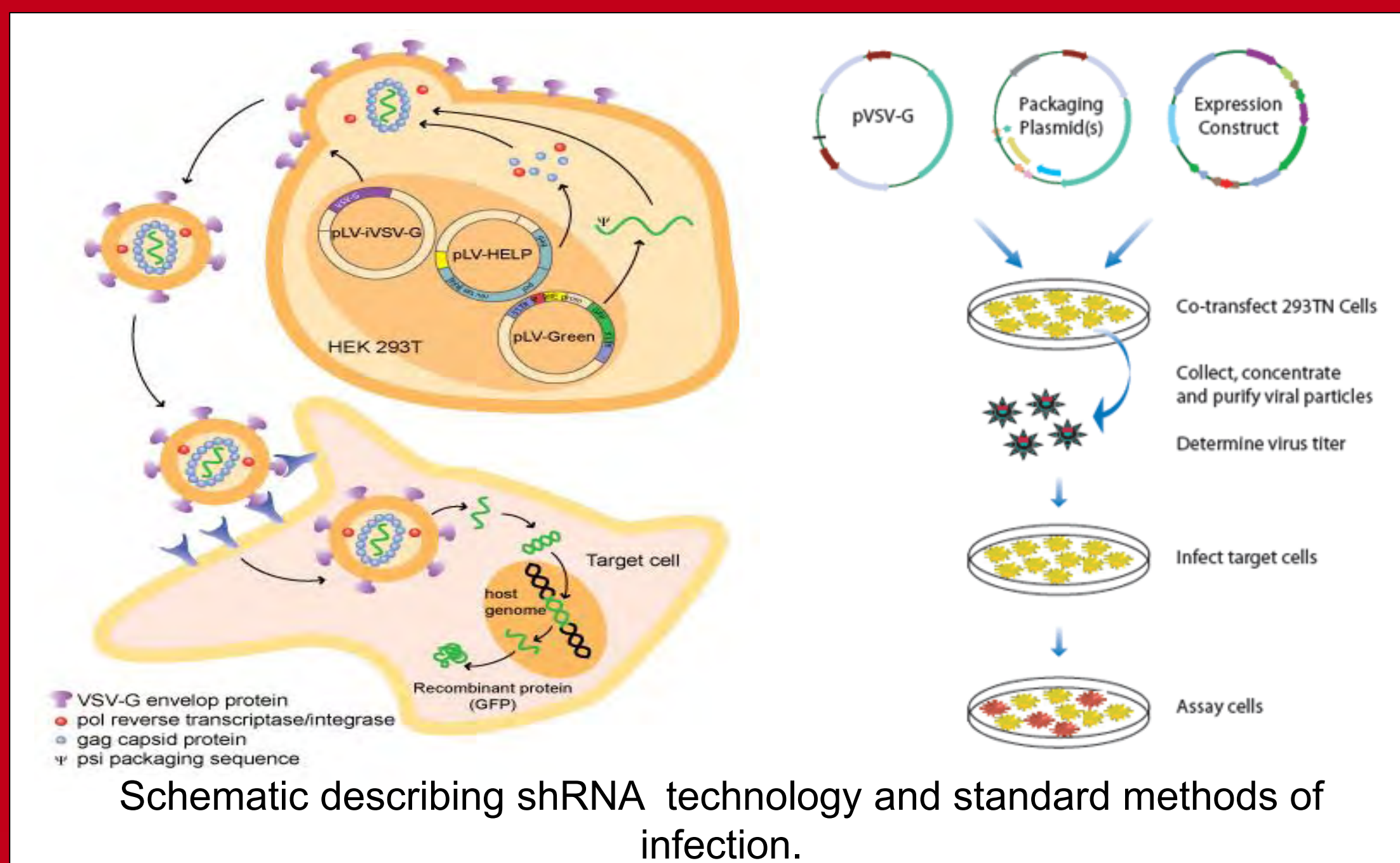
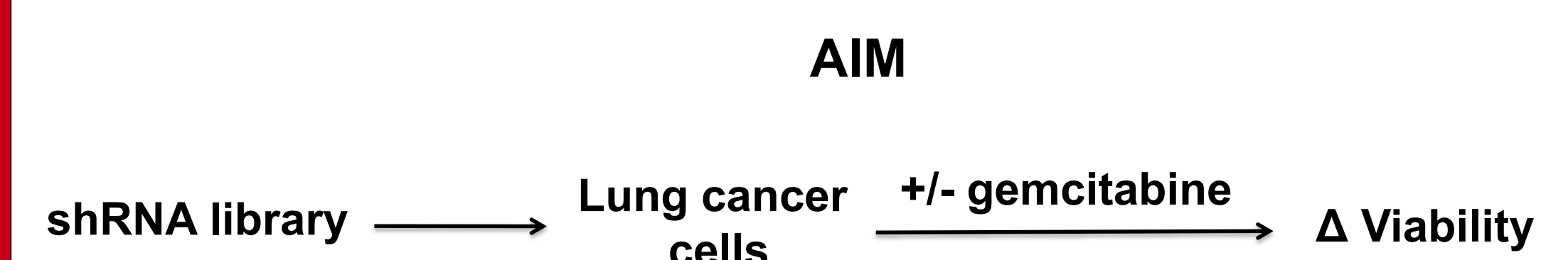
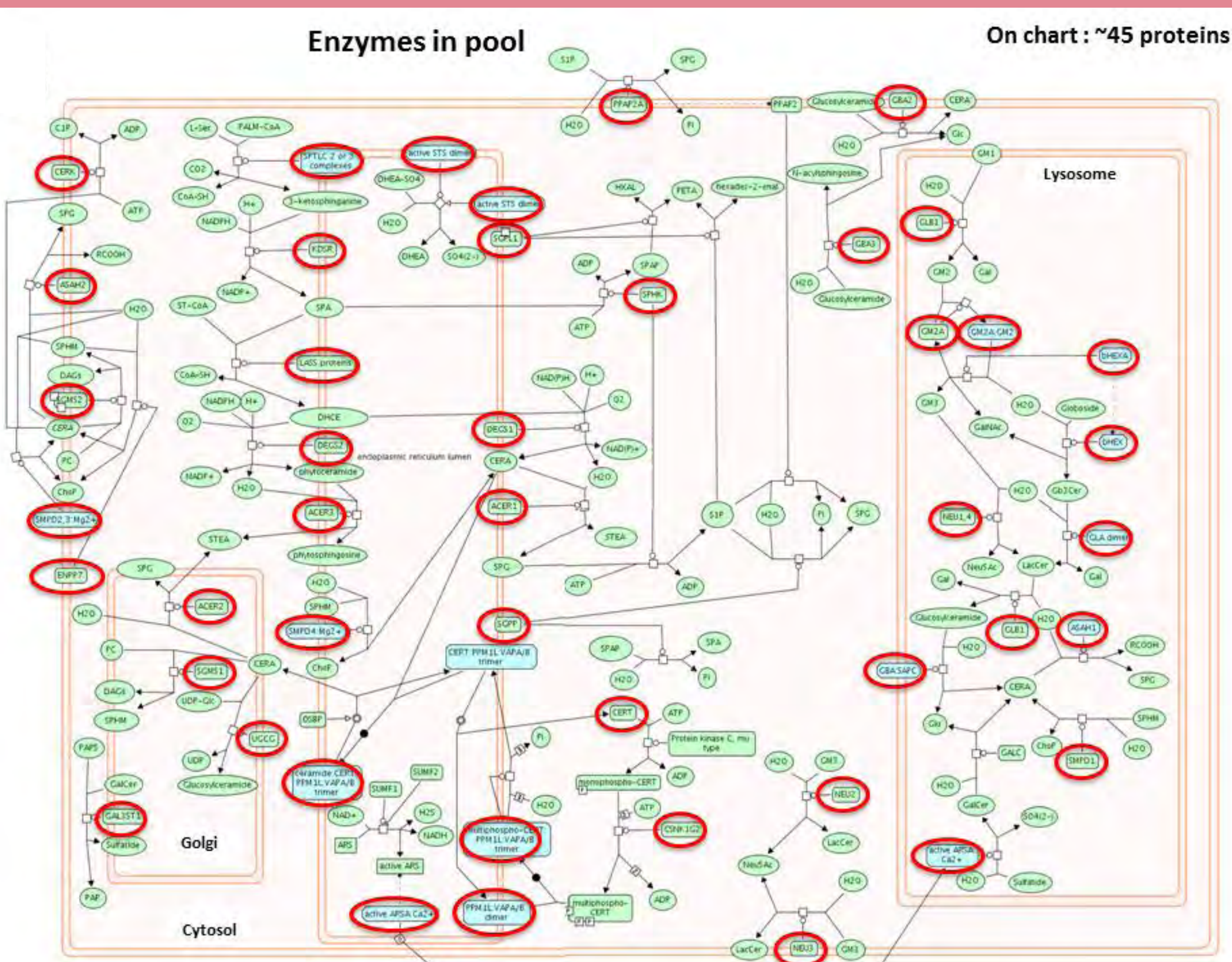
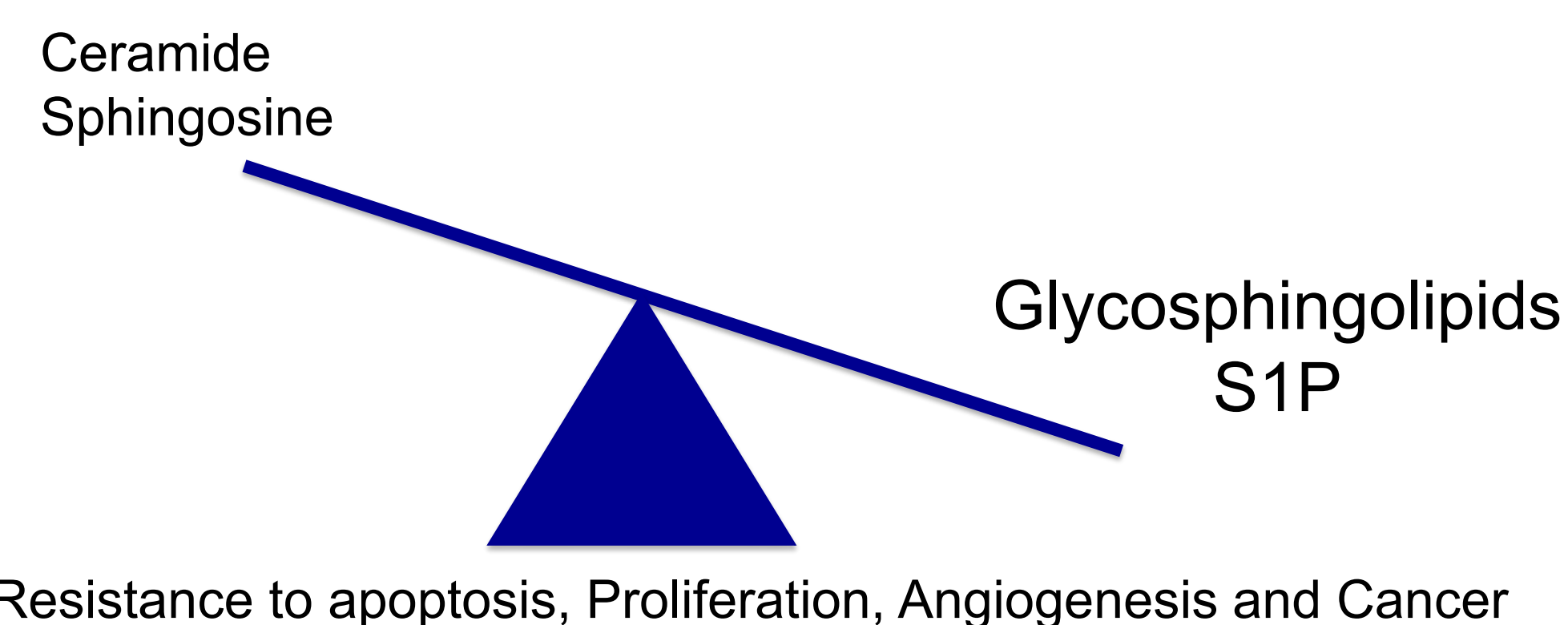
We seek to develop a comprehensive and unbiased resource that will allow us to study of the role of sphingolipid metabolism in lung cancer biology. We are creating a library of viral vectors that will facilitate knockdown of every protein involved in sphingolipid metabolism. This library will be utilized in cellular models to identify sphingolipid genes involved in response of lung cancer to standard of care chemotherapeutics and will allow the scientific community to interrogate the entire sphingolipid metabolic pathway in an unbiased and comprehensive manner. This will increase our understanding of the biological processes regulated by sphingolipids and may lead to the identification of novel therapeutic targets.

## Basic Sphingolipid Metabolism

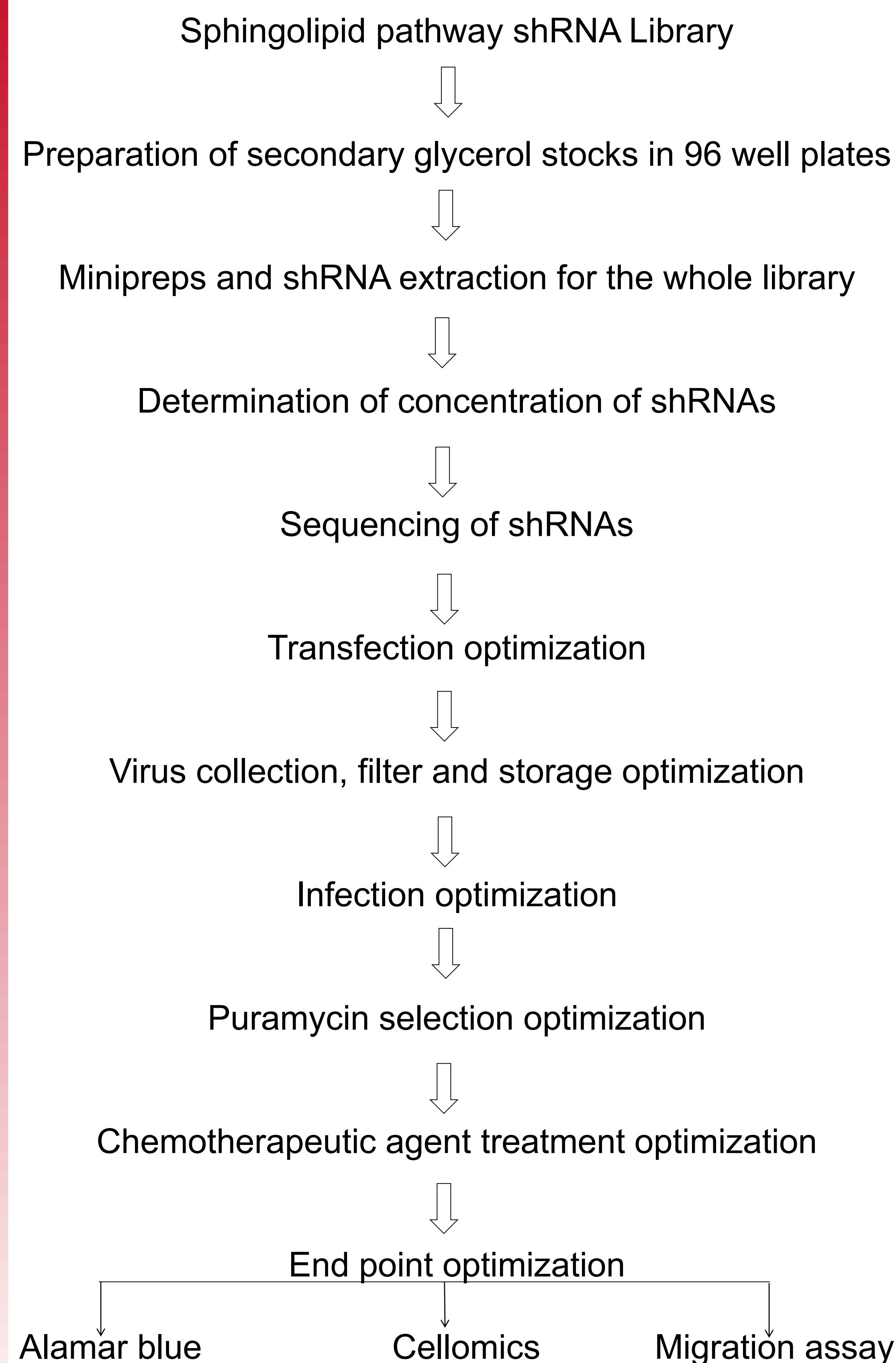


## Balance of Sphingolipids Dictates Cell Survival

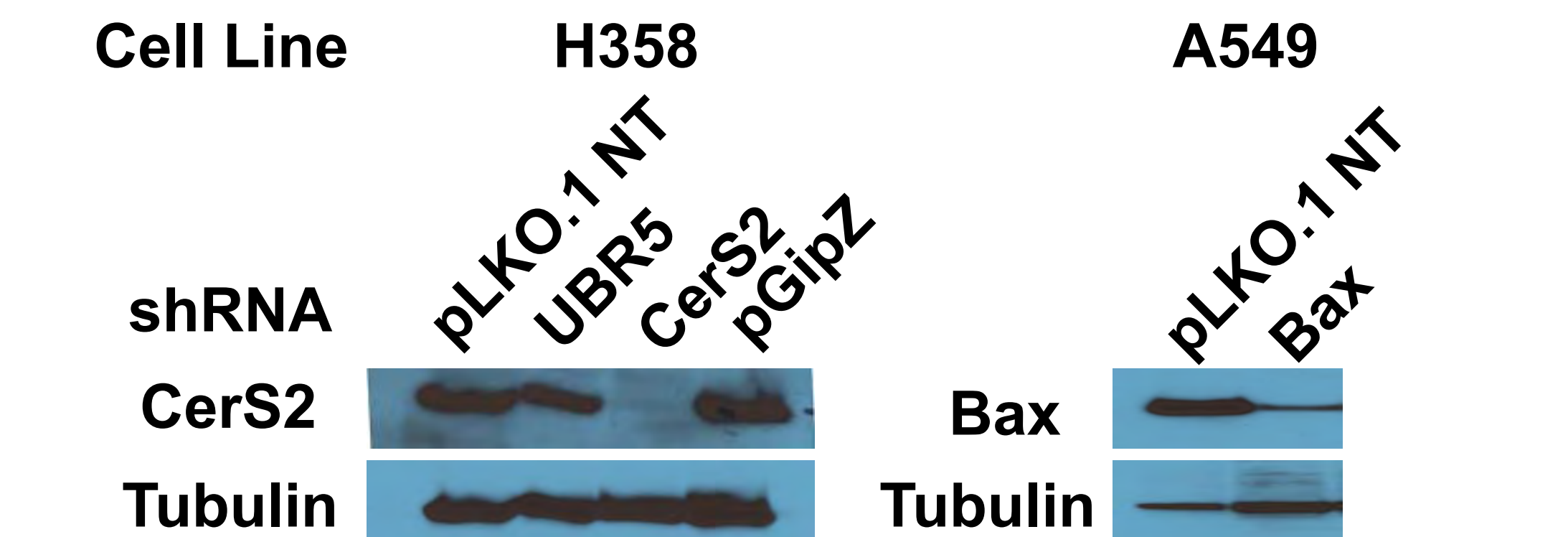
**Hypothesis:** Unbalanced sphingolipid metabolism in cancer cells results in an altered ratio of glycosphingolipids to ceramides, increasing resistance to apoptotic stimuli.



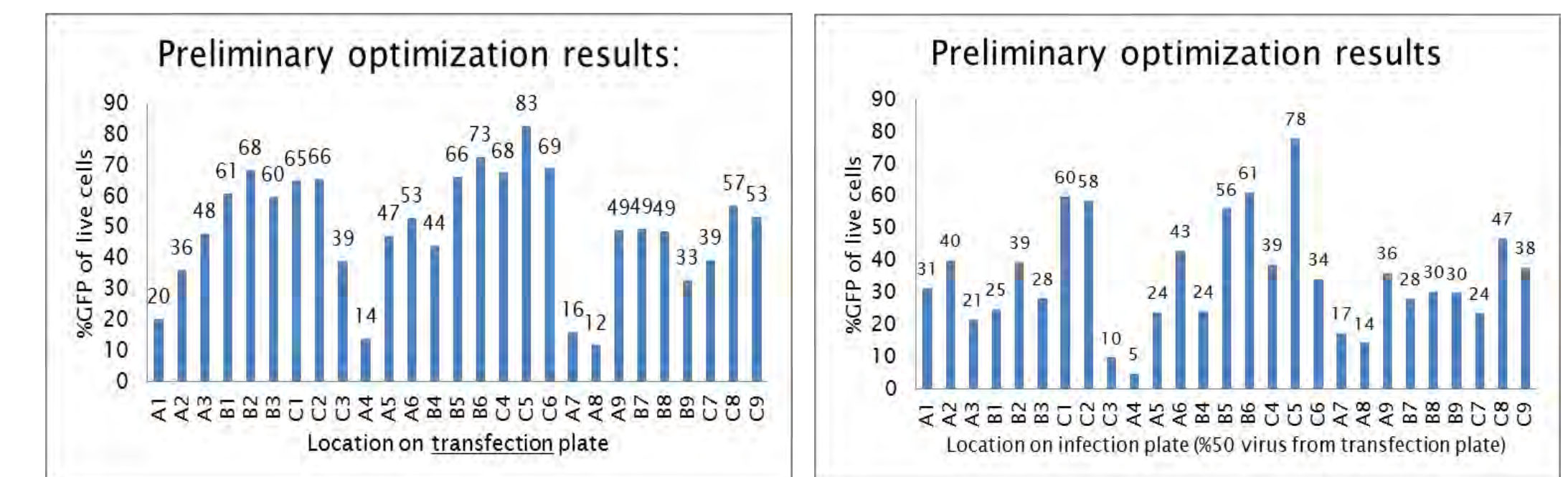
## Schematic of shRNA library screen in 96 well format



## shRNA validation /Proof of concept/proof of efficacy



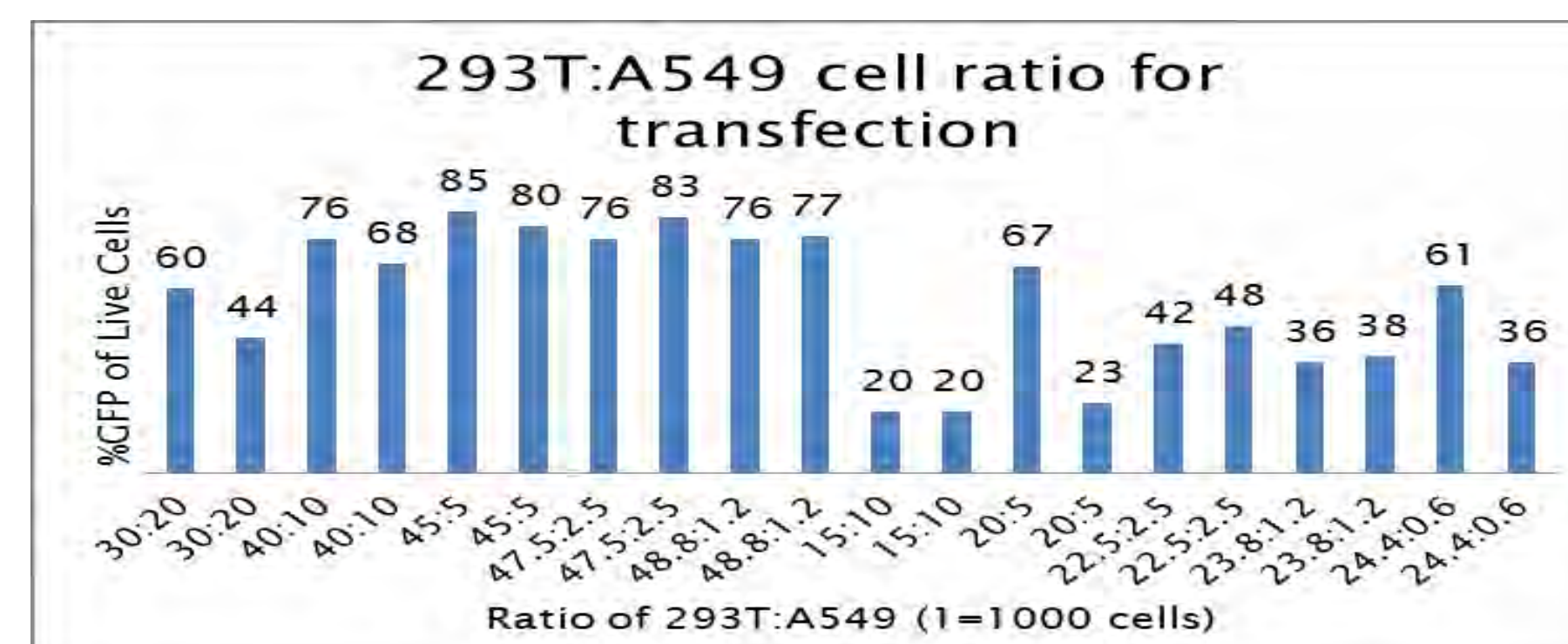
## Optimization of viral production for high throughput system



| DNA (µg) | 0.05  | 0.1          | 0.2 | 0.05 | 0.1          | 0.2 | 0.05 | 0.1           | 0.2 |    |
|----------|-------|--------------|-----|------|--------------|-----|------|---------------|-----|----|
| PEI/DNA  | 1:1   | A1           | A2  | A3   | B1           | B2  | B3   | C1            | C2  | C3 |
|          | 2.5:1 | A4           | A5  | A6   | B4           | B5  | B6   | C4            | C5  | C6 |
|          | 5:1   | A7           | A8  | A9   | B7           | B8  | B9   | C7            | C8  | C9 |
| Cell #   |       | 25,000 Cells |     |      | 50,000 Cells |     |      | 100,000 Cells |     |    |

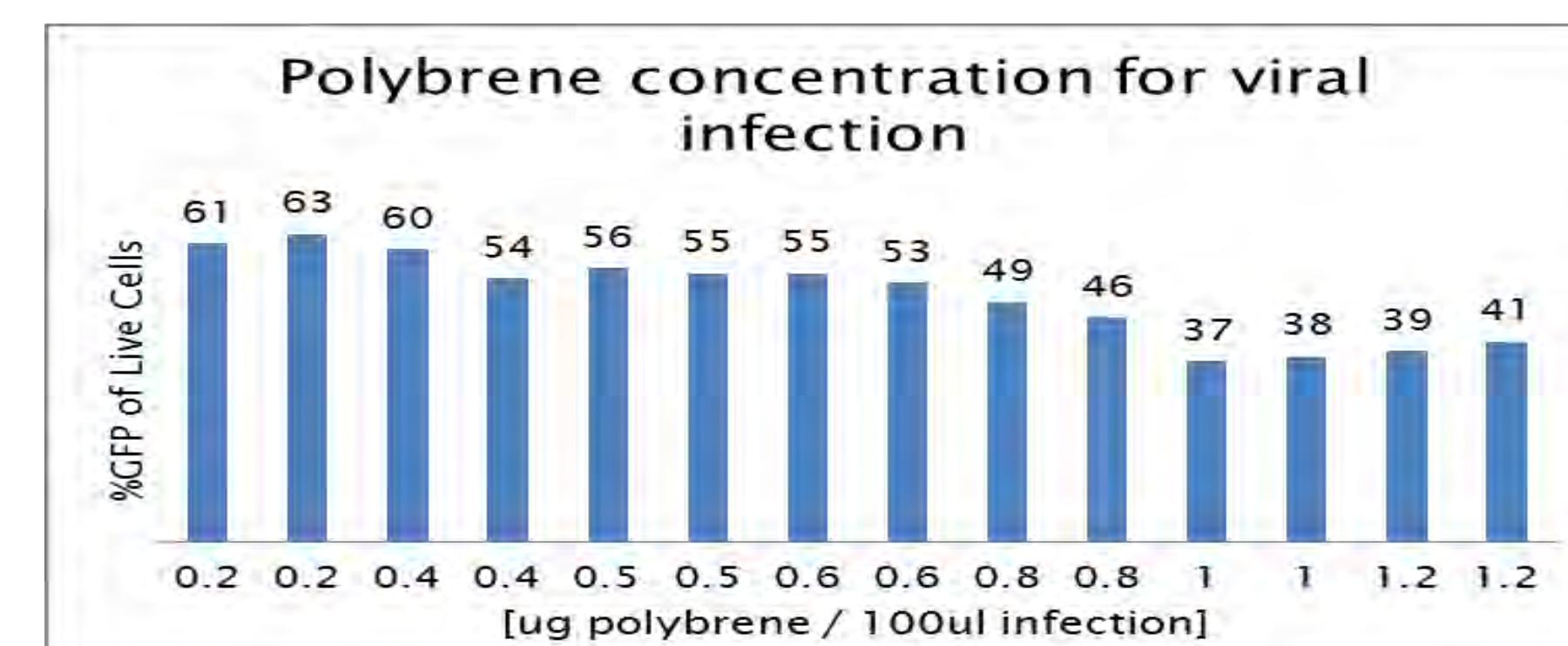
**Conclusion:** The best parameters for viral production were 100,000 cells, 0.1µg DNA, and 0.25µg PEI. During this experiment it was discovered that the low adherent nature of 293T cells was a problem that resulted in inefficient viral production.

## Improvement of cellular adhesion during viral production



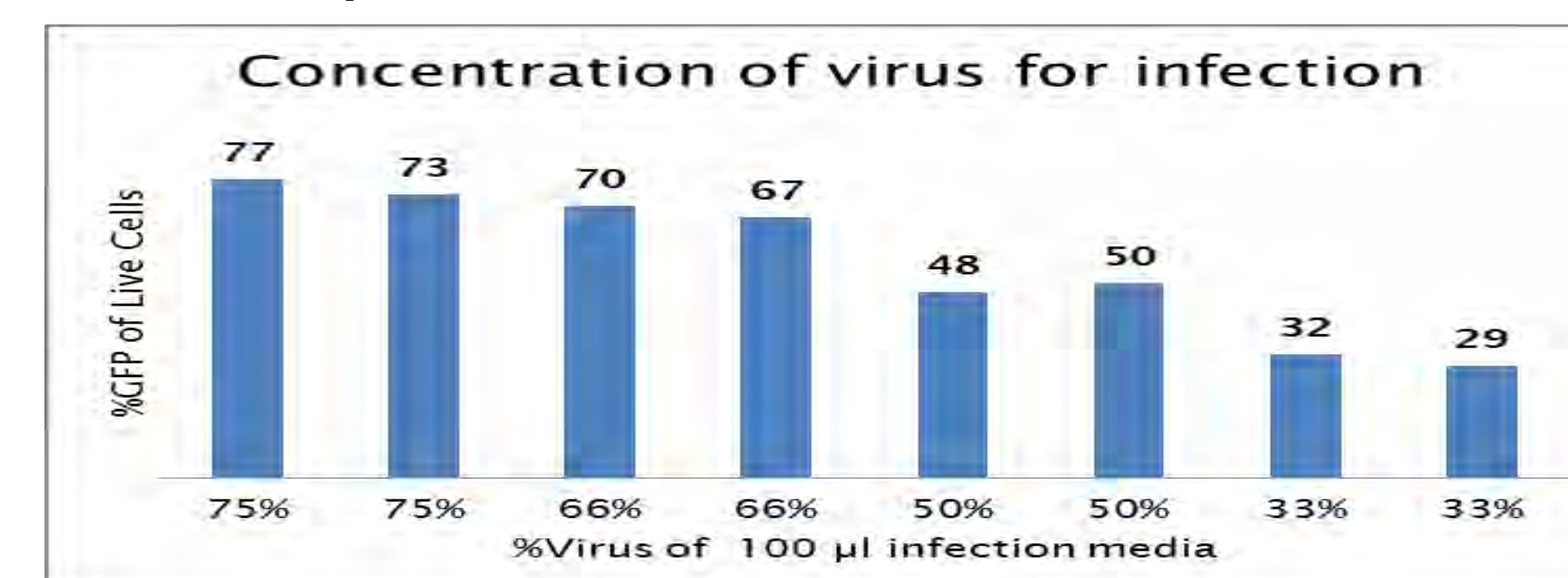
**Conclusion:** The addition of A549 cells greatly increased the adherence of 293T cells and the optimal ratio of 293T to A549 cells was 45,000 to 5,000.

## Infection optimization: concentration of polybrene



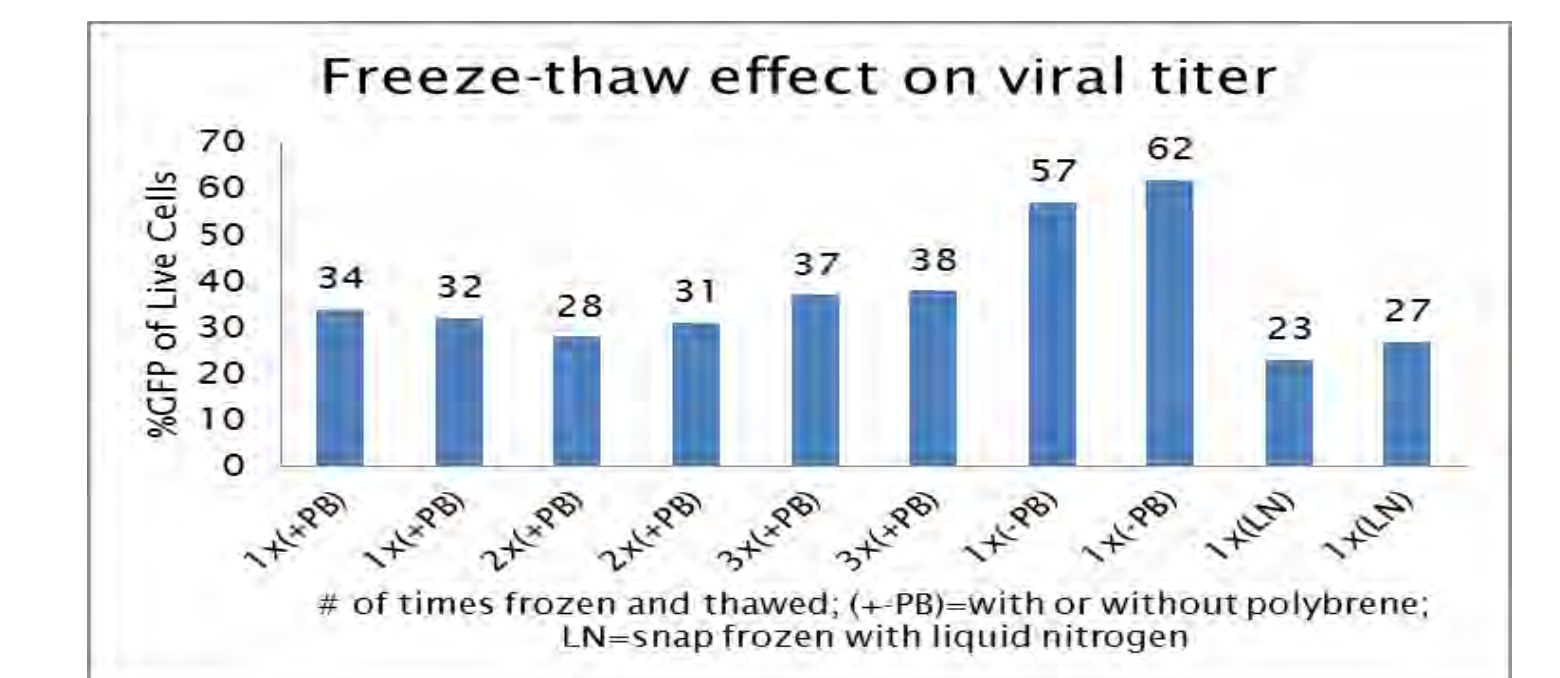
**Conclusion:** 0.2µg Polybrene per well resulted in the greatest viral infection rate.

## Infection optimization: viral concentration for infection



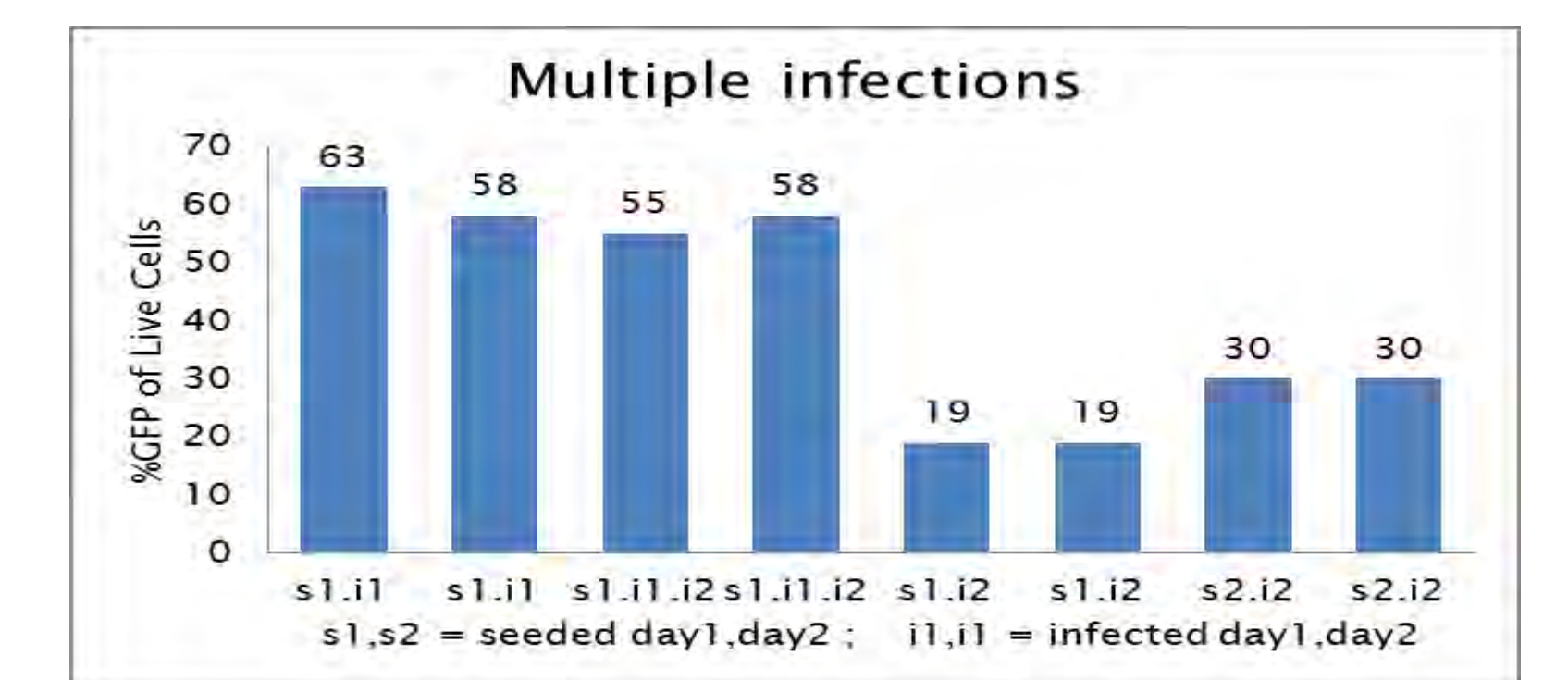
**Conclusion:** The concentration of the virus was directly proportional to the infection rate of live cells, thus, concentration of virus used to infect target cells should be maximized in order to maximize the infection rate.

## Infection optimization: viral storage conditions



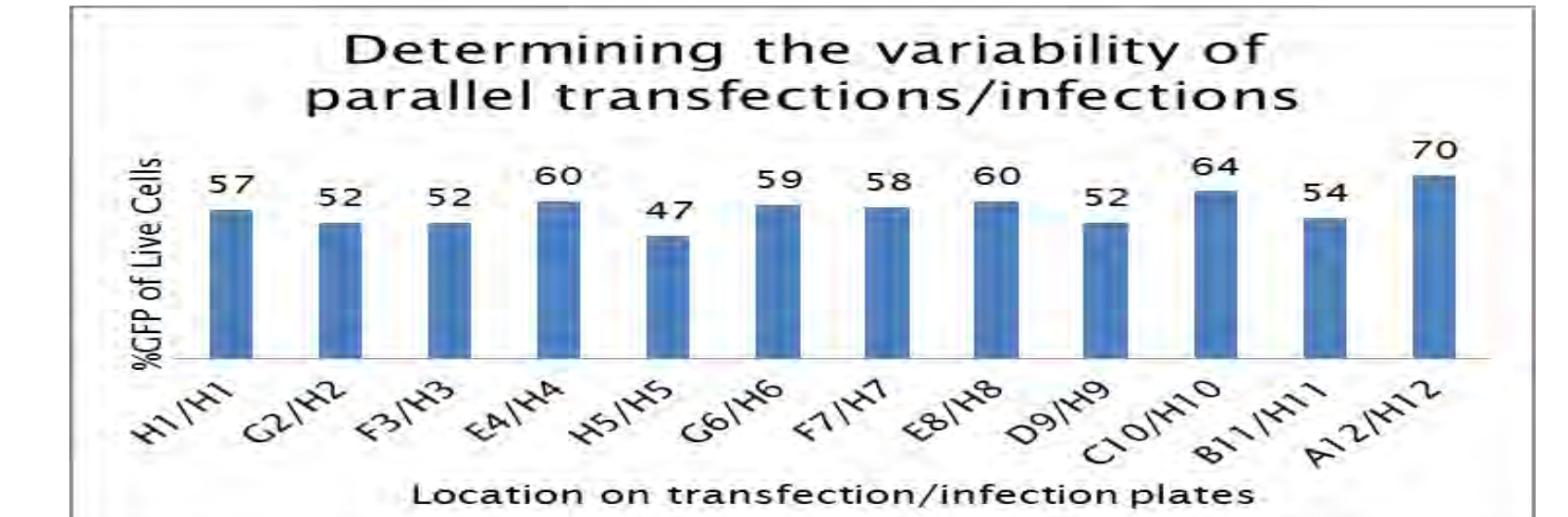
**Conclusion:** Freezing virus at -80° C with polybrene reduces the infectivity by almost half.

## Infection optimization: single vs multiple infections



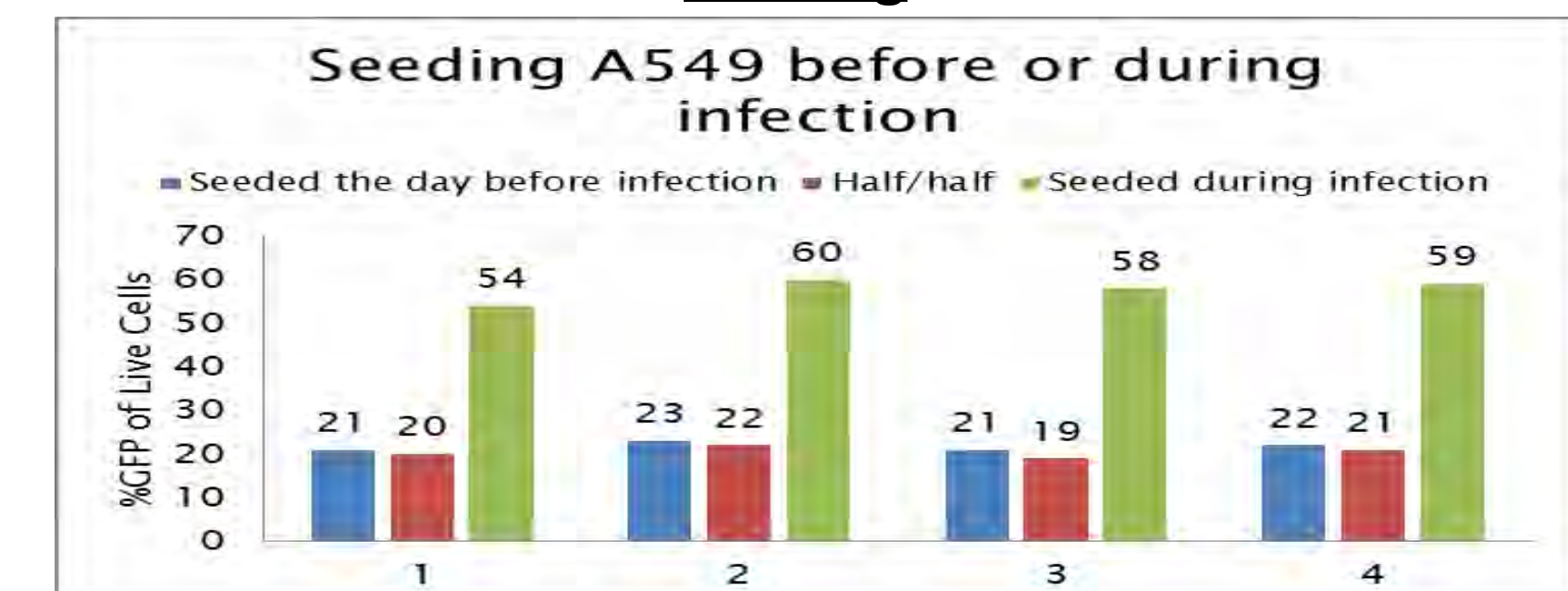
**Conclusions:** Infecting target cells more than once does not increase the rate of infection.

## Infection optimization: variability among infections



**Conclusion:** Variability in the process should be minimized before utilizing the library in high throughput studies.

## Infection optimization: timing of infection relative to cell seeding



**Conclusions:** Seeding cells prior to infection lowers infection rates. Seeding and infection should be done simultaneously.

## Summary and future directions

- Complete optimization and perform primary screens.
- Initial targets will be validated using several different established and primary lung cancer cell lines.
- Using the shRNA libraries as novel tools, we will identify which genes involved in sphingolipid metabolism alter the response of lung cancer cells to standard of cancer treatments.
- This high throughput technique will be invaluable resources that we, and others, can utilize for a myriad of applications.

## Acknowledgements

This work was supported by NCI grant R25 CA134283 to the University of Louisville. This work is also supported by the National Institute of Diabetes and Digestive and Kidney Diseases of the National Institutes of Health, [R01DK093462] (to L.J.S.), Kosair Pediatric Cancer Research Program award (to L.J.B.) and the James Graham Brown Cancer Center.

# The Hepatic "Matrisome" Responds Dynamically to Stress: Novel Characterization of the ECM Proteome

Christine E. Dolin<sup>1,2</sup>, Veronica L. Massey<sup>1,2</sup>, Lauren G. Poole<sup>1,2</sup>, Michael L. Merchant<sup>1,3</sup>, Daniel W. Wilkey<sup>1,3</sup> and Gavin E. Arteel<sup>1,2</sup>

<sup>1</sup> Department of Pharmacology and Toxicology, <sup>2</sup> University of Louisville Alcohol Research Center, <sup>3</sup> Department of Medicine, University of Louisville Health Sciences Center, Louisville KY 40292, USA

## ABSTRACT

**Background.** Chronic liver disease (e.g., ALD) follows a common natural history that leads to end-stage liver disease and hepatocellular carcinoma (HCC). There are no therapies to halt or reverse this disease process. The hepatic ECM proteome (i.e., matrisome) responds dynamically to stress. However, outside the context of fibrotic liver disease, the nature and impact of these responses to stress are poorly understood. The goal of the current work was to develop a proteomic method to characterize changes to the hepatic matrisome and compare the impact of ethanol and lipopolysaccharide (LPS) on this compartment.

**Methods.** Mice were fed ethanol-containing or isocaloric control diet for 6 weeks and injected with LPS or a vehicle 24 hours prior to sacrifice. Liver sections from these mice were diced and processed in a series of increasingly rigorous extraction buffers to separate proteins by age and crosslinking. Proteins in the resulting samples were identified using liquid chromatography-tandem mass spectrometry (LC-MS/MS). These data were filtered to show proteins that are extracellular by GO annotation, and further filtered based on current literature for matrisome proteins. Matrisome proteins were categorized by primary function; these variables were compared between the experimental groups. Immunoblotting was also performed using primary antibodies against fibrin and osteopontin, proteins previously found to be significant in ALD-associated ECM remodeling.

**Results.** The extraction methods yielded distinct pools of ECM proteins that were readily identifiable by LC-MS/MS. The ECM proteome responded dynamically to stress. For example, ethanol feeding caused a dramatic ~30% increase in the number of proteins associated with the ECM proteome. A similar response was observed 24 h after LPS injection. Interestingly, the enhancement of LPS-induced liver damage caused by ethanol preexposure was associated with changes unique to that treatment. Indeed, the combination of LPS and EtOH produced a highly cross-linked fibrin(ogen) signal.

**Conclusions.** These results suggest that this approach can be used to document qualitative changes to the ECM proteome (i.e., presence and absence). Future work will focus on quantitative changes to the matrix, as well as the qualitative changes summarized here.

## BACKGROUND

Alcoholic liver disease (ALD), is a major cause of morbidity and mortality worldwide (1). ALD progresses in stages from steatosis to steatohepatitis, followed by fibrosis/cirrhosis and eventually hepatocellular carcinoma (HCC). Currently there is no FDA approved therapy to halt or reverse ALD. In order to identify a potential therapeutic target, a greater understanding of the mechanisms by which ALD progresses, particularly in earlier stages, must be established. Changes to the extracellular matrix (ECM) during ALD are the most dramatic at the fibrosis/cirrhosis stage, which is characterized by the accumulation of collagen I, as well as laminin, fibronectin and fibrinogen (2). However, previous work has identified key roles for ECM remodeling during earlier phases of the disease (3). Previous work by this group has illustrated a pivotal role of fibrin in ALD-associated ECM remodeling (Figure 1) (3). Work by others has also shown the importance of fibronectin (4) and osteopontin (5). The contribution of other ECM proteins to the progression of inflammatory liver injury during ALD is not known.

To examine the role of the ECM in the inflammation stage of ALD, mice were pair fed EtOH for 6 weeks. Select pairs were also injected with lipopolysaccharide (LPS) 24 hours prior to sacrifice to stimulate an inflammatory response. Liver sections from these mice were extracted using the 'Texas 3-Step' method by de Castro Bras et al. (Figure 2) (6). This method produces three fractions of ECM proteins that correspond to increasing age and crosslinking; the final insoluble pellet contains highly cross-linked ECM proteins. Fractions were then analyzed with LC-MS/MS (Table 1; Figure 3) and immunofluorescent staining (Figure 4) to evaluate the ECM proteome.

## MATERIALS AND METHODS

**Animals and Treatments:** Male C57B6/J mice were fed ethanol-containing or isocaloric control diet using the standard Lieber-DeCarli protocol. After 6 weeks, mice were injected with 10 mg/kg LPS or vehicle (saline) and sacrificed 4 or 24 h later. Chunks of liver were immediately frozen in liquid nitrogen and stored at -80°C.

**Sample Extraction:** Pieces of liver were diced and processed through increasingly rigorous extraction buffers (see Figure 2). The supernatants and final pellet were resuspended in deglycosylation buffer to remove post-translational modifications of ECM proteins. Samples from 5 separate mouse livers were pooled for subsequent LC-MS/MS analysis.

**Liquid Chromatography and Data Acquisition:** An EASY n-LC (Thermo) UHPLC system was used for LC separation. A Nanospray Flex source (Thermo) was used to position the end of the emitter near the ion transfer capillary of the mass spectrometer. The ion transfer capillary temperature of the mass spectrometer was set at 225°C, and the spray voltage was set at 1.6kV. An Orbitrap Elite - ETD mass spectrometer (Thermo) was used to collect data from the LC eluate. An Nth Order Double Play with ETD Decision Tree method was created in Xcalibur v2.2. The lock mass option was enabled (0% lock mass abundance) using the 371.101236m/z polysiloxane peak as an internal calibrant.

**Data Analysis:** Proteome Discoverer v1.4.0.288 and Scaffold Q+ v4.3.2 Proteome Discoverer v1.4.0.288 was used to analyze the data collected by the mass spectrometer. The database used in Mascot v2.4 and SequestHT searches was the 6/2/2014 version of the UniProtKB *Mus musculus* reference proteome canonical and isoform sequences. In order to estimate the false discovery rate, a Target Decoy PSM Validator node was included in the Proteome Discoverer workflow. The workflow allows for extraction of MS2 scan data from the Xcalibur RAW file, separate searches of CID and ETD MS2 scans in Mascot and Sequest, and collection of the results into a single file (.msf extension). The resulting .msf files from Proteome Discoverer were loaded into Scaffold Q+ v4.3.2. Scaffold was used to calculate the false discovery rate using the Peptide and Protein Prophet algorithms. The results were annotated with mouse gene ontology information from the Gene Ontology (GO) Annotations Database ([ftp.ebi.ac.uk](http://ebi.ac.uk)).

The resultant data were filtered by the GO annotation for "extracellular." The resultant filtered list was validated through published databases (e.g., <http://web.mit.edu/hyneslab/matrisome/>) to be part of the ECM proteome (proteoglycans and glycoproteins, ECM associated proteins, collagens, proteases and protease inhibitors). The relative size and content of each fraction were determined. The impact of ethanol and LPS injections were compared.

**Immunoblots:** Protein extracts from the ECM extraction fractions and total protein extract from a different section of the same liver in RIPA buffer were used. Samples were loaded onto (SDS)-polyacrylamide gels of 12% (wt:vol) acrylamide followed by electrophoresis and western blotting. Primary antibodies against fibrin (Dako 59D8) and osteopontin (Abcam 8448) were used.

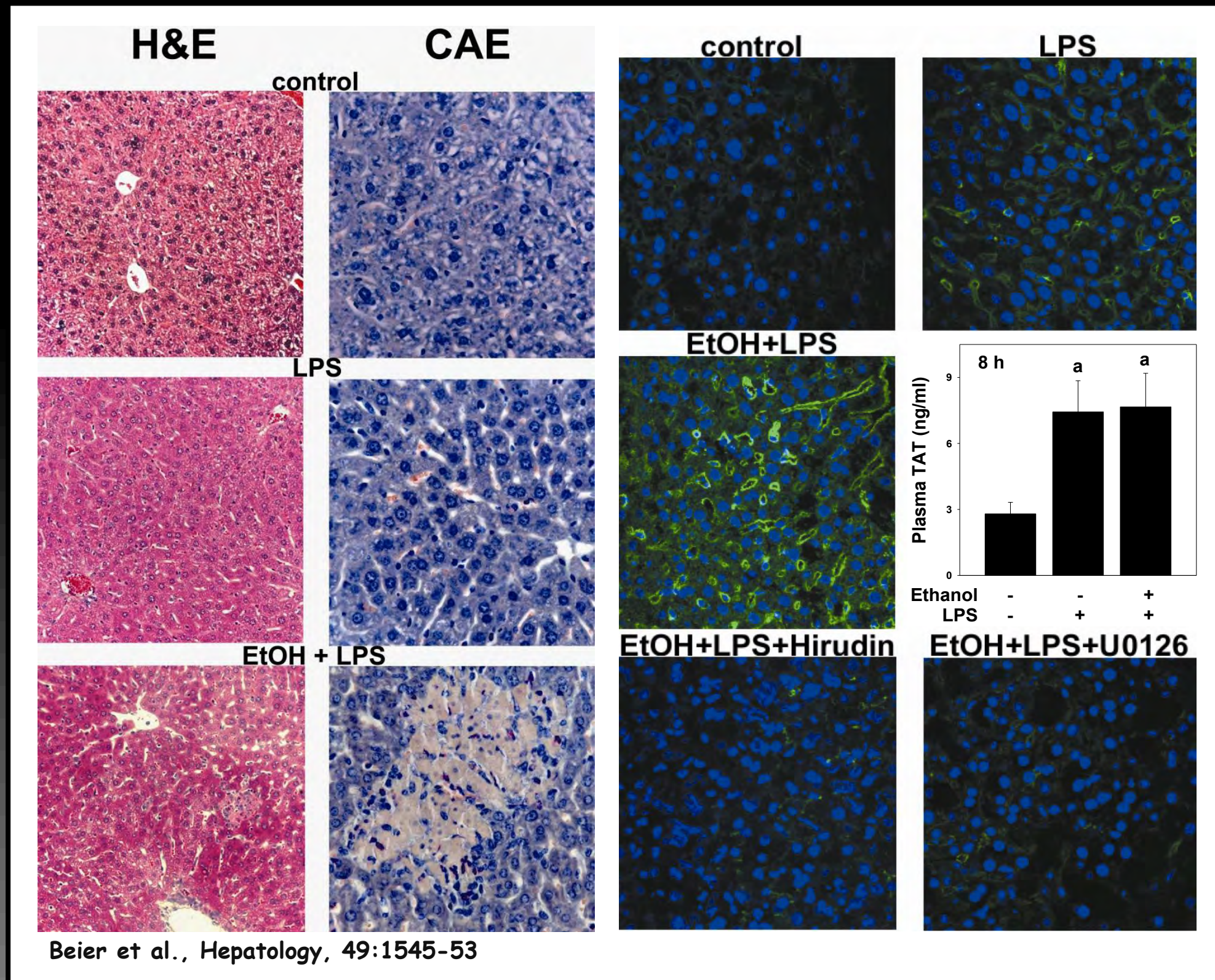


**Figure 1: Injury and fibrin deposition with EtOH and LPS treatment.** Mice were exposed to ethanol or control administration and subsequently injected with LPS. Representative photomicrographs depicting liver injury (H&E), inflammation (CAE) and fibrin immunofluorescence are shown. The inset shows plasma thrombin activity (TAT dimers).

As is well-known, ethanol preexposure enhanced inflammatory liver injury caused by LPS administration. Injury under these conditions correlated with perisinusoidal fibrin deposition. Administrations that prevented fibrin accumulation (e.g., hirudin and U0126) blocked injury. These data indicate that fibrin accumulation contributes to inflammatory liver damage caused by ethanol.

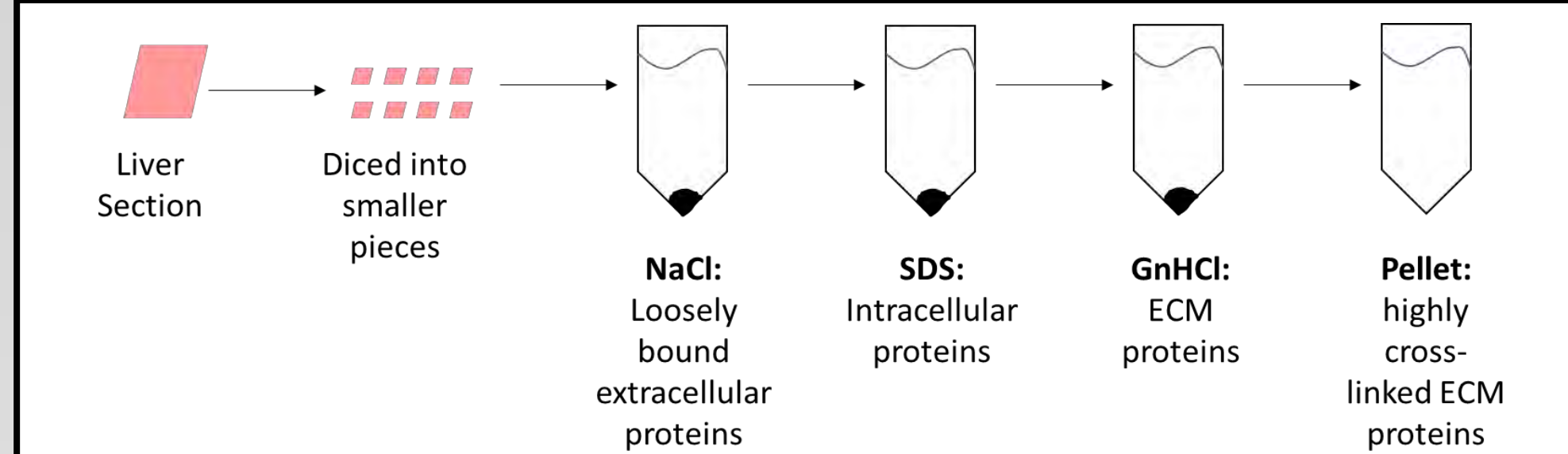


**Figure 2: ECM Extraction Process.** Liver sections from mice were diced into smaller pieces and then extracted in NaCl, SDS and GmHCl. Supernatants and the final pellet from the GmHCl fraction were resuspended in deglycosylation buffer for further analysis.

The NaCl fraction is expected to be enriched with loosely bound extracellular proteins and newly formed ECM, while the SDS fraction is expected to be enriched with transitional ECM. The GmHCl fraction and pellet are expected to be enriched with ECM proteins, the latter containing highly cross-linked ECM proteins. These fractions were deglycosylated and analyzed by LC-MS/MS.

| Protein Name                             | Accession Number | Molecular Weight |
|--|------------------|------------------|
| <b>Proteoglycans and glycoproteins</b>   |                  |                  |
| Fibrinogen gamma chain                   | F1BG_MOUSE       | 49 kDa           |
| Protein Fga                              | EPV24_MOUSE (-1) | 87 kDa           |
| Lumican                                  | LUM_MOUSE        | 38 kDa           |
| Decorin                                  | DCRN_MOUSE (-1)  | 63 kDa           |
| Haptoglobin                              | HPT_MOUSE        | 39 kDa           |
| Keratin, type 2 cytoskeletal 13          | K13L3_MOUSE      | 48 kDa           |
| Cornadecanin                             | CD3N_MOUSE       | 54 kDa           |
| <b>Other ECM-associated proteins</b>     |                  |                  |
| Superoxide dismutase [Cu-Zn]             | SODC_MOUSE       | 16 kDa           |
| Serum amyloid A-1 protein                | SA4A1_MOUSE      | 14 kDa           |
| Serum amyloid A-2 protein                | SA4A2_MOUSE      | 14 kDa           |
| Apolipoprotein A-I                       | APOA1_MOUSE      | 31 kDa           |
| Apolipoprotein E                         | APOE_MOUSE       | 36 kDa           |
| Apolipoprotein A-II                      | APOA2_MOUSE      | 49 kDa           |
| Anexin A2                                | ANXA2_MOUSE      | 39 kDa           |
| Anexin A1                                | ANXA1_MOUSE      | 39 kDa           |
| Actin, alpha skeletal muscle             | ACTB_MOUSE       | 42 kDa           |
| Actin, cytoplasmic 1                     | ACTA1_MOUSE (-1) | 37 kDa           |
| Vimentin                                 | VIME_MOUSE       | 54 kDa           |
| 14-3-3 protein sigma                     | 1433S_MOUSE      | 28 kDa           |
| Thioredoxin                              | TXND_MOUSE       | 12 kDa           |
| 14-3-3 protein epsilon                   | 1433E_MOUSE      | 29 kDa           |
| Peptidyl-prolyl cis-trans isomerase PPIA | PPIA_MOUSE       | 18 kDa           |
| 14-3-3 protein zeta/delta                | 1433Z_MOUSE      | 28 kDa           |
| Endoplasmic                              | ENPL_MOUSE       | 92 kDa           |
| Calnexin                                 | CALN_MOUSE (-1)  | 37 kDa           |
| Alpha-actinin-4                          | ACTN4_MOUSE (-3) | 105 kDa          |
| <b>Proteases and protease inhibitors</b> |                  |                  |
| Alpha-1-antitrypsin 1-1                  | A1AT1_MOUSE (-1) | 46 kDa           |
| Serpin B5                                | SPB5_MOUSE       | 42 kDa           |
| Lysostzyme C-1                           | LYZ1_MOUSE       | 17 kDa           |
| <b>Collagens</b>                         |                  |                  |
| Collagen alpha-2(I) chain                | COL1A2_MOUSE     | 130 kDa          |

**Table 1: Sample results table.** Liver sections from mice were extracted and analyzed by LC-MS/MS. The results listed are from the insoluble pellet fractions.

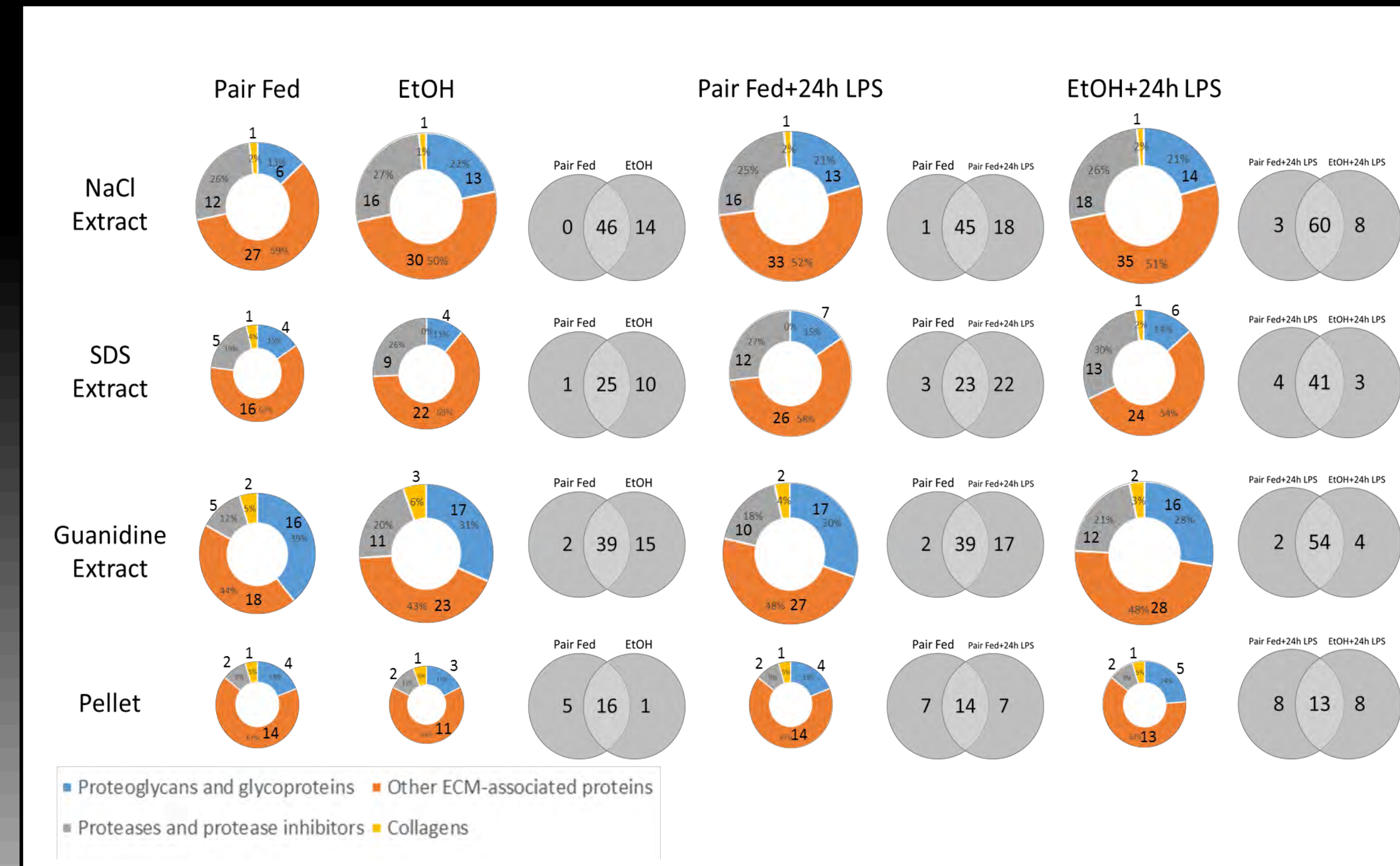


**Figure 3: Effects of EtOH and LPS on 'matrisome proteins'.** The effects of 6 weeks of chronic alcohol ingestion and/or injection with LPS 24 hours prior to sacrifice on the number of ECM proteins in various fractions were determined. The size of the pie charts corresponds to relative amount of protein found in that fraction.

The ECM proteome responded dynamically to stress. For example, 6 wks of ethanol feeding caused a dramatic ~30% increase in the number of proteins associated with the ECM proteome. A similar response was observed 24 h after LPS injection. Interestingly, the enhancement of LPS-induced liver damage caused by ethanol preexposure was associated with changes unique to that treatment. Indeed, the combination of LPS and EtOH produced a highly cross-linked fibrin(ogen) signal (see Figure 1). These results suggest that this approach can be used to document qualitative changes to the ECM proteome (i.e., presence and absence).

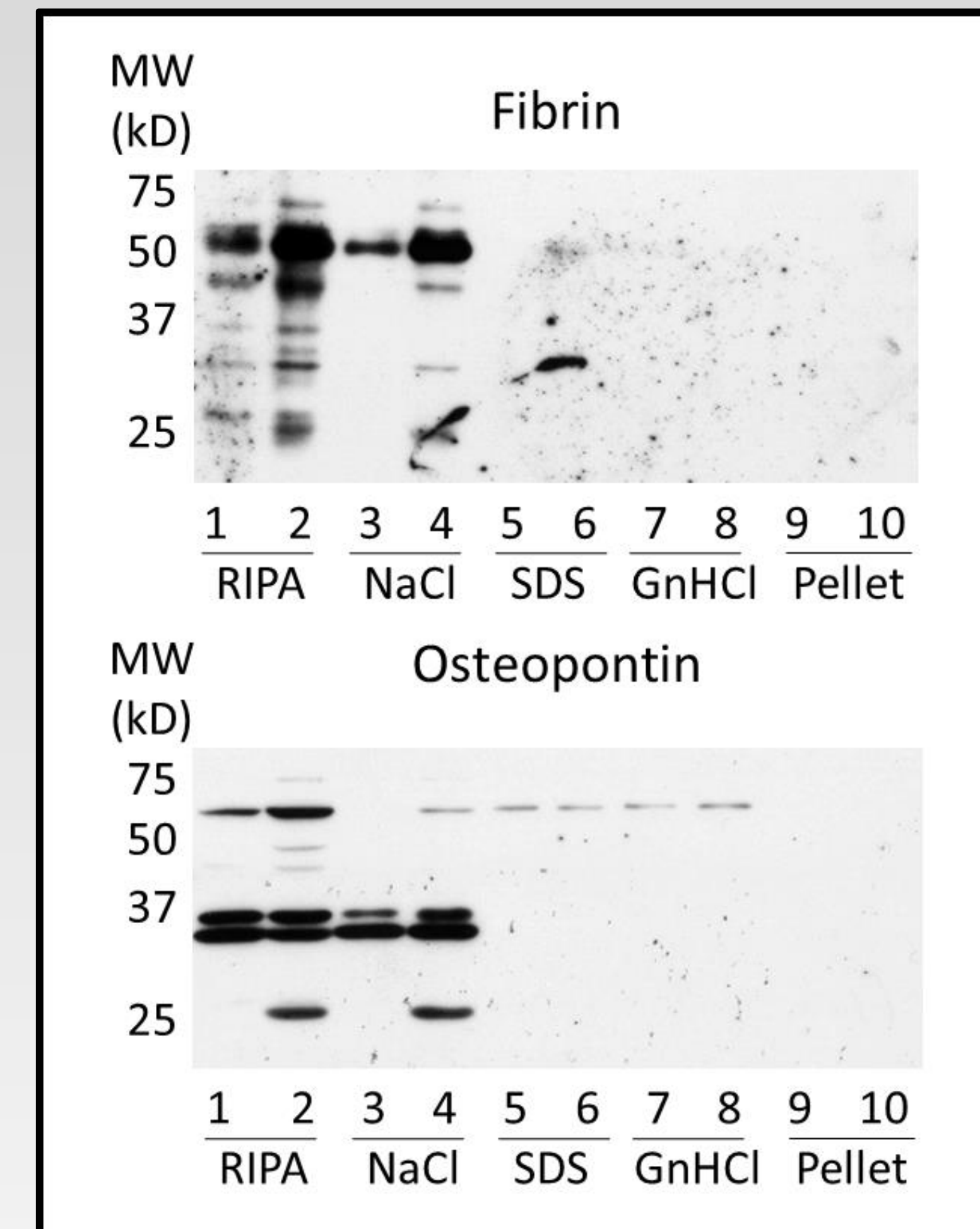


**Figure 4: Western validation of results.** The presence of known ECM proteins (e.g., fibrin and osteopontin) were determined in total (RIPA) extracts, as well as the various extracts from the 'Texas 3-step.' Foci up to this point have been on proteins previously shown to be involved in experimental ALD (e.g., fibrin and osteopontin).

As has been observed previously by this group and others, EtOH exposure increased the amount of fibrin and osteopontin in the liver of mice. These approaches not only validate the LC/MS results, but also serve to document quantitative changes in the ECM proteome.

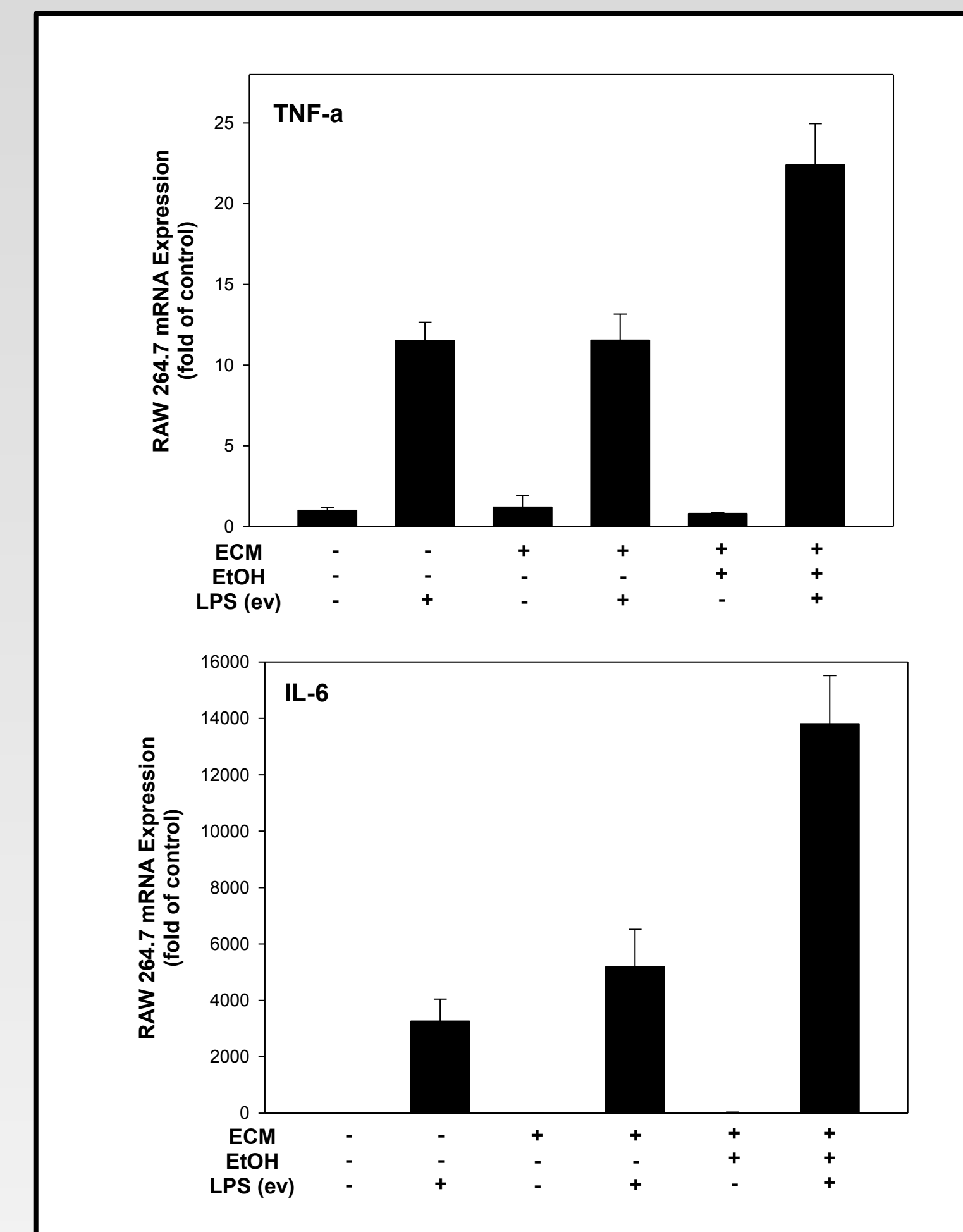


**Figure 5: ECM from alcohol-treated mice enhanced macrophage activation.** ECM was extracted from livers and served as a substratum for RAW macrophages. The cells were then stimulated with LPS and cytokine expression was measured by rtPCR.

In the absence of LPS stimulus, there was no difference between control RAW cells (no ECM) and those grown on ECM extract substratum. EtOH preexposure dramatically enhanced the expression of both IL-6 and TNF $\alpha$  by these cells. These data further support the hypothesis that changes in the ECM proteome caused by alcohol exposure enhance inflammation (Figure 1).

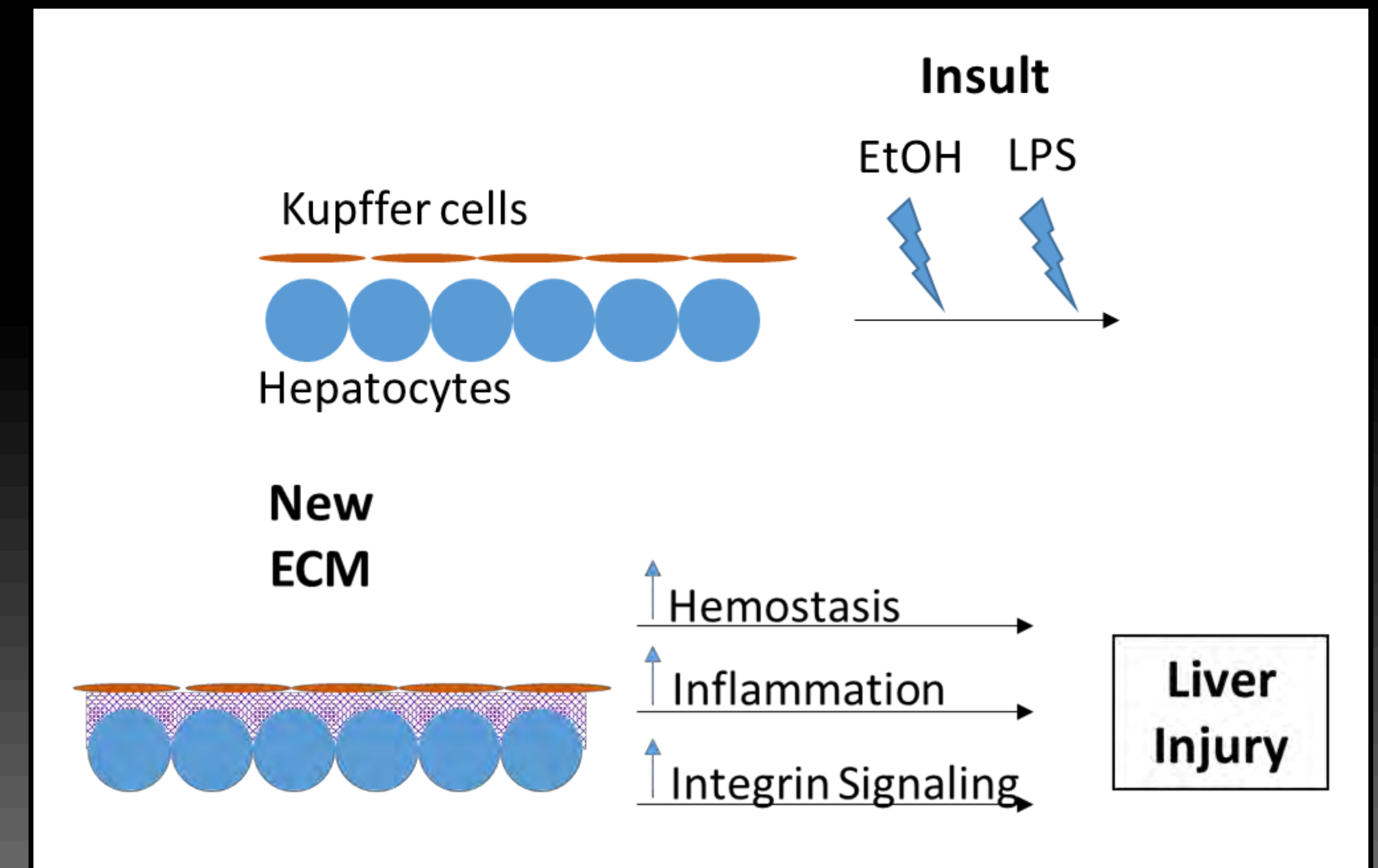


**Figure 7: Role of the ECM in liver injury.** Ethanol and/or LPS exposure leads to ECM remodeling. This response is dynamic and correlates with an enhanced inflammatory phenotype during steatohepatitis. The matrix may contribute to liver inflammation and injury indirectly (e.g., via hemostasis), via direct effects on inflammatory cells (Figure 5), and/or via altered signaling in hepatic cells (e.g., via integrins). These mechanisms are not mutually exclusive and can work additively to mediate the observed effects.

## SUMMARY

1. A new method for documenting changes in the hepatic ECM proteome ('matrisome') is described.
2. Sequential extractions characterize qualitative changes to this proteome.
3. The hepatic matrisome responds dynamically to stress both chronic (ethanol diet) and acute (LPS).
4. The combination of ethanol and LPS cause a unique matrisome signature.
5. ECM matrices from ethanol-exposed livers enhanced activation of macrophages in culture, in-line with previous in vivo studies.
6. Future work will focus on quantitative changes to the matrix, as well as the qualitative changes summarized here.

## REFERENCES

1. Grant B, Dufour M, Harford T. Epidemiology of alcoholic liver disease. *Seminars in Liver Disease*. 1988; 8:12-25.
2. Schuppan D, Ruhl M, Somasundaram R, Hahn E. Matrix as a modulator of hepatic fibrosis. *Seminars in Liver Disease*. 2001; 21:351-72.
3. Beier JJ, Luyendyk JP, Guo L, von Montfort C, Staunton DE, Arteel GE. Fibrin accumulation plays a critical role in the sensitization to lipopolysaccharide-induced liver injury caused by ethanol in mice. *Hepatology*. 2009; 5:1545-53.
4. Aziz-Seible RS, McVicker BL, Kharbanda KK, Casey CA. Cellular fibronectin stimulates hepatocytes to produce factors that promote alcohol-induced liver injury. *World Journal of Hepatology*. 2011; 2:45-55.
5. Ge X, Leung TM, Arriazu E, Lu Y, Urtasun R, Christensen B, et al. Osteopontin binding to lipopolysaccharide lowers tumor necrosis factor- $\alpha$  and prevents early alcohol-induced liver injury in mice. *Hepatology*. 2014; 4:1600-16.
6. de Castro Bras LE, Ramirez TA, DeLeon-Pennell KY, Chiao YA, Ma Y, Dai Q, et al. Texas 3-Step decellularization protocol: Looking at the cardiac extracellular matrix. *Journal of Proteomics*. 2013; 36:43-52.

## FUNDING SUPPORT

Support of NIH/NCI (5R25CA134283-03) and NIH/NIAAA (1R01AA021978-01) are gratefully acknowledged.

# Viability of Losartan as a Combination Therapy with Oncolytic Adenovirus

Harry Gao, Xiao-Mei Rao, M.D., Steven Wechman, B.S., Kelly McMasters, M.D. PhD., Heshan Sam Zhou, PhD.

Department of Surgery, Brown Cancer Center, Departments of Pharmacology and Toxicology, Microbiology and Immunology, University of Louisville School of Medicine

## Abstract

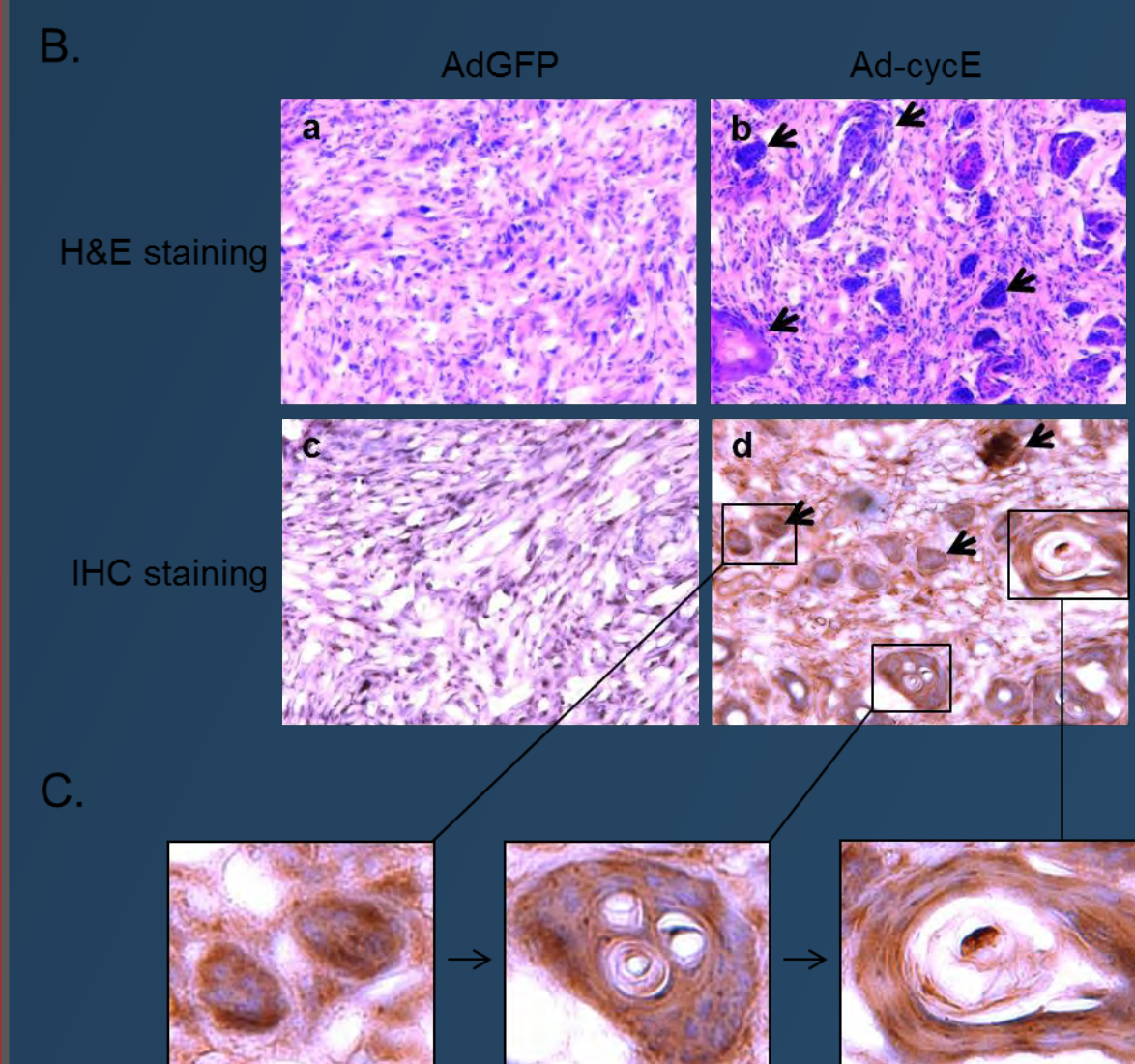
Cancer-selective oncolytic adenoviruses have great conceptual potential as an emerging lung cancer therapy. However, one of the major obstacles in oncolytic virotherapy is maximizing the spread of the virus therapy throughout the tumor. Tumors have an extracellular matrix that is dense enough to retard or outright halt the distribution of therapeutic nanoparticles like viruses. Combination treatments aimed at degrading, or limiting extracellular matrix production hold great promise.

Losartan is a clinically-approved hypotensive drug with anti-fibrotic properties; it has been shown in mouse models to increase the distribution of some therapeutic nanoparticles by limiting extracellular matrix production. *In vitro* experiments were performed to verify the suitability of losartan as a combination treatment with oncolytic adenoviruses. Toxicity tests showed that Losartan had no anti-cancer properties of its own. Various cell lines in culture were then treated with a combination of Losartan and adenovirus. The effects were verified through visual examination of AdGFP fluorescence expression, crystal staining of adherent cells, Western blot analysis for viral protein expression, and virus titer produced in infected cells.

In several cell lines, the combination treatment of Losartan and adenovirus was markedly more effective than the adenovirus alone. H1299 cells responded particularly well to the combination treatment, with positive results in each of the four analytical methods used. More testing is needed to understand the full range of Losartan's effects and how to maximize its positive effect on viral efficacy. Losartan appears to be a viable option to increase adenovirus distribution in tumors.

## Introduction

Oncolytic viruses ought to be an effective and self-sustaining weapon against cancer. However, the dense extracellular matrix in tumors prevents therapeutic nanoparticles from spreading through the tumor and greatly limits the efficacy of adenoviral therapy. Moreover, tumors grown in immunocompetent mice have also been demonstrated to form capsule structures. These structures appear to be an active tumoral response to viral infection that serves to contain the spread of virus particles. Given all this, increasing the distribution of viruses in tumors is vital to increase virotherapy efficacy. Preliminary tests were run to verify the drug Losartan's suitability for this purpose.



200x HE stains of ED1 tumors in immunocompetent mice with virus containment capsules. White structures are the spaces where cells were infected and killed by adenovirus; no cells outside these structures were infected.

400x IHC staining for E1A in ED1 tumors. White structures are the spaces where cells were infected and killed by adenovirus; no cells outside these structures were infected.

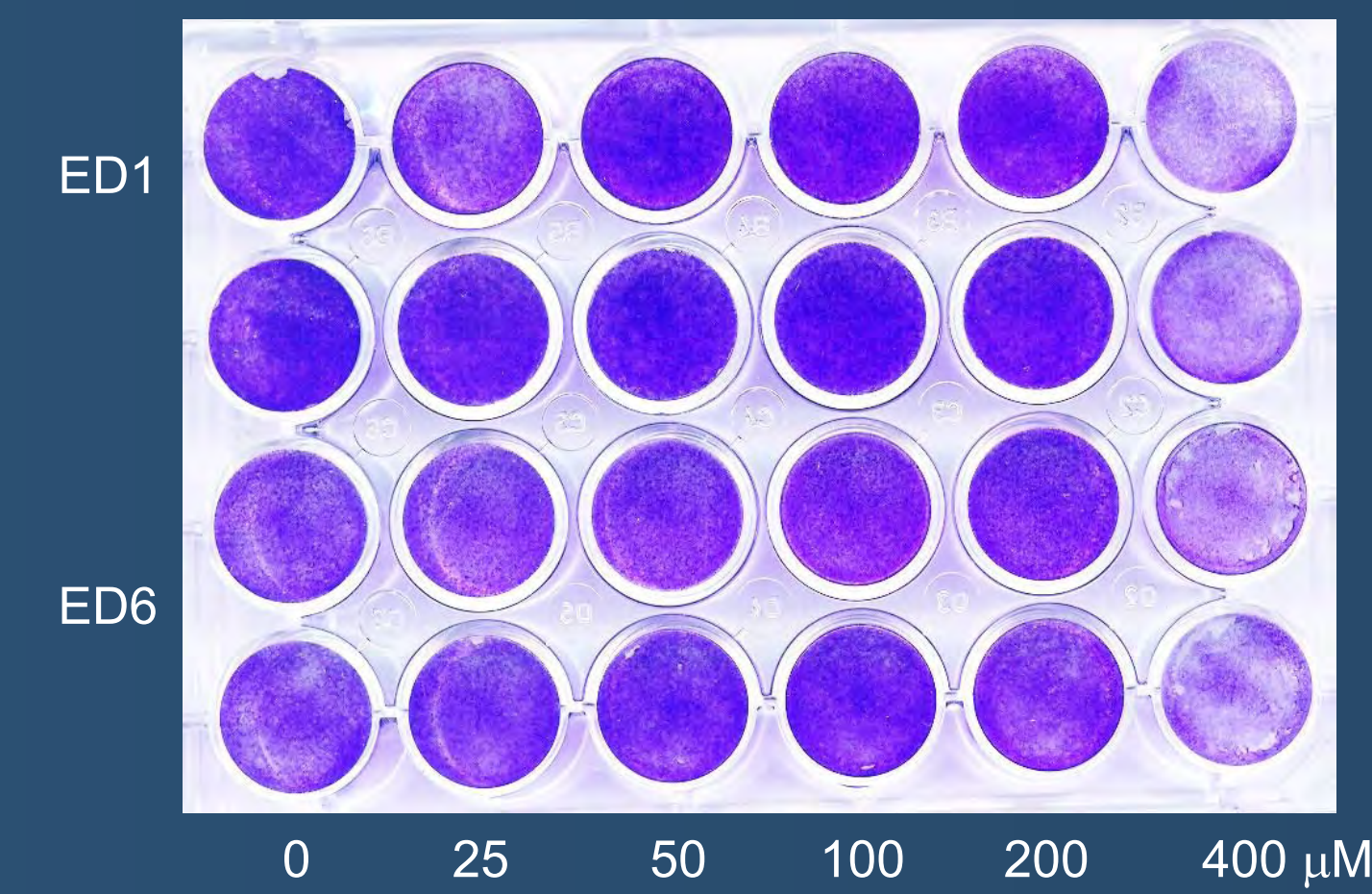


Fig. 1: Crystal stain of one of the initial Losartan toxicity tests. No significant effect on cell viability was seen until about 200  $\mu$ M.

Fig. 2: Representative images taken of H1299 cells in a combination treatment trial prior to crystal violet staining. Virus treatments were at 2.5 MOI.

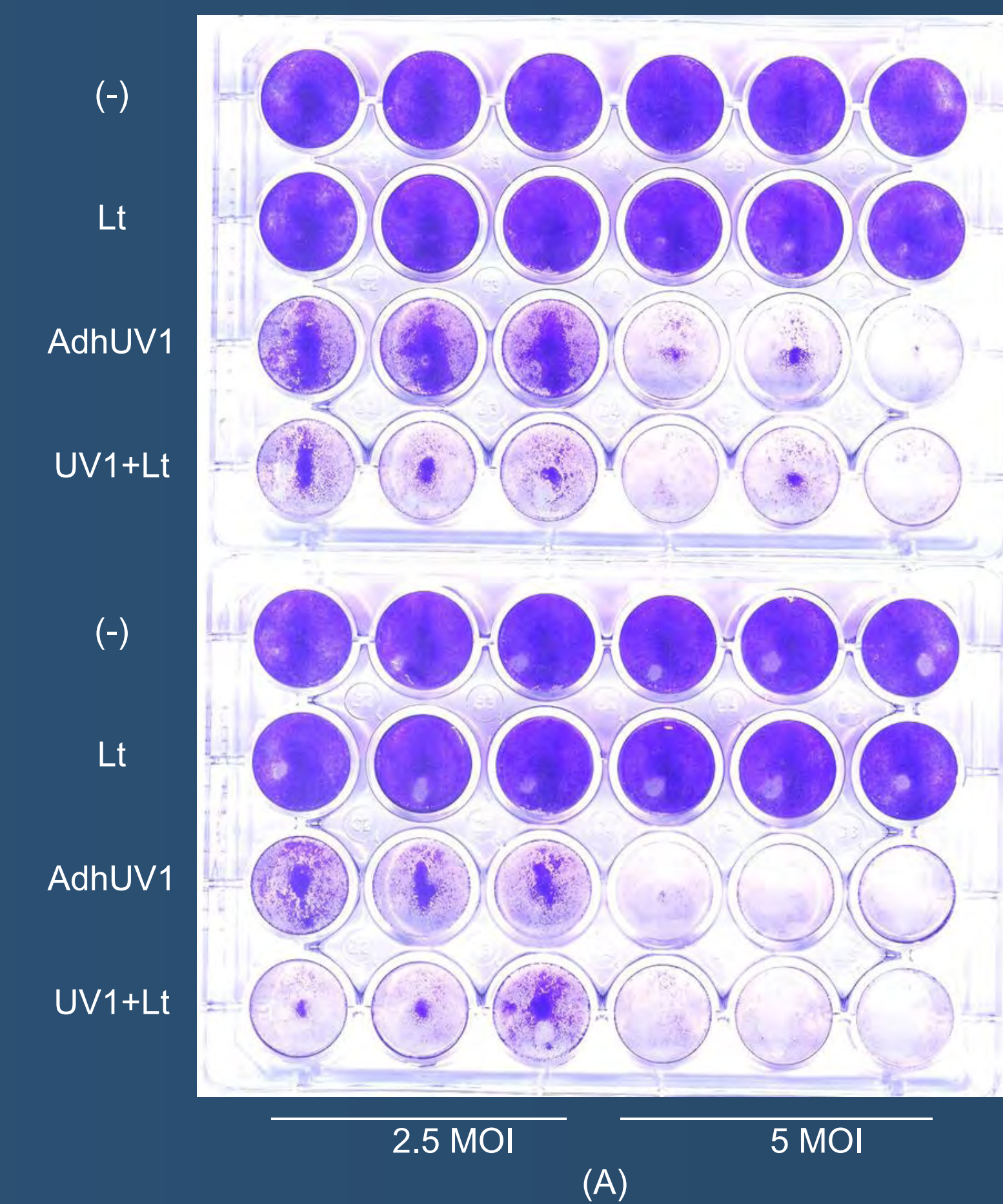
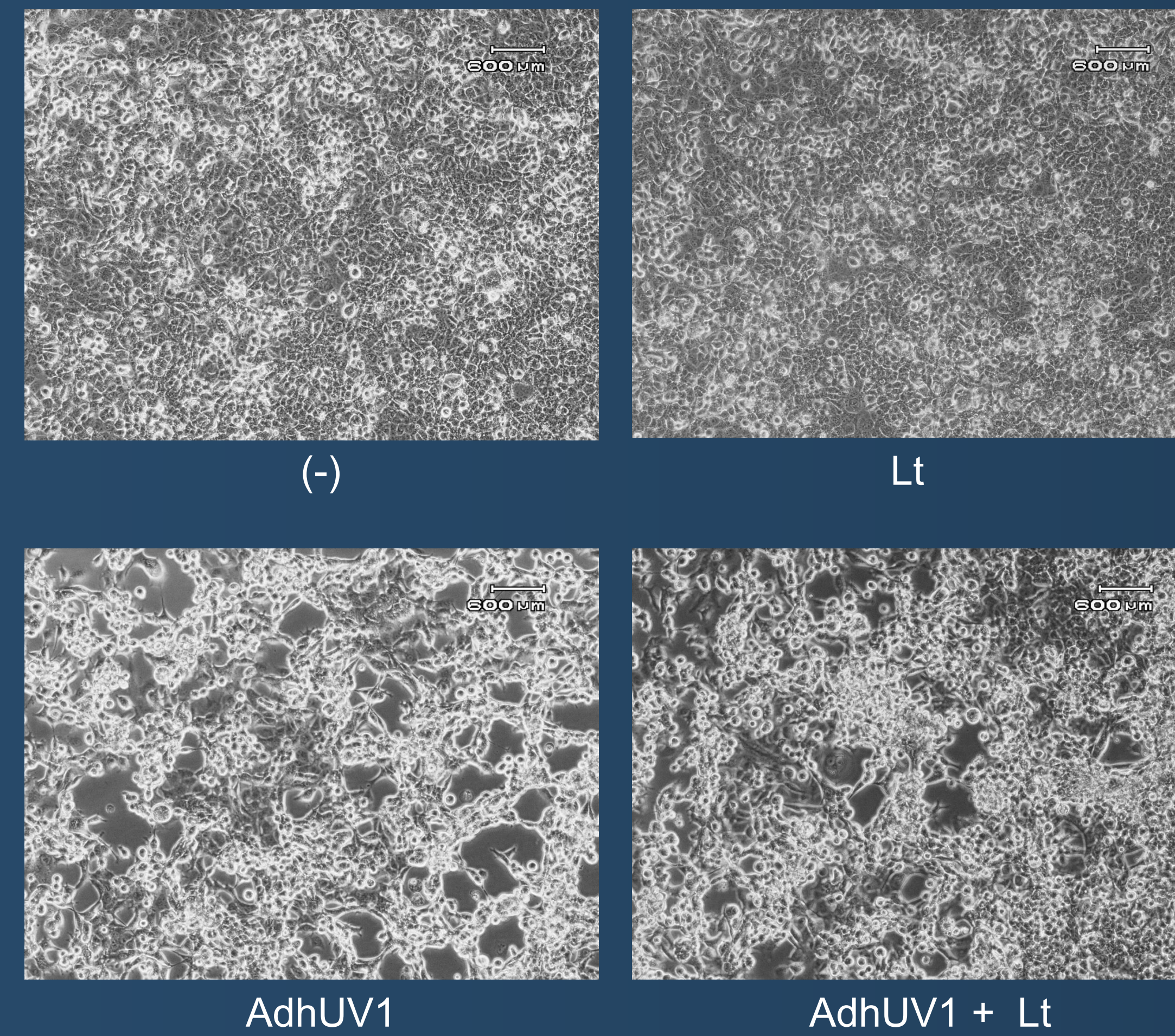


Fig. 4: Effects of Losartan and Losartan + adenovirus combination treatments relative to cells not treated with Losartan. (A) Before the AdhUV1 was applied, some H1299 cells were pretreated for a day with 20 $\mu$ M of Losartan (twice the clinical dose). Plates were fixed and stained on day three of the infection. (B) Stain readings were collected and analyzed. Each point represents the mean of at least three wells  $\pm$  (SD; bars).

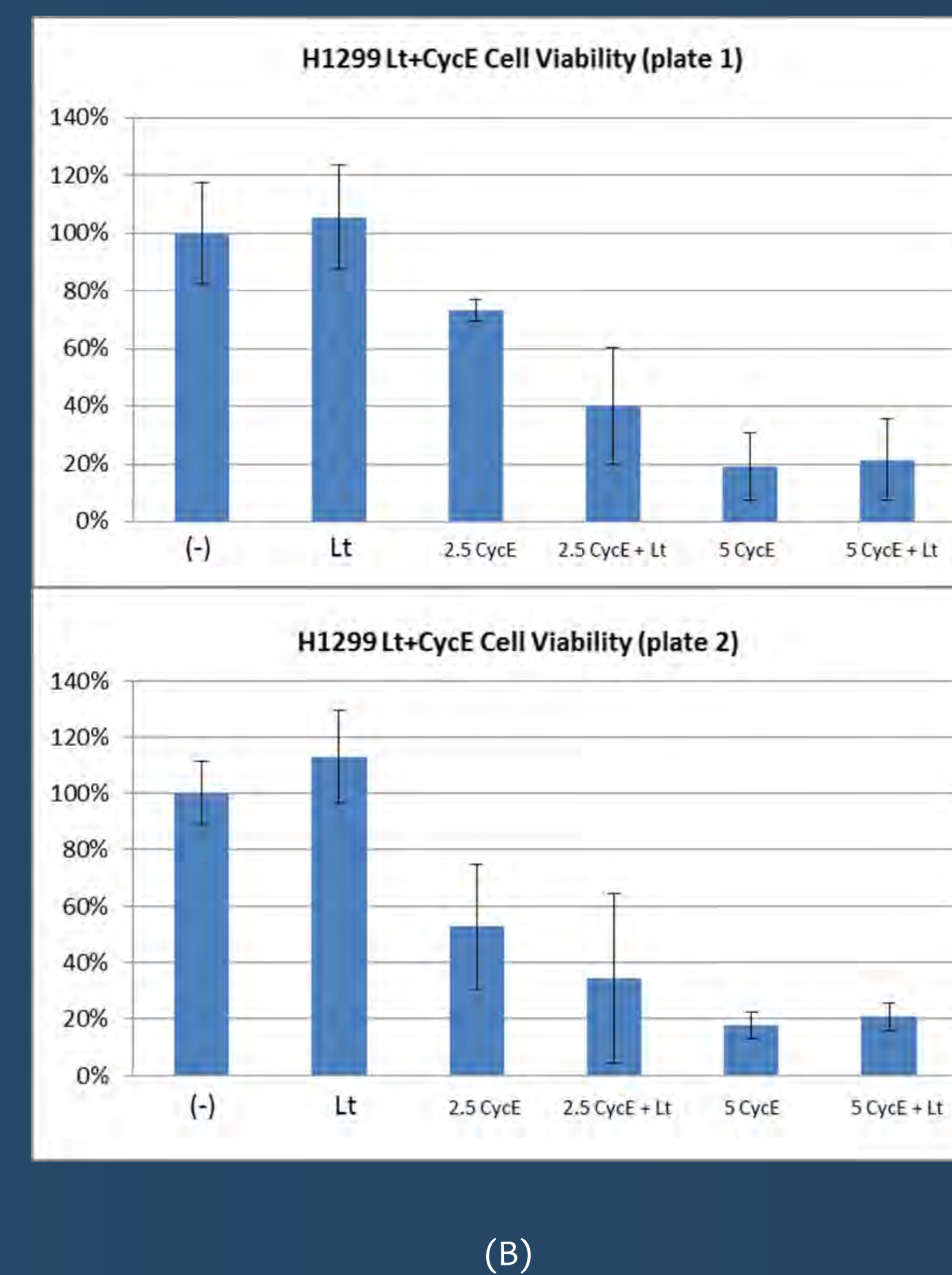


Fig. 5: Virus produced in cells treated with both Losartan and AdhUV1 and cells treated with only AdhUV1.

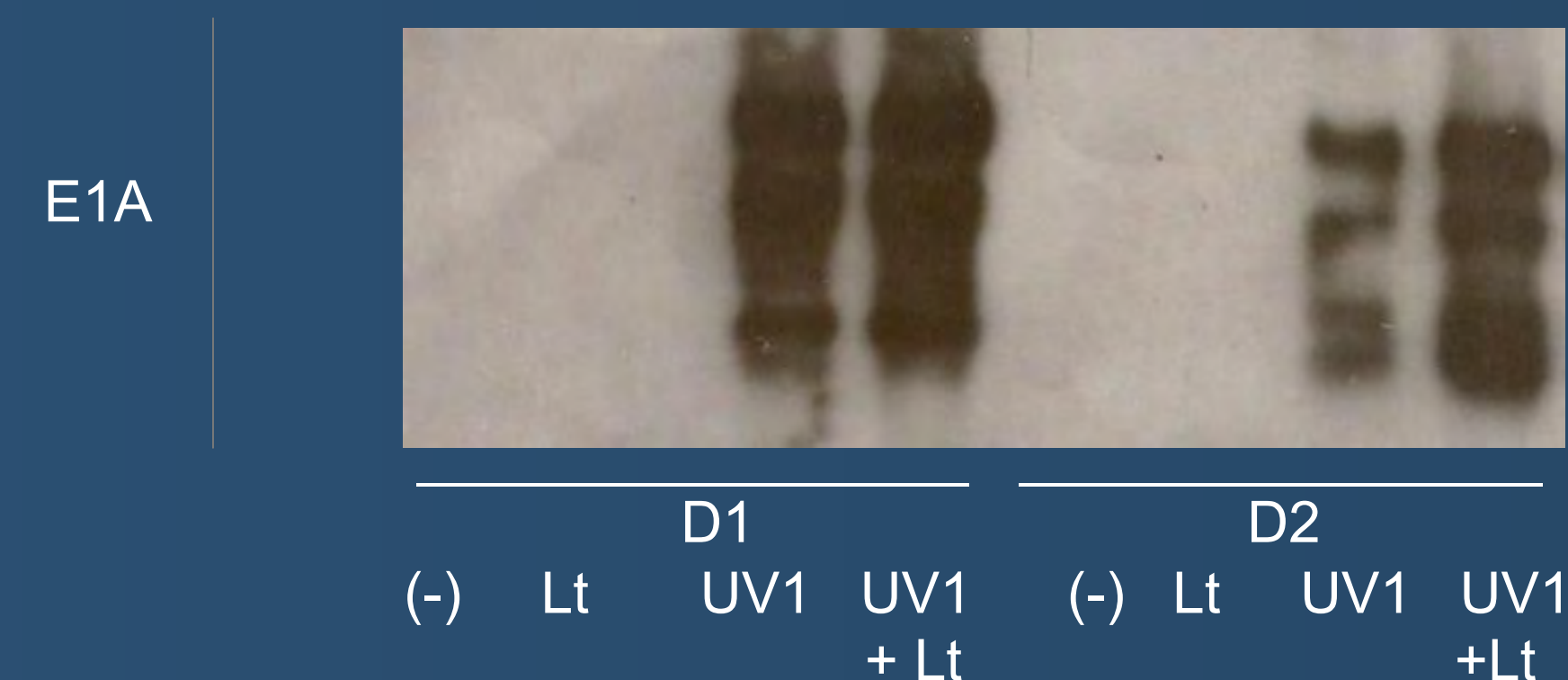


Fig. 6: Expression of adenoviral E1A genes in H1299 cells treated with Losartan + AdhUV1 or AdhUV1 only. Pellet samples were taken from dish cultures and analyzed through Western blot.

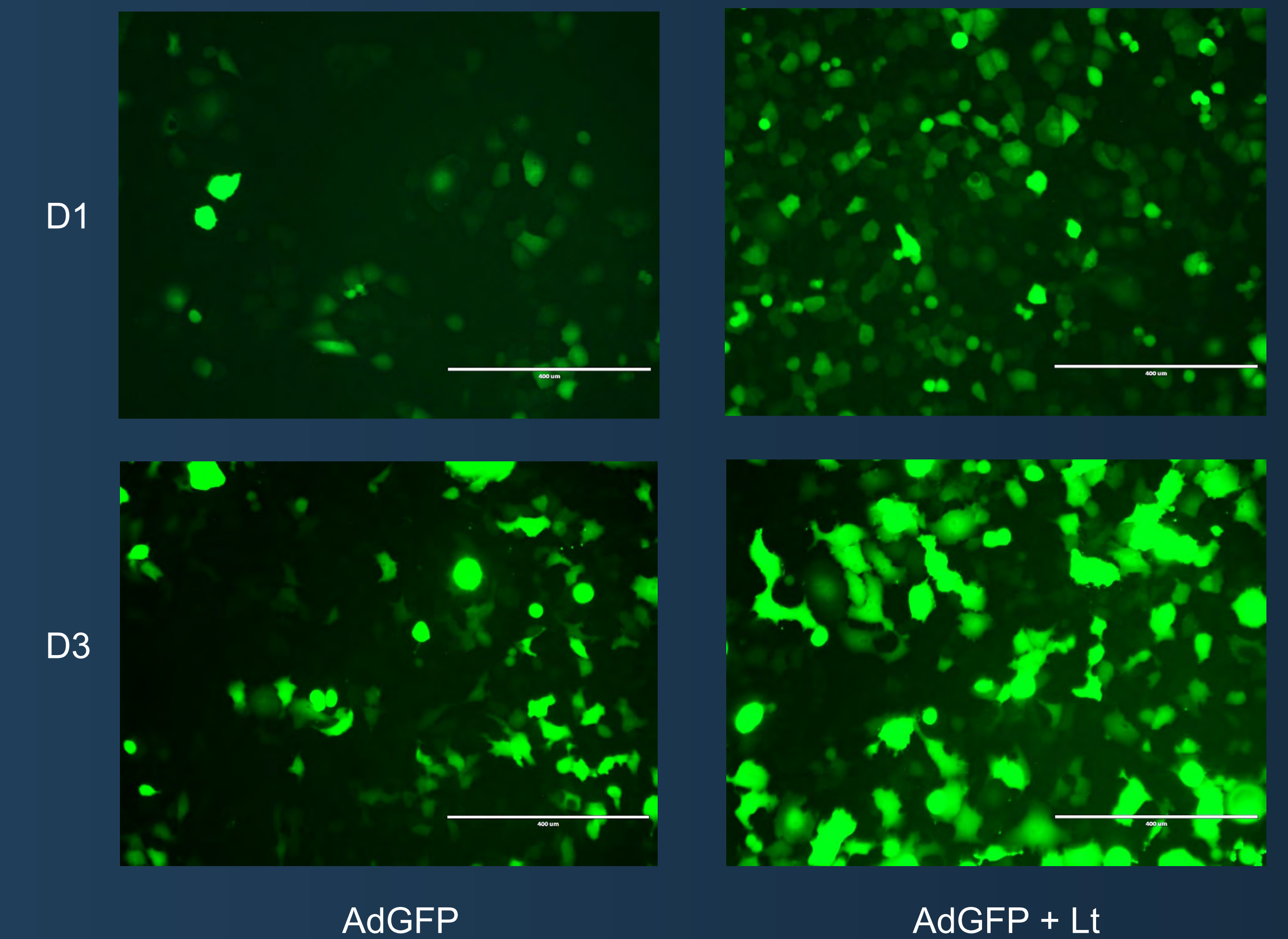


Fig. 3: H1299 cells were infected with AdGFP. Half of them were pre-treated for a day with Losartan before infection. The strength of AdGFP expression in both treatments was examined under a fluorescent filter and representative images were taken.

## Conclusions

- AdGFP experiments show that Losartan increases the initial penetration and distribution of the virus.
- Viral replication appears to be increased in the presence of Losartan, as shown by the virus titers.
- Losartan exhibits a positive effect on viral cytotoxicity and increases the efficacy of adenovirus therapy, particularly at low MOI's.

## Acknowledgements

Research was partially supported by NCI grant R25 CA134283 to the University of Louisville (Dr. D. Hein).